SMIP93

SEMINAR ON
SEISMOLOGICAL AND ENGINEERING IMPLICATIONS
OF RECENT STRONG-MOTION DATA

Sacramento, California
May 20, 1993

PROCEEDINGS

Sponsored by

Strong Motion Instrumentation Program
Division of Mines and Geology
California Department of Conservation

Supported in Part by

California Seismic Safety Commission

The California Strong Motion Instrumentation Program (SMIP) is a program within the Division of Mines and Geology of the California Department of Conservation and is advised by the Strong Motion Instrumentation Advisory Committee (SMIAC), a committee of the California Seismic Safety Commission. Current program funding is provided by an assessment on construction costs for building permits issued by cities and counties in California, with additional funding from the California Department of Transportation, the Office of Statewide Health Planning and Development, and the California Department of Water Resources.

DISCLAIMER

Neither the sponsoring nor supporting agencies assume responsibility for the accuracy of the information presented in this report or for the opinions expressed herein. The material presented in this publication should not be used or relied upon for any specific application without competent examination and verification of its accuracy, suitability, and applicability by qualified professionals. Users of information from this publication assume all liability arising from such use.

SMIP93

SEMINAR ON
SEISMOLOGICAL AND ENGINEERING IMPLICATIONS
OF RECENT STRONG-MOTION DATA

Sacramento, California
May 20, 1993

PROCEEDINGS

Edited by

M.J. Huang

Sponsored by

Strong Motion Instrumentation Program
Division of Mines and Geology
California Department of Conservation

Supported in Part by

California Seismic Safety Commission

PREFACE

The California Strong Motion Instrumentation Program (SMIP) in the Division of Mines and Geology of the California Department of Conservation promotes and facilitates the improvement of seismic codes through the Data Interpretation Project. The objective of this project is to increase the understanding of earthquake strong ground shaking and its effects on structures through interpretation and analysis studies of SMIP and other applicable strong-motion data. The ultimate goal is to accelerate the process by which lessons learned from earthquake data are incorporated into seismic code provisions and seismic design practices.

Since the establishment of SMIP in early 1970s, over 500 stations, including 130 buildings, 20 dams and 10 bridges, have been installed. Significant strong-motion records have been obtained from many of these stations. One of the most important sets of strong-motion records is from the 1989 Loma Prieta earthquake during which strong-motion records were obtained from 53 ground-response stations and 41 extensively-instrumented structures. The most recent sets are from the Cape Medocino (Petrolia) earthquake of April 25, 1992, the Landers and Big Bear earthquakes of June 28, 1992. These records have been and will be the subject of SMIP data interpretation projects.

The SMIP93 Seminar is the fifth in a series of annual events designed to transfer recent interpretation findings on strong-motion data to practicing seismic design professionals and earth scientists. In both oral presentations and poster sessions, seven investigators will provide state-of-the-art data and analysis results from recent interpretation studies of SMIP data during the past year. In addition, papers are presented by two invited speakers on the topics of special interest.

The papers in this Proceedings volume represent interim results obtained by the investigators. Following this seminar the investigators will be preparing final reports with their final conclusions. These reports will be more detailed and will update the results presented here. SMIP will make these reports available after the completion of the studies.

SMIP93 Seminar Proceedings

TABLE OF CONTENTS

SMIP93 Seminar Proceedings

SMIP93 Seminar Proceedings

SMIP93 SEMINAR ON

SEISMOLOGICAL AND ENGINEERING IMPLICATIONS

OF RECENT STRONG MOTION DATA

Radisson Hotel, Sacramento, California
May 20, 1993

PROGRAM

8:30-9:30	**Registration**
9:30-9:40	**Welcoming Remarks** *James F. Davis*, State Geologist, Division of Mines and Geology and *LeRoy Crandall*, Seismic Safety Commission, and Chair, Strong Motion Instrumentation Advisory Committee (SMIAC)
9:40-9:45	**Introductory Remarks** *Anthony Shakal*, Manager, Strong Motion Instrumentation Program
SESSION I	**Ground Response** **Moderator:** *Bruce Bolt*, UC Berkeley/Seismic Safety Commission Chair, SMIAC Ground-Response Subcommittee
9:45-10:10	**Variation of Response Spectrum with Tectonic Environment and Focal Depth** *G. Lindley and R. Archuleta*, UC Santa Barbara
10:10-10:30	**Strong Motion Data from the Large California Earthquakes of 1992** *R. Darragh, T. Cao, C. Cramer and A. Shakal*, SMIP
10:30-10:50	**Empirical Prediction of Strong Ground Motion for Earthquakes** *R. Youngs*, Geomatrix Consultants, San Francisco (Invited)
10:50-11:10	Break
SESSION II	**Building Response 1** **Moderator:** *Wilferd Peak*, Consulting Engineering Geologist Chair, SMIAC Data Interpretation Subcommittee
11:10-11:35	**Simulation of the Recorded Response of Unreinforced (URM) Infill Buildings** *J. Kariotis, T. Guh, G. Hart, J. Hill and N. Youssef*, Kariotis & Associates, South Pasadena
11:35-12:00	**Quantifying the Effects of Soil Structure Interaction for Use in Building Design** *C. Poland, J. Soulages, J. Sun and L. Mejia*, H.J. Degenkolb Associates, San Francisco
12:00-12:30	**Poster Session for Sessions I & II**

SMIP93 Seminar Proceedings

12:30-2:10 **Lunch**
Welcome by *Edward Heidig*, Director, Department of Conservation
Introduction by *LeRoy Crandall*, Chair, SMIAC
Keynote Speaker: *Egor Popov*, EERI Distinguished Lecturer

SESSION III **Building Response 2**
Moderator: *Chris Poland*, H.J. Degenkolb Associates
Chair, SMIAC Buildings Subcommittee

2:10-2:35 **Expected Seismic Performance of Buildings**
W. Holmes, Rutherford & Chekene, San Francisco (Invited)

2:35-3:00 **Analysis of Records from Four Base-Isolated Buildings During the 1992 Landers Earthquake**
M. Huang, P. Malhotra and A. Shakal, SMIP

3:00-3:20 Break

SESSION IV **Lifeline Structure Response**
Moderator: *Vern Persson*, Division of Safety of Dams, DWR
Chair, SMIAC Lifelines Subcommittee

3:20-3:45 **Dynamic Response Analyses of Cogswell Dam During the 1991 Sierra Madre and the 1987 Whittier Narrows Earthquakes**
R. Boulanger, J. Bray, S. Merry and L. Mejia, UC Davis

3:45-4:10 **Seismic Performance and Design Considerations of a Long-Span Suspension Bridge**
W. Liu, R. Imbsen and A. Kiureghian, Imbsen & Associates, Sacramento

4:10-4:40 **Poster Session for Sessions III and IV**

SMIP93 Seminar Proceedings

VARIATION OF RESPONSE SPECTRUM WITH TECTONIC ENVIRONMENT AND FOCAL DEPTH

Grant T. Lindley* and Ralph J. Archuleta#

*Institute for Crustal Studies
University of California
Santa Barbara CA 93106-1100

#Department of Geological Sciences and
Institute for Crustal Studies
University of California
Santa Barbara CA 93106-1100

ABSTRACT

The variation of response spectral shapes is examined for the 1980 Mammoth Lakes, 1983 Coalinga, and 1992 Southern California earthquake sequences. Significant variations of the response spectra are found between earthquakes of the Southern California earthquake sequence and earthquakes of the Mammoth Lakes and Coalinga sequences. These variations do not correspond simply to variations with tectonic environment. Variation of response spectral shape with focal depth is found for microearthquakes, but not for large, potentially damaging earthquakes (M >6). Response spectral shapes vary with magnitude and the variation is significant when the difference in magnitude is approximately 2 or larger.

INTRODUCTION

The 1991 Unified Building Code (UBC) gives normalized response spectra to be used in the design of structures. The shapes of these spectra vary depending on geotechnical site parameters but not on earthquake source characteristics. Source characteristics are taken into account primarily by the peak ground acceleration. Various studies have found the peak ground acceleration of earthquakes to vary with focal depth and/or tectonic environment [e.g. *McGarr*, 1984; *Campbell*, 1981]. The variation of source properties with tectonic environment or focal depth may affect the shape of the response spectrum as well as the peak ground acceleration. This study uses a simple seismological model of the earthquake source to analyse data from three regions of California to examine how response spectral shapes vary with focal depth, tectonic environment, and earthquake magnitude.

DATA

Data recorded in three different regions has been analysed. The three regions were chosen to represent three different tectonic environments. Earthquakes of the 1992 Southern California sequence are predominantly strike-slip. Earthquakes of the 1983 Coalinga sequence are predominantly thrust although strike-slip and normal faulting also occurred. Earthquakes of the 1980 Mammoth Lakes sequence are predominantly a combination of strike-slip and normal faulting.

The 1992 Southern California earthquake sequence included the M 7.4 Landers, the M 6.5 Big Bear, and the M 6.1 Joshua Tree earthquakes. A total of 9 CSMIP ground response recordings [Darragh et al., 1992; CSMIP staff, 1992] and 5 TERRAscope recordings [*Kanamori et al.*, 1990] of the Landers main shock have been analysed. In addition, 40 earthquakes ranging in magnitude from 4.0 to 6.5 recorded at the Pasadena TERRAscope station and 688

microearthquakes (M 1.5 to 3.6) recorded by digital PASSCAL instruments deployed by the Southern California Earthquake Center have been analysed.

Earthquakes from Coalinga include the M 6.7 Coalinga main shock and its larger aftershocks. The main shock was analysed using recordings from 40 CSMIP ground response stations. In addition, 32 recordings of 5 aftershocks (M 5.0 to 6.0) were analysed from CSMIP stations [*Shakal and McJunkin*, 1983; *Shakal and Ragsdale*, 1983]. Aftershocks were also recorded by the U. S. Geological Survey [*Mueller et al.*, 1984] and the analysis includes 32 recordings of 8 earthquakes (M 4.0 to 5.3) and 106 earthquakes from magnitude 2.5 to 4.0.

The data from the Mammoth Lakes area are recordings from the May-June 1980 earthquake sequence recorded by CSMIP [*Turpin*, 1980] and the U. S. Geological Survey [*Mueller et al.*, 1981; *Spudich et al.*, 1981] . A total of 28 recordings of 11 earthquakes ranging from M 4.0 to 6.2 were studied including four magnitude 6-6.2 earthquakes. In addition, 162 earthquakes ranging from 2.5 to 4.0 in magnitude were included in the analysis from data recorded by the USGS.

DETERMINATION OF EARTHQUAKE STRESS DROP

In order to determine the variation of the response spectrum with tectonic environment and focal depth, the data are analysed using a simple seismological model of the earthquake source. The analysis also includes the effect of attenuation. From this analysis, estimates are made of the earthquake stress drop and source Fourier amplitude spectrum for different focal depths and tectonic environments. Finally, the source Fourier spectra are converted to source response spectra.

In order to determine the earthquake stress drop, the Fourier amplitude spectra of S-waves are analyzed by finding non-linear least squares best fits to the spectra. The Fourier spectra are fit to the logarithm of the functional form [*Boatwright*, 1978]

$$D(f) = \frac{\Omega_0 \exp(-\pi f t^*)}{\left[1 + (f/f_c)^{2\gamma}\right]^{1/2}} \qquad (1)$$

where D(f) is the Fourier displacement amplitude, Ω_0 is the low frequency spectral asymptote, f is the frequency, f_c is the corner frequency, γ is the source spectral falloff, and t* is the integral of the travel time divided by the quality factor of attenuation Q. The parameter γ is taken to be 2.0. The parameter t* determines the attenuation. The best fit for a particular spectrum is the combination of parameters that minimizes the sum of squared residuals. The residual at each value of the Fourier spectrum is the spectrum minus the fit to the spectrum. The best fitting combination of parameters is identically the same whether fitting to the displacement, velocity, or acceleration spectrum. An example of a spectral fit is shown in Figure 1.

Stress drops for S-waves are calculated using the equation [*Brune*, 1970, 1971]

$$\Delta\tau = 7/16\ (2\pi f_c/2.34\beta)^3\ M_0 \qquad (2)$$

where $\Delta\tau$ is the stress drop, β is the shear wave velocity, and M_0 is the seismic moment. The moments for S-waves are determined by

$$M_o = 4\pi \rho\beta^3 r\Omega_o/2R_{\theta\phi} \quad (3)$$

where ρ is the density and r is the hypocentral distance. The value of $R_{\theta\phi}$ is determined by the radiation pattern for which an average value of 0.55 is used [*Boore and Boatwright*, 1984]. The shear wave velocity is taken to be 3.3 km/sec and the density 2.9 g/cm^3.

Table 1 lists the M > 4 events studied in this anlaysis and gives average values for the seismic moment and stress drop.

Table 1. M > 4 earthquakes and source parameters.

Event	Mag.	Depth (km)	# stations	log-avg. moment dyne-cm	log-avg. stress drop bars
1980 Mammoth Lakes:					
5/25 16:33	6.1	10.13	1 CSMIP	$7\ 10^{24}$	220
5/25 16:49	6.0	6.28	2 CSMIP	$2\ 10^{24}$	312
5/25 19:44	6.1	15.26	1 CSMIP	$9\ 10^{24}$	281
5/25 20:35	5.7	0.03	1 CSMIP	$3\ 10^{23}$	177
5/26 18:57	5.7	5.61	1 CSMIP	$5\ 10^{23}$	68
5/27 14:50	6.2	14.73	3 CSMIP	$3\ 10^{24}$	289
5/28 5:16	4.9	5.07	2 USGS	$7\ 10^{22}$	90
5/31 10:11	4.3	5.55	5 USGS	$7\ 10^{21}$	181
6/1 06:47	4.5	7.00	3 USGS	$4\ 10^{22}$	255
6/2 10:22	4.0	6.77	4 USGS	$9\ 10^{21}$	59
6/2 20:34	4.1	7.41	5 USGS	$3\ 10^{21}$	116
1983 Coalinga:					
5/2 23:42	6.7	9.65	40 CSMIP	$1\ 10^{25}$	576
5/9 2:49	5.3	11.75	10 CSMIP + 8 USGS	$3\ 10^{23}$	388
5/9 7:40	5.3	9.5	7 CSMIP	$2\ 10^{23}$	345
7/22 2:39	6.0	9.2	7 CSMIP	$2\ 10^{24}$	188
7/22 3:43	5.0	9.6	2 CSMIP	$1\ 10^{23}$	936
7/25 22:31	5.1	9.5	2 CSMIP	$1\ 10^{24}$	689
5/3 15:41	4.8	7.81	2 USGS	$5\ 10^{22}$	191
5/9 3:26	4.5	12.57	6 USGS	$3\ 10^{22}$	365
5/12 13:41	4.7	10.15	3 USGS	$2\ 10^{22}$	37
5/16 14:21	4.0	8.43	5 USGS	$7\ 10^{21}$	31
5/19 11:05	4.3	12.24	3 USGS	$3\ 10^{21}$	44
5/22 8:39	4.5	9.75	3 USGS	$7\ 10^{21}$	55
5/24 9:02	4.6	9.19	2 USGS	$6\ 10^{22}$	474
1992 Landers:					
6/28 11:57	7.4	9	9 CSMIP + 5 TERRAscope	$5\ 10^{26}$	221
6/29 14:13	5.4	9.88	1 TERRAscope	$7\ 10^{23}$	53
6/29 16:01	5.2	1.86	1 TERRAscope	$5\ 10^{23}$	11
6/30 12:34	4.2	4.57	1 TERRAscope	$9\ 10^{21}$	6.1

Event	Mag.	Depth (km)	# stations	log-avg. moment dyne-cm	log-avg. stress drop bars
6/30 14:38	5.0	0.84	1 TERRAscope	$4\ 10^{23}$	7.4
6/30 20:05	4.1	0.57	1 TERRAscope	$6\ 10^{21}$	3.0
7/01 7:40	5.4	9.00	1 TERRAscope	$1\ 10^{23}$	42
7/2 5:16	4.0	0.72	1 TERRAscope	$6\ 10^{21}$	1.6
7/5 21:18	5.4	0.36	1 TERRAscope	$2\ 10^{24}$	7.6
7/6 12:00	4.5	1.80	1 TERRAscope	$2\ 10^{22}$	3.2
7/7 8:21	4.0	3.24	1 TERRAscope	$6\ 10^{21}$	2.0
7/7 22:09	4.4	2.54	1 TERRAscope	$2\ 10^{22}$	10
7/2 2:23	4.9	6.00	1 TERRAscope	$1\ 10^{23}$	9.4
7/18 0:06	4.0	2.62	1 TERRAscope	$2\ 10^{21}$	1.4
7/20 4:08	4.1	0.41	1 TERRAscope	$1\ 10^{22}$	1.5
7/24 7:23	4.0	8.97	1 TERRAscope	$2\ 10^{21}$	1.4
7/24 18:14	5.0	9.08	1 TERRAscope	$4\ 10^{23}$	1.8
7/25 4:31	4.9	5.85	1 TERRAscope	$1\ 10^{23}$	4.2
8/4 19:06	4.0	0.01	1 TERRAscope	$9\ 10^{21}$	1.7
8/8 15:37	4.4	2.84	1 TERRAscope	$6\ 10^{22}$	2.1
8/11 6:11	4.3	0.75	1 TERRAscope	$6\ 10^{21}$	4.7
8/15 8:24	4.8	0.61	1 TERRAscope	$4\ 10^{22}$	22
1992 Big Bear:					
6/28 15:04	6.5	5.00	1 TERRAscope	$4\ 10^{25}$	378
6/28 15:24	4.8	6.00	1 TERRAscope	$4\ 10^{22}$	19
6/28 17:48	4.4	1.18	1 TERRAscope	$2\ 10^{22}$	3.8
7/1 10:32	4.1	0.35	1 TERRAscope	$3\ 10^{22}$	0.8
7/21 21:10	4.1	1.86	1 TERRAscope	$5\ 10^{21}$	16
8/17 20:41	5.3	11.73	1 TERRAscope	$9\ 10^{22}$	20
8/24 13:51	4.3	1.84	1 TERRAscope	$1\ 10^{22}$	4.4
11/27 16:00	5.3	1.54	1 TERRAscope	$2\ 10^{23}$	91
1992 Joshua Tree:					
4/23 4:50	6.1	12.38	1 TERRAscope	$6\ 10^{25}$	15
4/23 13:35	4.1	1.05	1 TERRAscope	$1\ 10^{22}$	1.0
4/23 18:56	4.4	3.42	1 TERRAscope	$9\ 10^{21}$	9.0
4/26 6:26	4.2	0.62	1 TERRAscope	$4\ 10^{22}$	3.7
4/27 3:11	4.2	0.01	1 TERRAscope	$2\ 10^{22}$	8.4
5/2 12:46	4.2	4.03	1 TERRAscope	$5\ 10^{21}$	9.0
5/4 1:16	4.1	5.97	1 TERRAscope	$8\ 10^{21}$	2.3
5/4 16:19	4.9	12.54	1 TERRAscope	$3\ 10^{23}$	3.3
5/6 2:38	4.7	7.31	1 TERRAscope	$8\ 10^{22}$	10
5/18 15:44	4.9	7.10	1 TERRAscope	$1\ 10^{23}$	15
6/11 00:24	4.3	0.82	1 TERRAscope	$5\ 10^{22}$	1.1

VARIATION OF STRESS DROP WITH DEPTH AND REGION

The variation of microearthquake stress drop with depth is shown in Figure 2 for the three regions. Some of the results for microearthquakes are from a previous anlaysis [Lindley and Archuleta, 1992]. A steady increase of earthquake stress drop with depth might be expected since the stress required for shear failure of rock should increase with the overburden pressure [see e.g. *Sibson*, 1974]. This increase of stress drop with depth is observed for Joshua Tree microearthquakes, but not for Coalinga or Mammoth Lakes microearthquakes. There is a large difference in stress drop between the three regions. Coalinga and Mammoth Lakes stress drops are approximately equal and are about a factor of five to ten larger than Joshua Tree stress drops.

A comparison of average stress drop for Joshua Tree microearthquakes and M >4 earthquakes of the 1992 Southern California earthquake sequence is shown in Figure 3. The Joshua Tree microearthquake stress drops are significantly smaller than the M >4 earthquake stress drops. The M >4 earthquake stress drops are still smaller than the stress drops for Coalinga or Mammoth Lakes (Figure 2). Both calculations show an increase of stress drop with depth. For the larger earthquakes (M>6), we expect that most of the radiated seismic energy will typically come from depths greater than about 5 or 6 km. Thus, the relatively low stress drops of the upper 6 km observed for the 1992 Southern California earthquake sequence would not be expected to alter the shape of the spectra of the potentially damaging earthquakes. It is only for earthquakes of magnitude less than about 5 with shallow focal depths that this low stress drop is likely to be observed.

Comparisons of stress drops for microearthquakes and M >4 earthquakes at Coalinga and Mammoth Lakes are shown in Figures 4 and 5. Again, the M >4 earthquakes have significantly higher stress drops than the microearthquakes. The difference between the stress drops at Coalinga and Mammoth Lakes is not significant. Coalinga and Mammoth Lakes M>4 earthquake stress drops are significantly larger than the M>4 earthquake stress drops of the 1992 Southern California earthquake sequence. This agrees with the results from the microearthquakes. This regional variation in the stress drop will result in significant differences in the response spectrum.

The observed stress drop difference between the three regions does not correspond to the expected variation based on tectonic environment [e.g. *Sibson*, 1974]. Based on tectonic environment, it would be expected that stress drops would be greatest at Coalinga (thrust), second greatest for the 1992 Southern California earthquake sequence (strike-slip), and smallest for Mammoth Lakes (normal/strike-slip). There are many other possible factors that could cause a change in stress drop between regions including earthquake repeat times, pore fluid pressure, rheology, or age of fault zones. The cause(s) for the differences in regional stress drops observed in this study are not readily apparent. Thus, while there are significant variations between the regions, it may be too early to attempt to include those variations in the UBC until a better understanding of the fundamental causes is obtained.

VARIATION OF RESPONSE SPECTRUM WITH REGION AND MAGNITUDE

The source parameters from the spectral fits and the seismological source model in equation (1) allow us to estimate the source Fourier amplitude spectrum. For engineering purposes, the response spectrum is usually more important than the Fourier spectrum. In order to calculate the response spectrum from the Fourier spectrum, random-vibration theory is used following *Joyner and Boore* [1988].

In order to compare the source response spectra between the three regions, hypothetical Fourier amplitude spectra are determined for a M6-6.5 event in each region (Figure 6). For the 1992 Southern California earthquake sequence, source parameters from the M 6.1 Joshua Tree and

M 6.5 Big Bear earthquakes were averaged together. For Coalinga, source parameters from the M 6.7 main shock and the M 6.0 aftershock were used, and for Mammoth Lakes, source parameters from the four main shocks (M 6.0 to 6.2) were averaged. The source response spectra were then calculated from the Fourier spectra following *Joyner and Boore* [1988].

As expected, the results indicate that the source response spectra at Coalinga and Mammoth Lakes are similar while the response spectra for the Southern California earthquake sequence are significantly different (Figure 7). The amplitude of the source response spectrum for the hypothesized M6-6.5 Southern California earthquake is larger at long periods and smaller at short periods compared to Coalinga or Mammoth Lakes. The reason for this is that the seismic moment is larger and the stress drop smaller for the same magnitude earthquake for the Southern California earthquake sequence as compared to Coalinga or Mammoth Lakes. The seismic moment controls the response at long periods boosting these levels and causing the source response spectrum for the Southern California earthquake to be larger at long periods.

It is interesting to compare one of the source response spectra (in this case Coalinga) to the 1991 UBC normalized response spectra (Figure 8). Also included is the source response spectrum with attenuation added ($t^* = 0.05$ s). The source response spectrum without attenuation is much larger than the UBC spectra at short periods. However, the shape of the source response spectrum with attenuation matches the shape of the UBC spectra, at least qualitatively. Thus, the rolloff of the response spectra typically observed for short periods appears to be controlled by attenuation while the falling amplitudes at long periods is controlled by the earthquake source.

It is also interesting to compare the source response spectra for different magnitude earthquakes of the 1992 Southern California earthquake sequence to see if magnitude affects the shape of the response spectra (Figure 9). From Figure 9 it appears that when the difference in magnitude is greater than or approximately 2, the response spectral shapes begin to become significantly different. The larger magnitude earthquake is observed to have greater amplitudes at long periods compared to the smaller magnitude earthquake. The explanation for this change in the source response spectral shape is that the corner frequency (see equation (1) and Figure 1) is smaller for the larger magnitude earthquake. This smaller corner frequency causes a boost in the source response spectrum for the larger earthquake at longer periods.

REFERENCES

Boatwright, J. (1978). Detailed spectral analysis of two small New York State earthquakes, *Bull. Seism. Soc. Am.*, **68**, 1117-1131.

Boore, D. M. and J. Boatwright (1984). Average body-wave radiation coefficients, *Bull. Seism. Soc. Am.*, **74**, 1615-1621.

Brune, J. N. (1970). Tectonic stress and the spectra of seismic shear waves from earthquakes, *J. Geophys. Res.*, **75**, 4997-5009. (Correction *J. Geophys. Res.*, **76**, 5002, 1971.)

Campbell, W. C. (1981). Near-source attenuation of peak horizontal acceleration, *Bull. Seism. Soc. Am.*, **71**, 2039-2070.

CSMIP staff (1992). Preliminary processed strong-motion data for the Landers earthquake of 28 June 1992, *California Division of Mines and Geology Report OSMS 92-11.*

Darragh, R., T. Cao, C. Cramer, F. Su, M. Huang, and A. Shakal (1992). Processed CSMIP strong-motion records from the Landers, CA earthquake of 28 June 1992: Release No. 2, *California Division of Mines and Geology Report OSMS 92-13.*

Joyner, W. B. and D. M. Boore (1988). Measurement, characterization, and prediction of strong ground motion, in *Earthquake Engineering and Soil Dynamics II - Recent Advances in Ground-Motion Evaluation*, J. L. Von Thun, editor, American Society of Civil Engineers Geotechnical Special Publication No. 20, 43-103.

Kanamori, H., E. Hauksson, and T. Heaton (1990). TERRAscope and CUBE project at Caltech, *Eos*, **72**, 564.

Lindley, G. T. and R. J. Archuleta (1992). Earthquake source parameters and the frequency dependence of attenuation at Coalinga, Mammoth Lakes, and the Santa Cruz Mountains, California, *J. Geophys. Res.*, **97**, 14,137-14,154.

McGarr, A. (1984). Scaling of ground motion parameters, state of stress, and focal depth, *J. Geophys. Res.*, **89**, 6969-6979.

Mueller, C., P. Spudich, E. Cranswick, R. Archuleta (1981). Preliminary analysis of digital seismograms from the Mammoth Lakes, California earthquake sequence of May-June, 1980, U.S. Geological Survey Open-File Report 81-155.

Mueller, C. S., E. Sembera, and L. Wennerberg (1984). Digital recordings of aftershocks of the May, 2 1983 Coalinga, California earthquake, U.S. Geological Survey Open-File Report 84-697.

Shakal, A. F. and R. D. McJunkin (1983). Preliminary summary of CDMG strong-motion records from the 2 May 1983 Coalinga, California, earthquake, California Division of Mines and Geology Report 83-5.2 (rev. 3).

Shakal, A. F. and J. T., Ragsdale (1983). Strong motion data from the Coalinga, California earthquake and aftershocks, in *The 1983 Coalinga, California, Earthquakes*, J. H. Bennett and R. W. Sherburne, editors, *Calif. Div. Mines Geol. Spec. Publ. 66*, 113-126.

Sibson, R. (1974). Frictional constraints on thrust, wrench, and normal faults, *Nature*, **249**, 542-544.

Spudich, P., E. Cranswick, J. Fletcher, E. Harp, C. Mueller, R. Navarro, J. Sarmiento, J. Vinton, R. Warrick (1981). Acquisition of digital seismograms during the Mammoth Lakes, California, earthquake sequence May-June 1980, U.S. Geological Survey Open-File Report 81-38.

Turpin, C. D. (1980). Strong-motion instrumentation program results from the May, 1980, Mammoth Lakes, Califorina earthquake sequence, in *Mammoth Lakes, California earthquakes of May 1980*, R. W. Sherburne, editor, *Calif. Div. Mines Geol. Spec. Publ. 150*, 75-90.

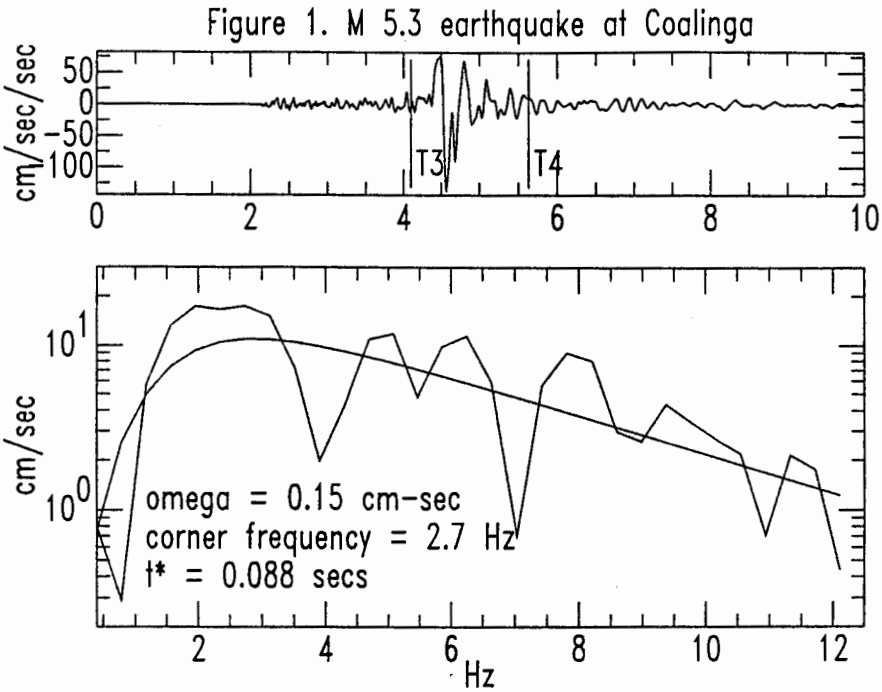

Figure 1. Example determination of earthquake source parameters and attenuation from the Fourier amplitude spectrum (M 5.3 aftershock from Coalinga). T3 and T4 mark the window for which the Fourier amplitude spectrum was calculated. The smooth curve in the spectrum is the fit to the Fourier spectrum.

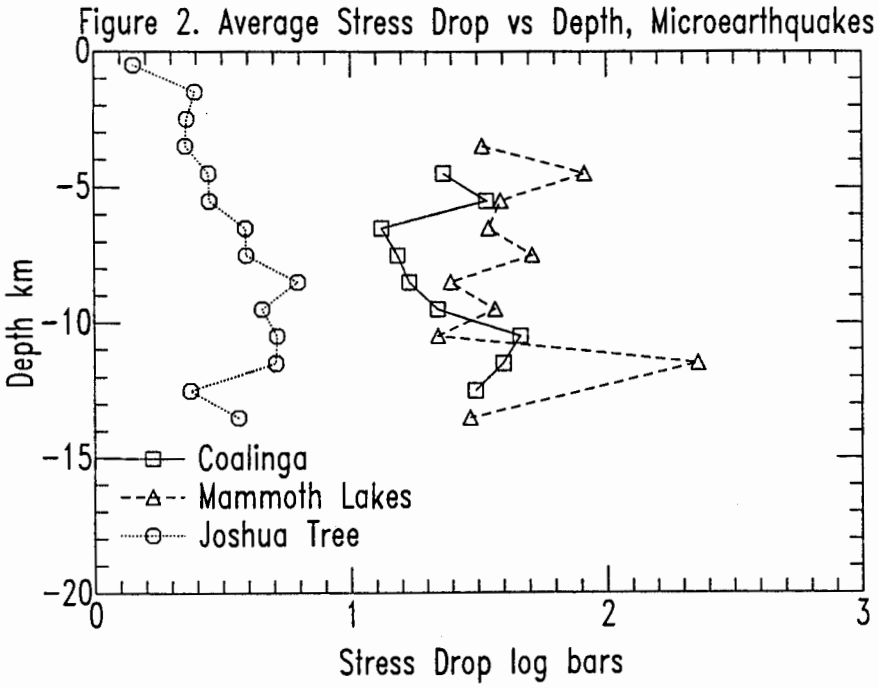

Figure 2. Variation of earthquake stress drop with depth for microearthquakes from three different regions of California. Data points are log-average stress drops for large numbers of microearthquakes in the three regions.

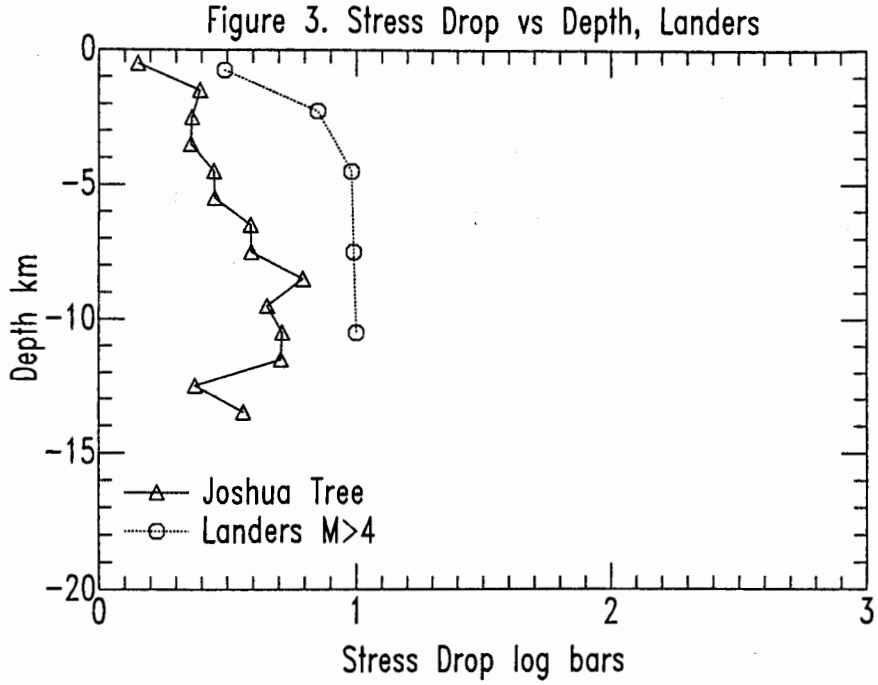

Figure 3. Stress drop versus depth for microearthquakes and M > 4 earthquakes from the 1992 Southern California earthquake sequence. Data points are log-average stress drops for the different depths.

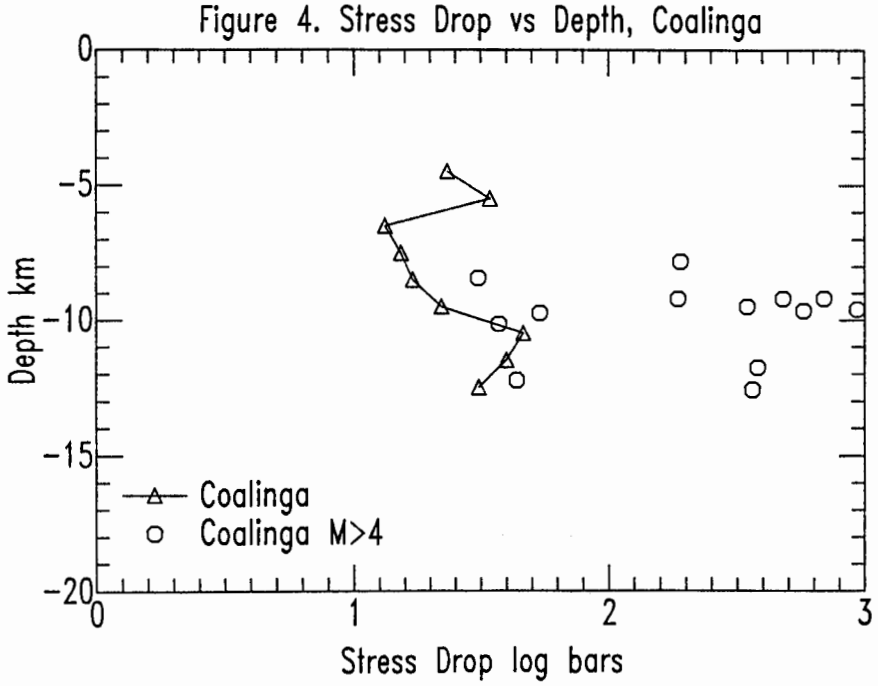

Figure 4. Stress drop versus depth for microearthquakes and M > 4 earthquakes from Coalinga. Circles are for individual M > 4 earthquakes.

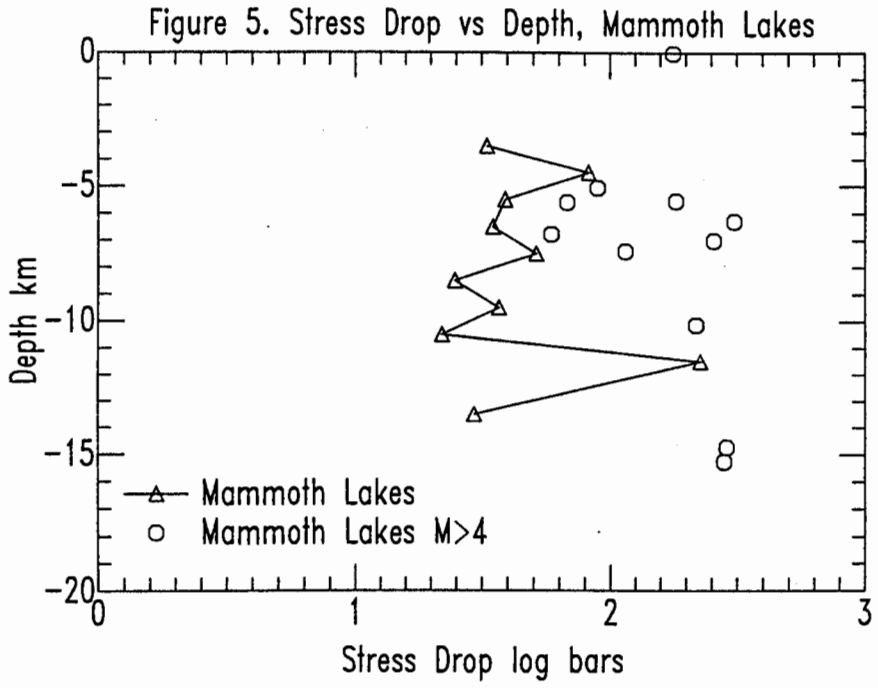

Figure 5. Stress drop versus depth for microearthquakes and M > 4 earthquakes from Mammoth Lakes. Circles are for individual M > 4 earthquakes.

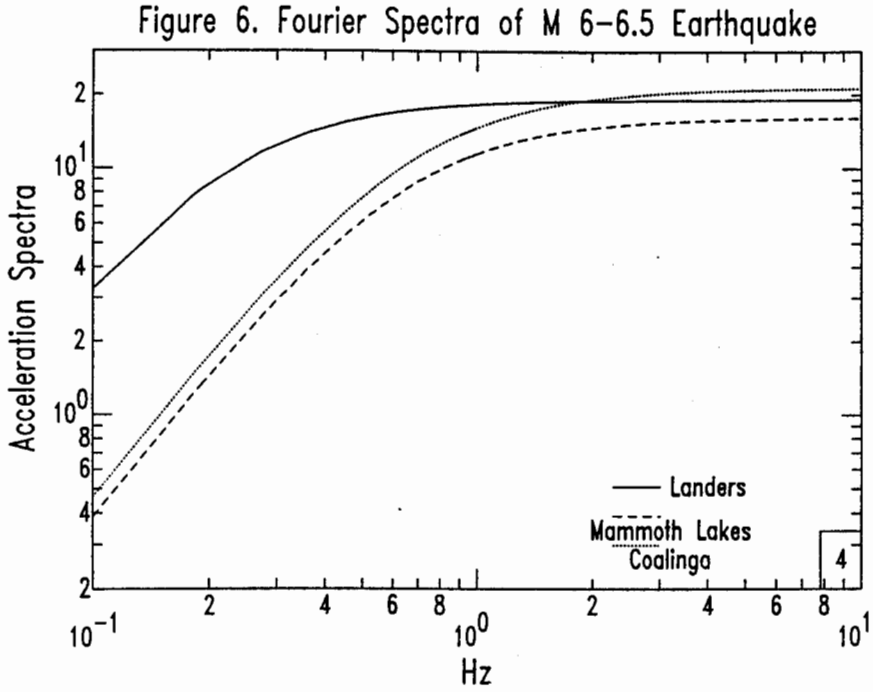

Figure 6. Source Fourier amplitude spectra for the three different regions for an hypothetical M 6-6.5 earthquake. The scale of the amplitude spectrum is arbitrary and depends on distance from the source.

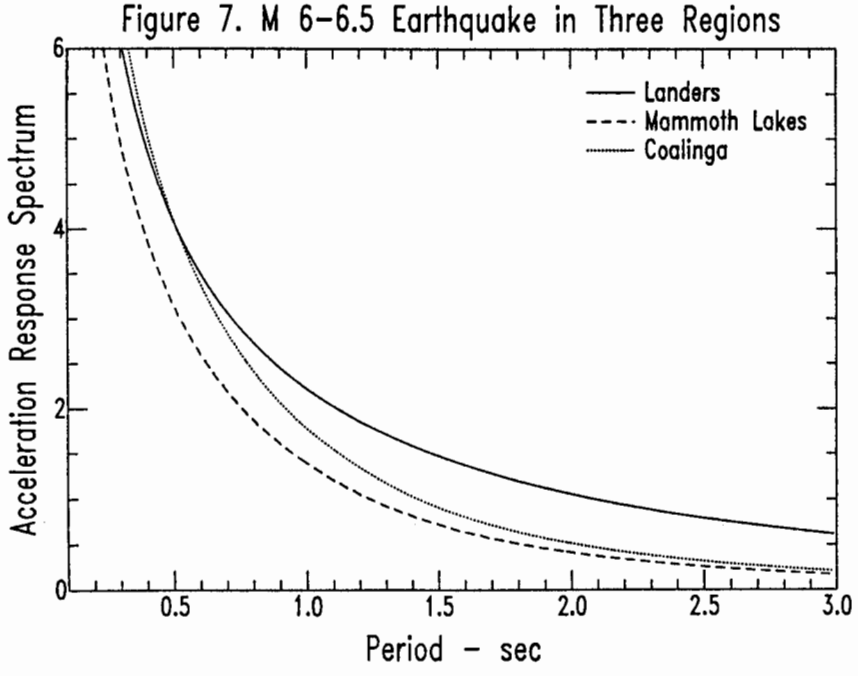

Figure 7. Source response spectra for the three different regions for an hypothetical M 6-6.5 earthquake. The scale of the amplitude spectrum is arbitrary and depends on distance from the source.

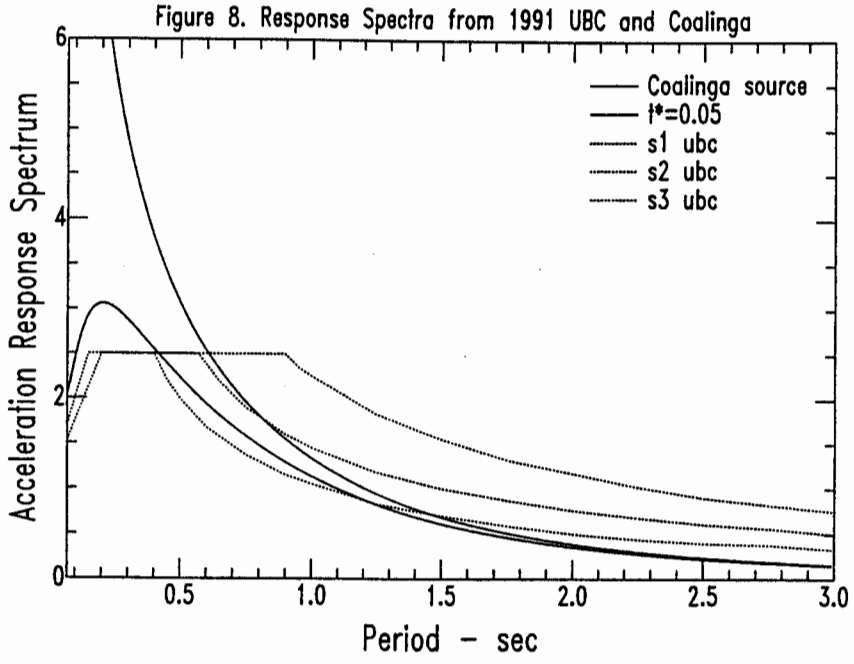

Figure 8. Source response spectrum for the Coalinga M 6-6.5 hypothetical earthquake, response spectrum with attenuation (t*=0.05 s), and normalized response spectra from the 1991 Uniform Building Code.

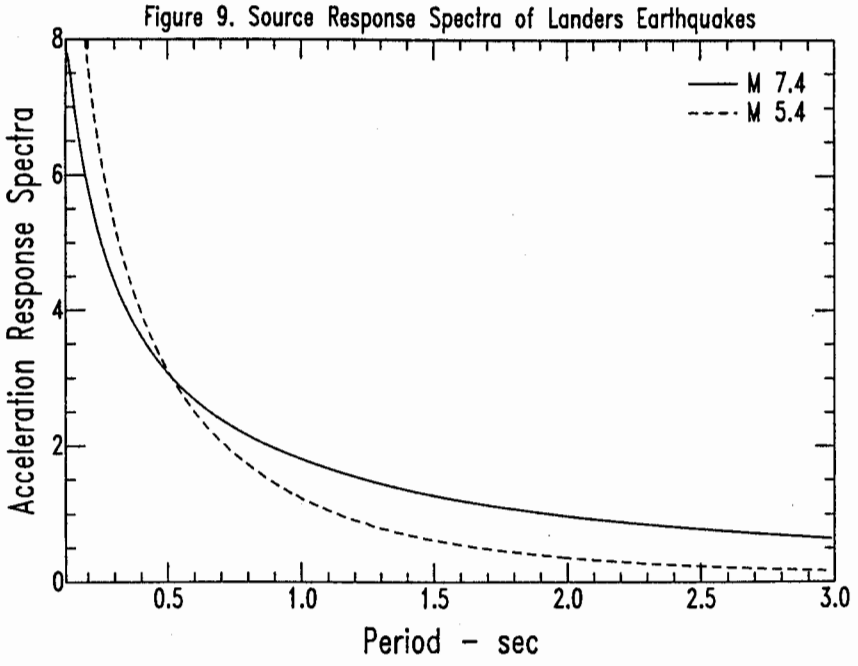

Figure 9. Source response spectra for the M 7.4 Landers main shock and for a nearby M 5.4 aftershock.

STRONG MOTION DATA FROM THE LARGE CALIFORNIA EARTHQUAKES OF 1992

R. B. Darragh, T. Q. Cao, C. H. Cramer and A. F. Shakal

California Department of Conservation
Division of Mines and Geology
Strong Motion Instrumentation Program

ABSTRACT

From April to July, 1992 six earthquakes occurred in California with magnitude greater than 6. The Cape Mendocino earthquake sequence in northern California includes a magnitude 7.0 mainshock and two aftershocks with magnitudes of 6.2 and 6.3. The Landers sequence in southern California includes the Joshua Tree, Landers and Big Bear earthquakes with magnitudes of 6.1, 7.3 and 6.2, respectively. Strong-motion records were recovered from more than 500 stations of the California Strong Motion Instrumentation Program (CSMIP) following these earthquakes. For example, the Landers earthquake produced an extensive set of strong motion accelerograms at 144 CSMIP stations that recorded the largest earthquake to occur in California since 1952.

We present four results obtained from the CSMIP strong motion data. First, the strong motion records from the Cape Mendocino mainshock have some of the highest accelerations ever recorded. The Cape Mendocino station recorded a peak acceleration near 2 g, the largest acceleration ever recorded in California. Also, one of the highest accelerations ever recorded on a structure, 1.4 g, occurred on the ground near the abutment of a freeway overpass near Rio Dell. Second, the most significant aspect of the records from the Landers earthquake is their long duration, compared to most records that have been obtained in California. For example, the duration of strong shaking was 2-3 times longer than for the magnitude 7 Loma Prieta earthquake of 1989. Third, recordings from both mainshocks have significantly more long period energy in the ground motion than seen in previous strong motion recordings. Fourth, the strong motion records from these earthquakes have larger peak accelerations than most existing attenuation models would predict. Also, the Landers peak accelerations show less attenuation with distance.

THE EARTHQUAKE SEQUENCES

Table I summarizes the earthquake magnitudes (moment (M_w), surface (M_S) and local (Richter) (M_L)) and mechanism as estimated by the U. S. Geological Survey, California Institute of Technology and University of California, Berkeley for the 1992 earthquakes. The moment magnitude scale is used throughout this paper. Important aspects of each sequence and CSMIP strong motion data recovered from these earthquakes are discussed briefly in the text and more extensively in the references given in the bibliography.

Cape Mendocino Sequence: The magnitude 7.0 mainshock was at the time the largest earthquake in California since the 1989 Loma Prieta earthquake. The sequence caused over 350 reported injuries, destroyed over 200 buildings and caused damage to an additional 900 structures mainly in the towns of Petrolia,

Ferndale, Rio Dell, Scotia and Fortuna (Oppenheimer and others, 1993). The two magnitude 6 aftershocks occurred northwest of the mainshock and all three earthquakes occurred within 25 km of each other. Because this earthquake sequence occurred near the southern end of the Cascadia subduction zone the records are important for prediction of ground shaking both in California and in the Pacific Northwest. Prior to these earthquakes the Cascadia subduction zone had exhibited little subduction-related seismic activity, and the mainshock recordings are the first strong-motion accelerograms from a large interplate earthquake.

Landers Sequence: The magnitude 6.1 Joshua Tree earthquake occurred on April 22 under the Little San Bernardino Mountains about 17 km east of Desert Hot Springs and 22 km northeast of Palm Springs and caused light to moderate damage near the epicenter. No primary surface faulting was observed. This earthquake has been considered a pre-shock of the Landers earthquake by Sieh and others (1993) because they consider the two earthquakes related in space and time.

The magnitude 7.3 Landers earthquake occurred 30 km north of the Joshua Tree epicenter on June 28. The mainshock is the largest earthquake to occur in the contiguous United States since 1952 and the largest earthquake with an extensive set of strong motion recordings. Extensive right-lateral strike-slip faulting was observed, with maximum horizontal offset of 6 meters, along faults that trend northwestward across the Mojave Desert for over 70 km (Sieh and others, 1993). Most of the damage and injuries were confined to the desert and mountain towns in the epicentral area.

Approximately 3 hours after the Landers earthquake, the magnitude 6.2 Big Bear earthquake occurred about 35 km west of the Landers epicenter. The epicenter is located in the San Bernardino Mountains, about 11 km southeast of Big Bear Lake and 45 km northeast of San Bernardino. No primary surface faulting was observed. Most of the damage due to this earthquake was confined to the mountain communities in the Big Bear area.

Table I

Earthquake Magnitude and Mechanism

Earthquake Name	Date	Depth	M_w	M_S	M_L	Mechanism
Cape Mendocino	4/25/92	11 km	7.0	7.1	7.0	Thrust
Aftershock No. 1	4/26/92	19 km	6.2	6.6	6.4	Strike-slip
Aftershock No. 2	4/26/92	22 km	6.3	6.6	6.4	Strike-slip
Joshua Tree	4/22/92	12 km	6.1	6.3	6.1	Strike-slip
Landers	6/28/92	9 km	7.3	7.6	6.8	Strike-slip
Big Bear	6/28/92	7 km	6.2	6.6	6.5	Strike-slip

STRONG MOTION DATA

Cape Mendocino Sequence Strong Motion Data: Strong-motion records were recovered from 14 CSMIP stations after the Cape Mendocino earthquakes of April 25-26, 1992. These 14 stations include 10 ground-response stations and 4

extensively-instrumented structures. The 4 structures include 2 buildings, a freeway overpass and a dam. The epicentral distance of the stations ranges from 4 km for the closest (Cape Mendocino) to about 110 km for the farthest (Fort Bragg).

The records recovered from the mainshock have some of the highest accelerations ever recorded. Peak accelerations near 2 g were recorded at the Cape Mendocino station, approximately 4 km southwest of the epicenter on hard sandstone. Figure 1 shows the acceleration, velocity and displacement waveforms in the north-south direction. A peak velocity of 126 cm/sec and a peak displacement near 70 cm (on the vertical component) was calculated. The duration of strong shaking was about 7 seconds at this station. Significant long-period energy was recorded at this site as shown by these waveforms. Figure 2 shows the response spectra from the Cape Mendocino record compared to that of the Taft (1952 Kern County earthquake) and El Centro (1940 Imperial Valley earthquake) stations. The Cape Mendocino spectrum is larger than the other spectrum for all periods shown.

Figure 3 shows horizontal peak ground acceleration from the mainshock compared to the Joyner-Boore attenuation relation (Joyner and Boore, 1988). Clearly, the data do not cluster about the median curve, but lie principally above it. For example, only 3 of the 16 values fall below the median peak acceleration curve.

Figure 4 shows the sensor locations for the Highway 101 Rio Dell overpass and the first 20 seconds of the acceleration waveforms for 5 transverse channels. As shown in the figure, this two-span skewed bridge recorded a transverse acceleration of 1.2 g at the deck level on the west end of the bridge. The corresponding peak acceleration at the east end was 0.69 g. Also, one of the highest accelerations ever recorded on a structure, 1.38 g, occurred on the ground near the west abutment. The duration of strong shaking was about 7 seconds at this station. The largest previous acceleration recorded at this bridge was 0.59 g during the 1982 Rio Dell earthquake.

During the two magnitude 6 aftershocks the largest accelerations recorded by ground-response stations were 0.60 and 0.57 g at Petrolia. The largest horizontal acceleration recorded on a structure was 0.91 g on the Rio Dell overpass structure located 42 km from the epicenter of the first aftershock. The acceleration in the free-field of the bridge was 0.55 g. At a 1-story supermarket in Fortuna 0.18 g horizontal acceleration was recorded at the ground floor and 0.87 g at the roof level in the out-of-plane direction at the top of the wall during the first aftershock. These are the largest accelerations ever recorded at this building. Similar large motions of the roof diaphragm have been recorded at other buildings with stiff walls and flexible diaphragms.

Landers Sequence Strong Motion Data: Strong-motion records were recovered from over 100 CSMIP stations after the magnitude 6.1 Joshua Tree earthquake on April 22. At the two closest CSMIP stations (Desert Hot Springs and Joshua Tree) peak accelerations of 0.22 and 0.32 g were recorded at 17 and 20 km from the epicenter. Duration of strong shaking was about 5 seconds at both stations.

Strong-motion records were recovered from a total of 144 CSMIP stations

after the Landers earthquake. The epicentral distance of the stations ranges from 14 km for the closest (Joshua Tree) to about 215 km for the farthest (Santa Felicia Dam). At these stations, a total of 224 records were obtained of the motion at over 1000 strong-motion sensors. The 144 stations include 88 ground-response stations and 56 extensively-instrumented structures. The 56 structures include 47 buildings, 6 dams and a major freeway interchange. The instrumented buildings included 4 that have been seismically isolated. These buildings are 2, 5, 8 and 9 stories in height and recorded peak accelerations at the foundation level were between 0.04 and 0.11 g. The acceleration response of these seismically isolated buildings was as high as 0.19 g at the roof (see Huang and others (1993) in this Proceedings).

Figure 5 shows horizontal peak ground acceleration from the mainshock compared to the Joyner-Boore (1988) attenuation relation. The peak acceleration values generally lie at or above the median curve and show less attenuation with distance than predicted by this model, especially at longer distances. Figure 6 shows the response spectra from three stations (Yermo, Joshua Tree and Inglewood) that recorded the Landers mainshock compared to response spectra at Taft (1952 Kern County earthquake) and El Centro (1940 Imperial Valley earthquake). The Landers spectra are generally larger than the other spectra, especially at long periods.

The most significant aspect of the records from the Landers earthquake is their long duration, compared to most records that have been obtained in California. For example, Figure 7 shows records from 4 California earthquakes (Landers, Loma Prieta, Big Bear and Whittier) recorded at similar distances (10 to 20 km). The record from the Landers earthquake has duration of strong shaking of about 30 seconds. This duration is 2 to 4 times longer than the duration of the other three records.

Evidence for the propagation of the Landers earthquake northward from the epicenter may be inferred by comparing the acceleration, velocity and displacement waveforms at two stations, Yermo and Joshua Tree (Figure 8). The station at Yermo, 84 km north of the epicenter has a peak acceleration near 0.24 g. The only other CSMIP station with higher peak acceleration is Joshua Tree (0.28 g) located 14 km southeast of the epicenter. Yermo has the largest peak velocity and displacement measured at CSMIP stations. The peak velocity is 50 cm/sec and the peak displacement is larger than 40 cm (1.3 feet). For comparison, the peak values at Joshua Tree are 43 cm/sec and 16 cm.

A peak acceleration of 0.88 g was recorded during the Landers earthquake at a Southern California Edison (SCE) station at Lucerne located 2 km from the fault. The six other SCE stations that recorded the Landers earthquake were located between 31 and 152 km from the fault (Hawkins and others, 1993).

An important set of records was obtained from the I-10/215 freeway overpass southwest of San Bernardino. The overpass instrumented is the connecting structure between I-10 from Los Angeles and I-215 toward San Bernardino. The bridge is a long and curved structure, typical of many in Southern California and similar to some which sustained heavy damage in the 1971 San Fernando earthquake. The bridge, about 2540 feet long and 90 feet high near the center, was recently strengthened by Caltrans and instrumented with 34 sensors by CSMIP. The ground motion near the bridge was 0.09 g. Higher accelerations (0.82 g) were recorded on the bridge deck. The motion at the footing of Bent

8 (channel 24) and at the deck level above Bent 8 (channel 20) are shown in Figure 9. Preliminary interpretation of the many spikes on some of the records indicate relative motion of the decks across the hinges (Malhotra and others, 1993). This is the first significant record from this type of bridge in California.

Four CSMIP stations located in the Los Angeles basin at an epicentral distance of approximately 165 km have peak displacements near 20 cm (8 inches). The peak accelerations at these stations are quite small (7% g and less). Large values of displacement despite the low levels of ground acceleration is a significant aspect of the records in the Los Angeles basin and may have contributed to the damage sustained by structures in the basin.

Strong-motion accelerograms were recorded at 132 CSMIP stations after the Big Bear earthquake. The epicentral distance of the stations ranges from 11 km for the closest (Big Bear Lake) to about 180 km for the farthest (Santa Felicia Dam). At the 132 CSMIP stations that recorded the Big Bear earthquake, a total of 218 records were obtained from over 950 strong-motion sensors. The 132 stations include 79 ground-response stations and 53 extensively-instrumented structures. The instrumented buildings included 4 that have been seismically isolated. The largest ground acceleration recorded by CSMIP ground-response stations was 0.57 g horizontal and 0.21 g vertical at Big Bear Lake (see Figure 7). The largest accelerations recorded on structures were 0.75 g recorded at a concrete tilt-up building and 1.02 g at the San Bernardino - I-10/215 Interchange.

ADDITIONAL STRONG-MOTION DATA

Several agencies in addition to CSMIP have strong-motion instruments in California. The U.S. Geological Survey maintains instruments of its own and of other agencies throughout the state (USGS, 1992a, 1992b). The University of Southern California maintains a network of 80 ground-response stations in southern California. In addition to these stations, smaller groups of stations are maintained by California Institute of Technology, Southern California Edison, Pacific Gas & Electric and other agencies. Finally, many private building owners in the City of Los Angeles have instruments in their buildings, as required by the City code.

ACKNOWLEDGEMENTS

The California Strong Motion Instrumentation Program extends its appreciation to the individuals and organizations which have permitted and cooperated in the installation of seismic strong-motion equipment on their property. CSMIP also extends its appreciation to the members of the Strong Motion Instrumentation Advisory Committee and its subcommittees. Funding for instrumenting the I-10/215 Interchange near San Bernardino was partially provided by the California Department of Transportation. Funding for instrumenting some of the hospitals was provided by the Office of Statewide Health Planning and Development. The authors would also like to recognize the CSMIP technicians for their diligence in installing and maintaining the instruments and recovering the records.

BIBLIOGRAPHY

Cramer, C., T. Cao, P. Fung, F. Su, R. Darragh, and A. Shakal (1992). Comparison of peak values and spectral parameters from CSMIP strong motion records for the M_S 6.9 Petrolia and the M_w 7.4 Landers, Calif. earthquakes with Joyner-Boore attenuation relations (abstract), EOS, Transactions of the American Geophysical Union, v. 73, no. 43 supplement, p. 380.

CSMIP (1992a). Quick Report on CSMIP Strong-Motion Records from the April 22, 1992 Desert Hot Springs, California, Report OSMS 92-03, 14 p.

CSMIP (1992b). Quick Report on CSMIP Strong Motion Records from the Petrolia, California Earthquakes of April 25-26, 1992, Report OSMS 92-04, 27 p.

CSMIP (1992c). Quick Report on CSMIP Strong-Motion Records from the June 28, 1992 Earthquakes near Landers and Big Bear, California, 22 p.

CSMIP (1992d). Second Quick Report on CSMIP Strong-Motion Records from the June 28, 1992 Earthquakes near Landers and Big Bear, California, 10 p.

CSMIP (1992e). Preliminary processed strong-motion data for the Landers earthquake of 28 June 1992, Calif. Div. Mines and Geology, Office of Strong Motion Studies, Report No. OSMS 92-11, 60 p.

Darragh, R., T. Cao, C. Cramer, M. Huang and A. Shakal (1992). Processed CSMIP strong-motion data from the Cape Mendocino/Petrolia earthquake of April 25, 1992: Release No. 1, Calif. Div. Mines and Geology, Office of Strong Motion Studies, Report No. OSMS 92-12, 130 p.

Darragh, R., T. Cao, C. Cramer, F. Su, M. Huang and A. Shakal (1992). Processed strong-motion records from the Landers earthquake of 28 June 1992: Release No. 2, Calif. Div. Mines and Geology, Office of Strong Motion Studies, Report No. OSMS 92-13, 156 p.

Darragh, R., T. Cao, M. Huang and A. Shakal (1993). Processed strong-motion records from the Landers earthquake of 28 June 1992: Release No. 3, Calif. Div. Mines and Geology, Office of Strong Motion Studies, Report No. OSMS 93-01, 104 p.

Joyner, W. B., and D. M. Boore (1988). Measurement, characterization, and prediction of strong ground motion, Proceedings of Earthquake Engineering & Soil Dynamics II GT Div/ASCE, Park City, Utah, June 27-30, 1988, p. 1-60.

Hawkins, H. G., D. K. Ostrom and T. A. Kelly (1993). Comparison of strong motion records, Landers earthquake 28 June 1992, near Lucerne Valley, California (abstract), Seismological Research Letters, v. 64, no. 1, p. 19.

Huang, M., A. Shakal, T. Cao, P. Fung, R. Sherburne, R. Sydnor, P. Malhotra, C. Cramer, F. Su, R. Darragh and J. Wampole (1992). CSMIP strong-motion records from the Big Bear, California earthquake of 28 June 1992, Calif. Div. Mines and Geology, Office of Strong Motion Studies, Report No. OSMS 92-10, 236 p.

Huang, M., P. Malhotra, and A. Shakal (1993). Analysis of records from four base-isolated buildings during the 1992 Landers earthquake, Proceedings of the SMIP93 Seminar on Seismological and Engineering Implications of Recent Strong-Motion Data, Sacramento, California, May 20, 1993, 14 p.

Malhotra, P., M. Huang, and A. Shakal (1993). Interaction at separation joints of a long bridge during 1992 earthquakes in California (abstract), submitted to Fifth U.S. National Conference on Earthquake Engineering.

Oppenheimer, D., G. Beroza, G. Carver, L. Dengler, J. Eaton, L. Gee, F. Gonzalez, A. Jayko, W. H. Li, M. Lisowski, M. Magee, G. Marshall, M. Murray, R. McPherson, B. Romanowicz, K. Satake, R. Simpson, P. Somerville, R. Stein, D. Valentine (1993). The Cape Mendocino, California earthquake sequence of April, 1992: Subduction at the triple junction, Science (in press).

Sieh, K., L. Jones, E. Hauksson, K. Hudnut, D. Eberhart-Phillips, T. Heaton, S. Hough, K. Hutton, H. Kanamori, A. Lilje, S. Lindvall, S. McGill, J. Mori, C. Rubin, J. Spotila, J. Stock, H. Thio, J. Treiman, B. Wernicke and J. Zachariasen (1993). Near-field investigations of the Landers earthquake sequence April to July 1992, Science, vol. 260, p. 171-176.

Shakal, A., R. Darragh, M. Huang, T. Cao, R. Sherburne, R. Sydnor, P. Malhotra, C. Cramer, J. Wampole, P. Fung and C. Petersen (1992). CSMIP strong-motion records from the Petrolia, California earthquakes of April 25-26, 1992, Calif. Div. Mines and Geology, Report No. OSMS 92-05, 74 p.

Shakal, A., M. Huang, T. Cao, R. Sherburne, R. Sydnor, P. Fung, P. Malhotra, C. Cramer, F. Su, R. Darragh and J. Wampole (1992). CSMIP strong-motion records from the Landers, California earthquake of 28 June 1992, Calif. Div. Mines and Geology, Office of Strong Motion Studies, Report No. OSMS 92-09, 330 p.

USGS (1992a). U. S. Geological Survey Strong-Motion Records from the Northern California (Petrolia) earthquake of April 25, 1992. 7 p.

USGS (1992b). Selected Accelerograms from U.S. Geological Survey Stations that Recorded the Landers and Big Bear Earthquakes of June 28, 1992, 13 p.

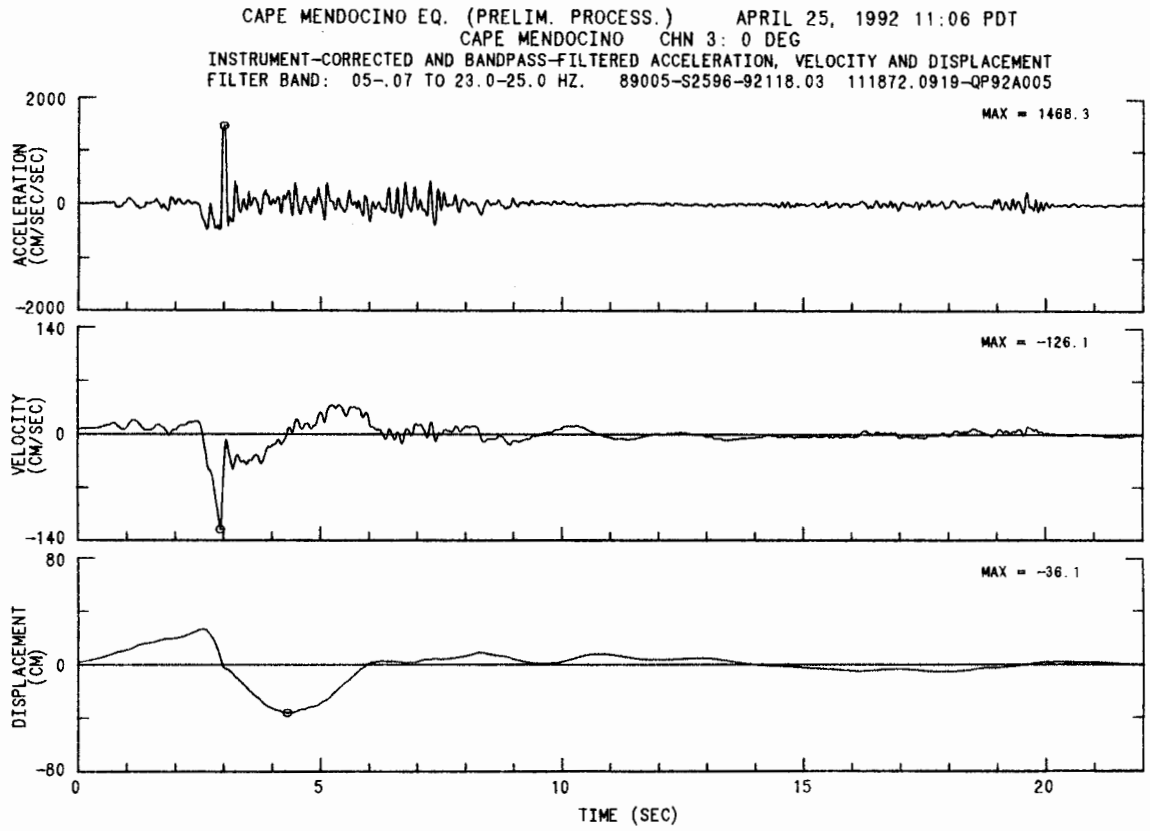

Figure 1: Acceleration, velocity and displacement time-histories (instrument-corrected and band-pass filtered) for the north-south component at the Cape Mendocino station.

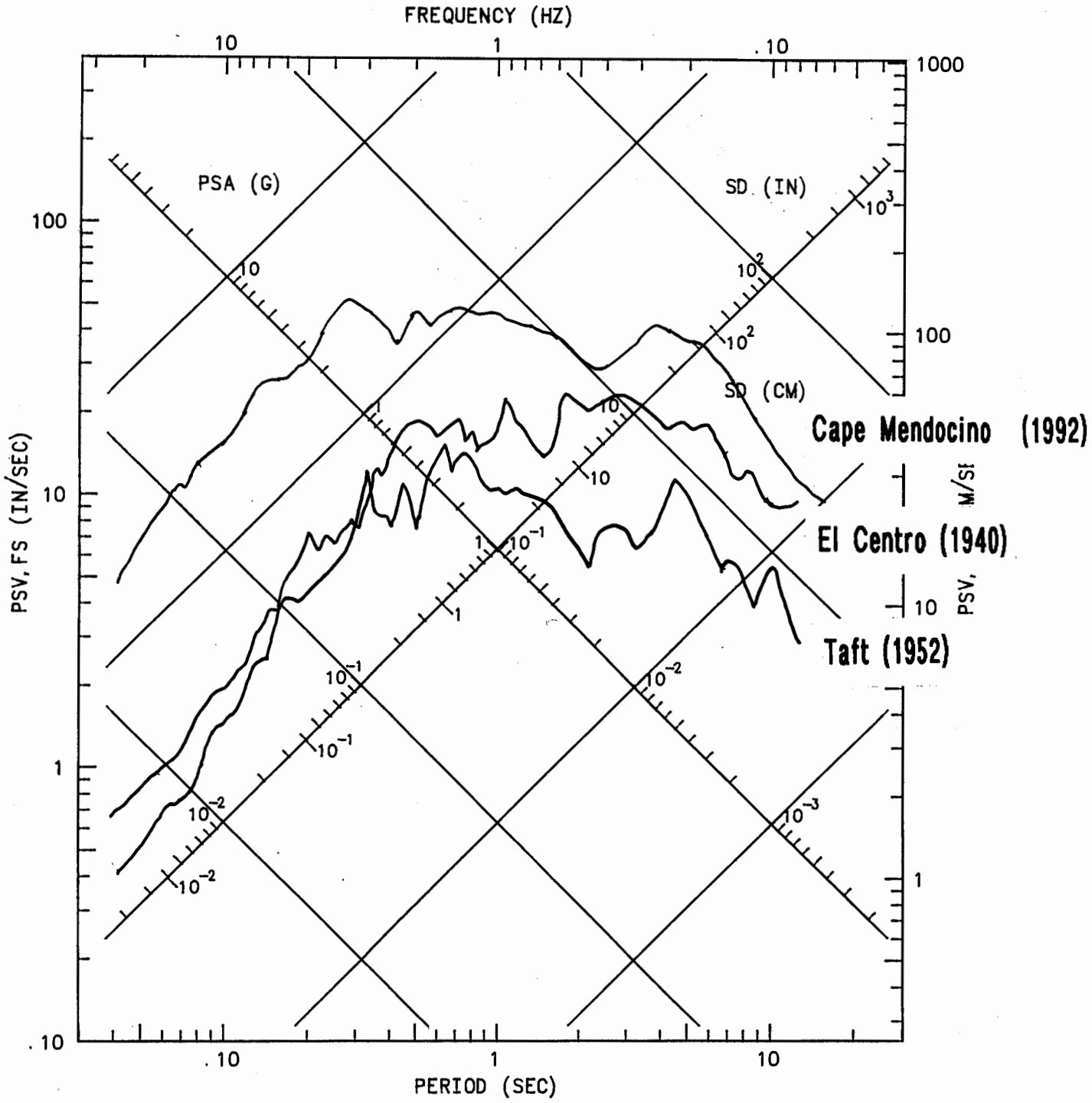

Figure 2: 5% damped response spectra from the Cape Mendocino station (1992 Cape Mendocino mainshock), Taft (1952 Kern County earthquake) and El Centro (1940 Imperial Valley earthquake).

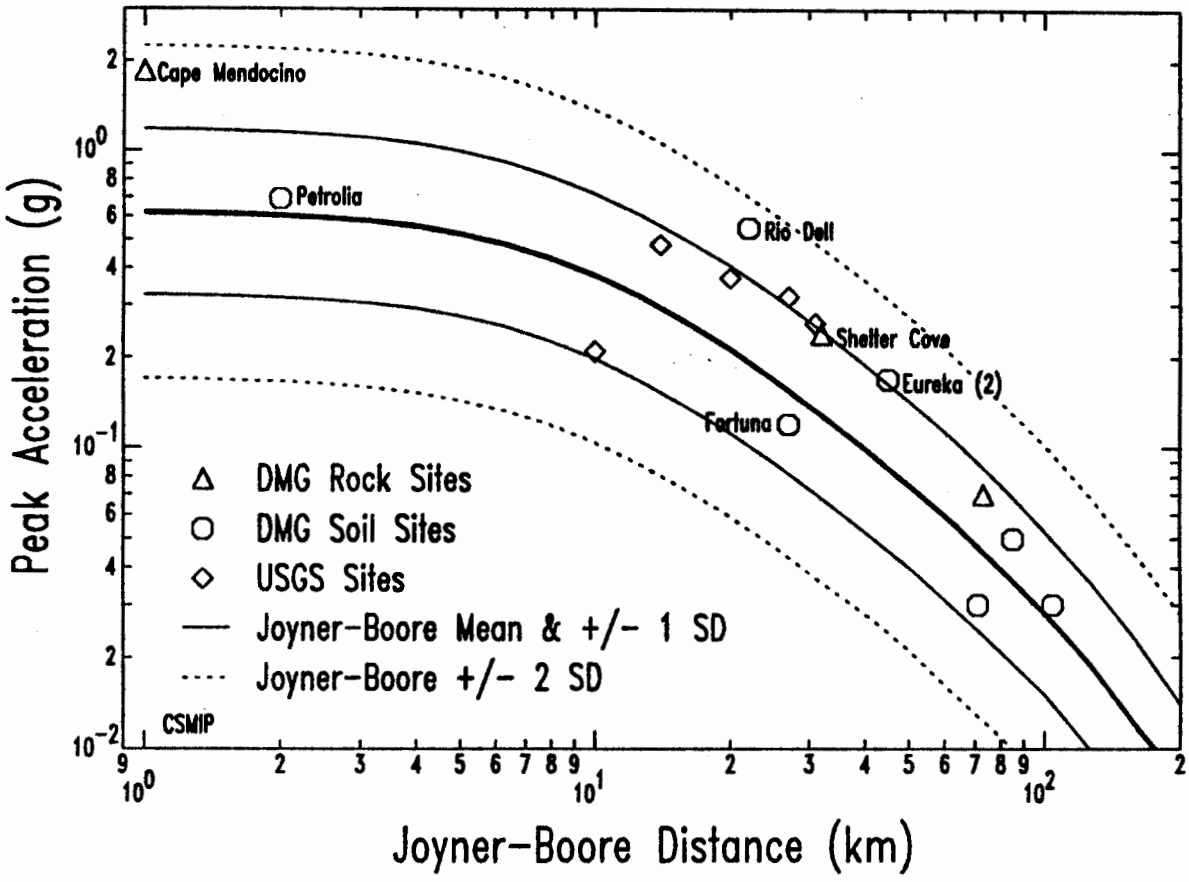

Figure 3: Peak horizontal acceleration versus distance for the Cape Mendocino mainshock. Distance measured from the surface projection of the aftershock zone to the station as defined by Joyner and Boore (1988). Largest of the two horizontal components is plotted. Bold solid curve is the median curve of Joyner and Boore (1988) for a magnitude 7.0 earthquake. Light solid lines indicate $\pm$ 1 standard deviation. Dashed lines indicate $\pm$ 2 standard deviations. Triangles indicate CSMIP stations located on rock; hexagons, on alluvium; diamonds indicate USGS stations.

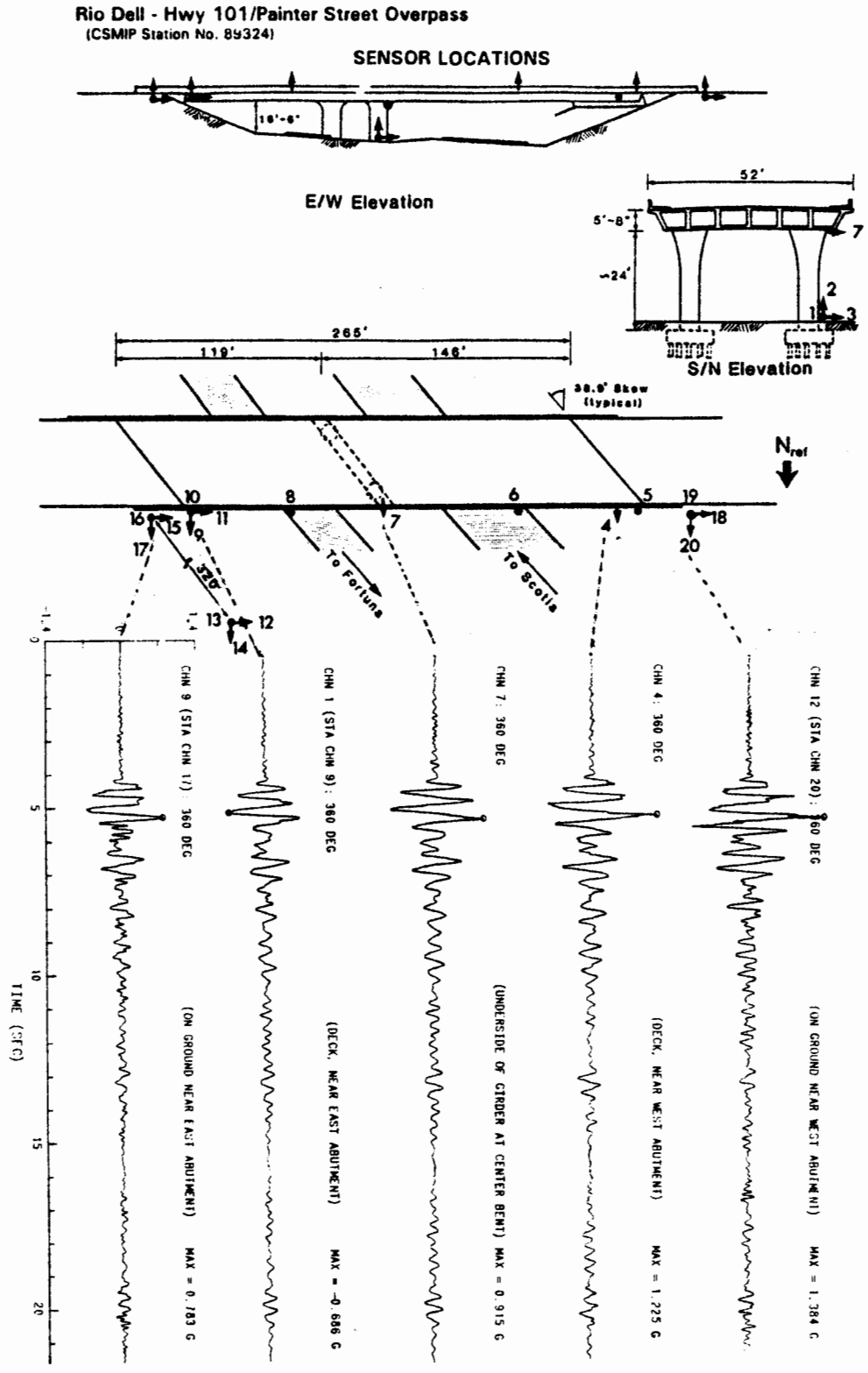

Figure 4: Sensor locations for the Rio Dell - Hwy 101/Painter Street Overpass. Accelerograms at five locations show the transverse motion of different parts of the bridge structure during the 1992 Cape Mendocino mainshock.

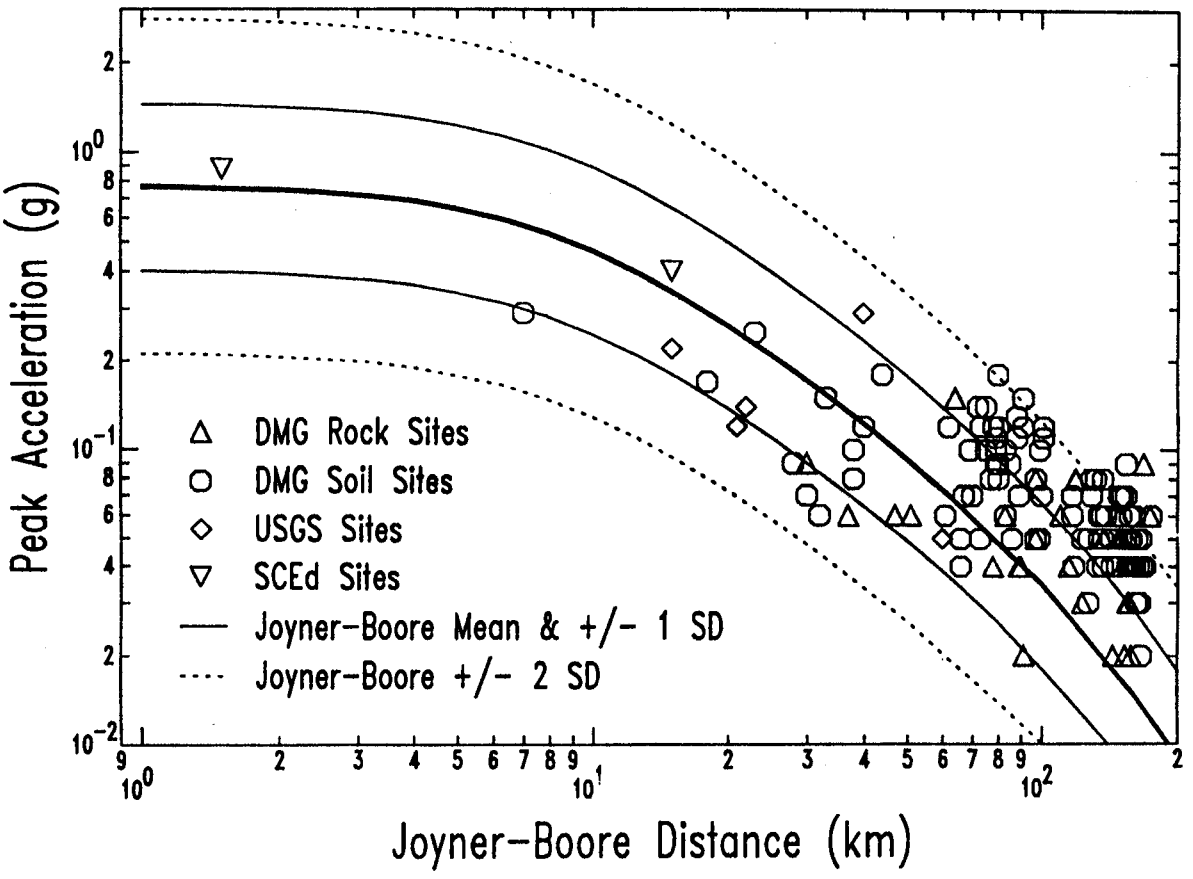

Figure 5: Peak horizontal acceleration versus distance for the Landers earthquake. Distance measured from the surface rupture to the station as defined by Joyner and Boore, 1988. Largest of the two horizontal components is plotted. Bold solid curve is the median curve of Joyner and Boore (1988) for a magnitude 7.3 earthquake. Light solid lines indicate $\pm$ 1 standard deviation. Dashed lines indicate $\pm$ 2 standard deviations. Triangles indicate CSMIP stations located on rock; hexagons, on alluvium; diamonds indicate USGS stations; inverted triangles indicate Southern California Edison stations.

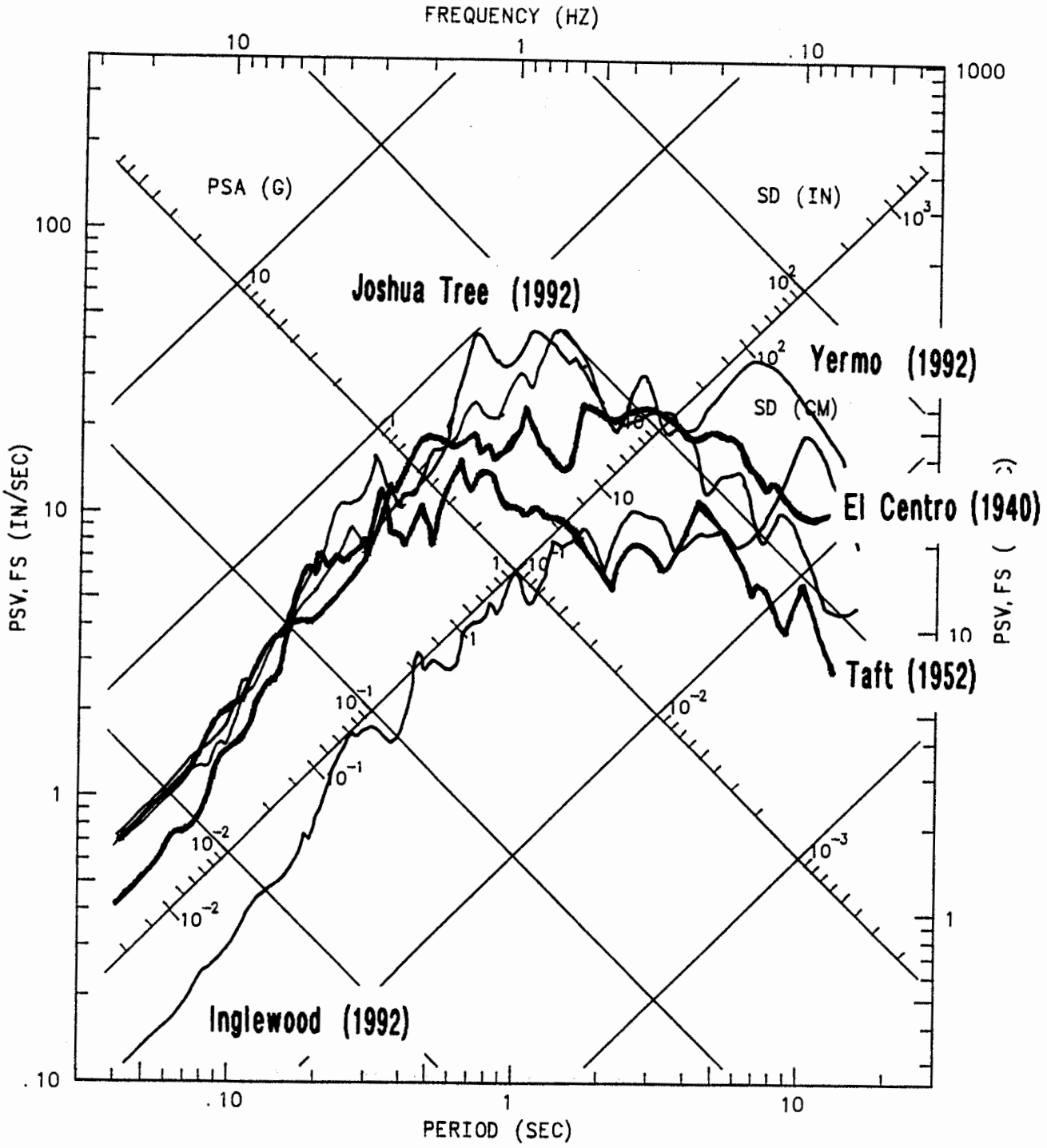

Figure 6: The 5% damped response spectra from the Joshua Tree, Yermo and Inglewood stations (1992 Landers earthquake) are shown by thin lines. The 5% damped response spectra from Taft (1952 Kern County earthquake) and El Centro (1940 Imperial Valley earthquake) are shown by thick lines.

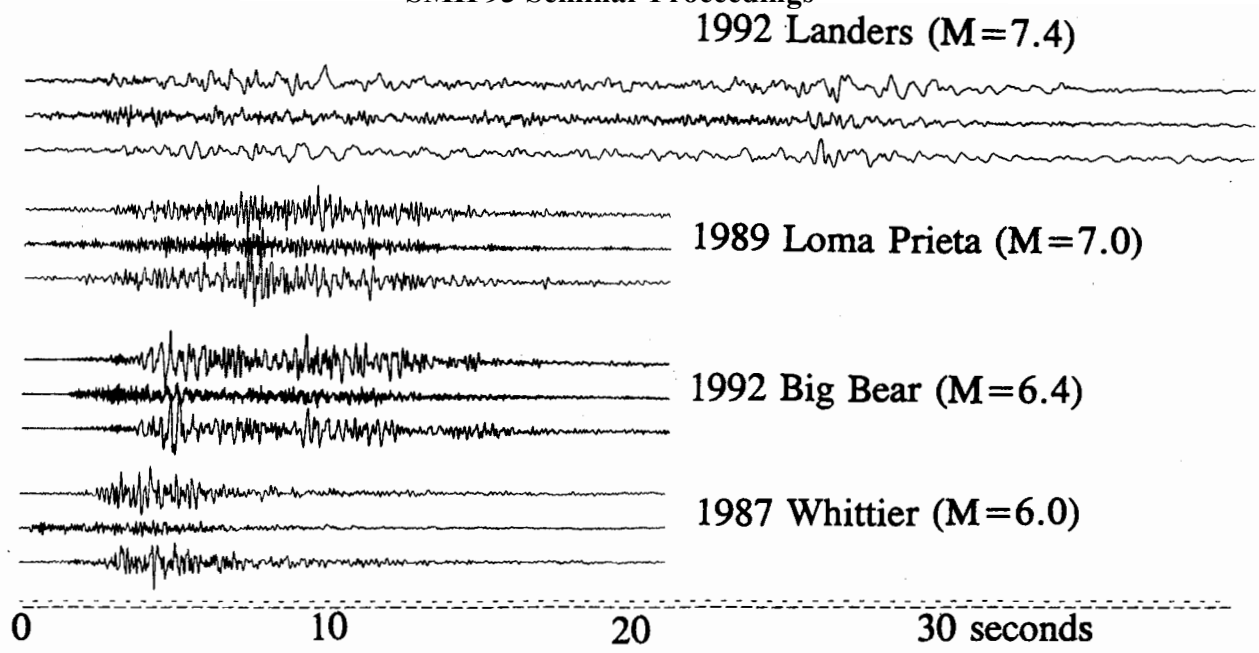

Figure 7: Duration of strong ground shaking. Accelerograms recorded for 4 different magnitude earthquakes at stations with similar distances (10 - 20 km).

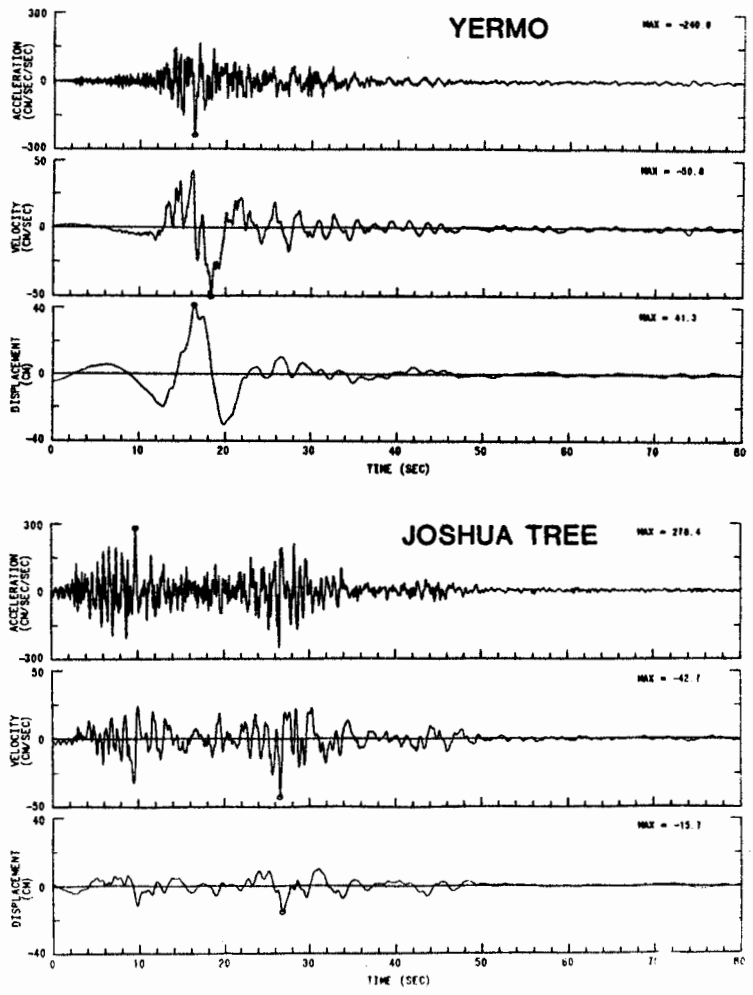

Figure 8: Comparison of Yermo and Joshua Tree acceleration, velocity and displacement waveforms (instrument-corrected and band-pass filtered) from the Landers earthquake.

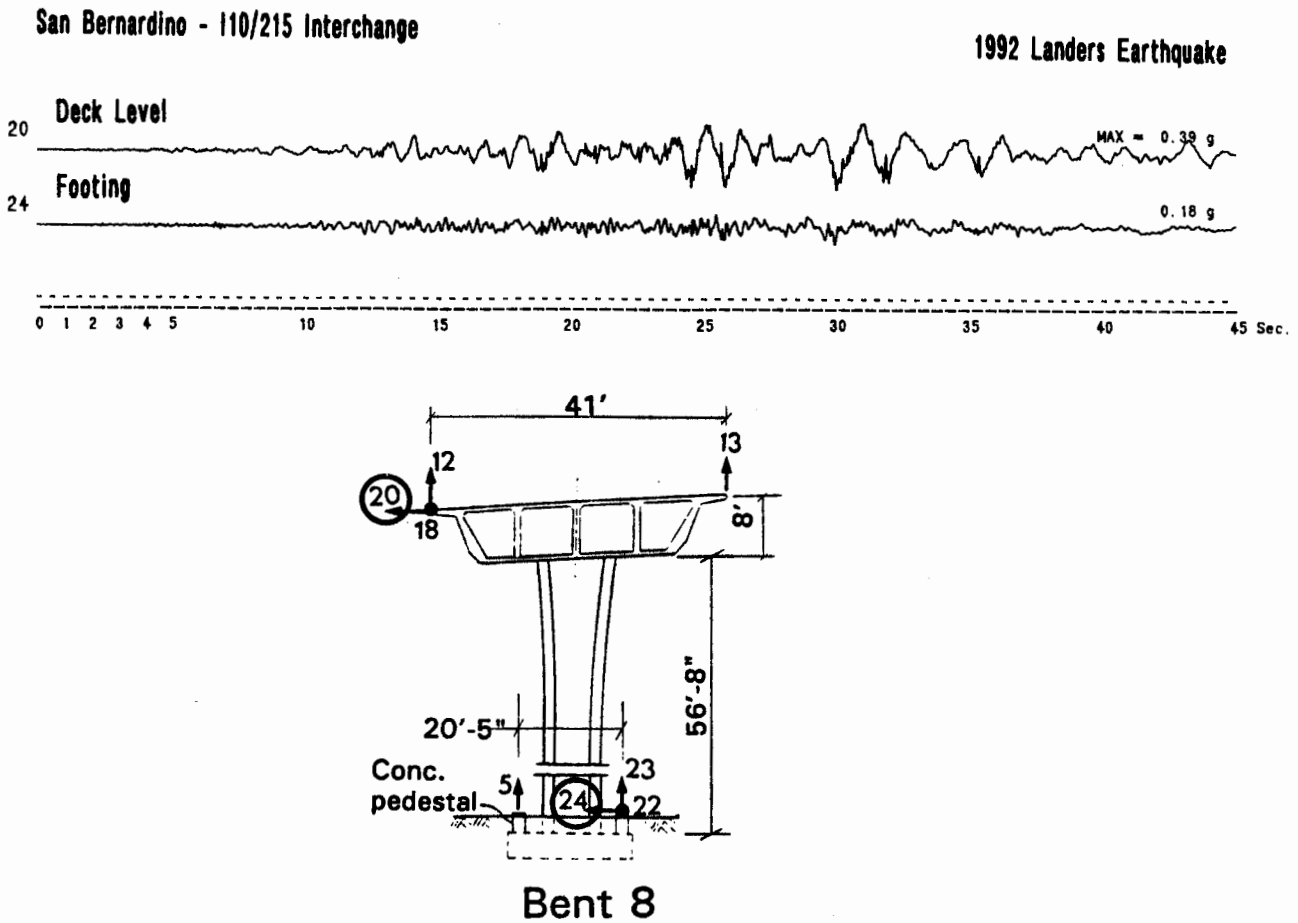

Figure 9: Two accelerograms recorded at the I-10/215 Interchange near San Bernardino. The channels show the motion at the footing of Bent 8 (channel 24) and at the deck level above Bent 8 (channel 20). A total of 34 acceleration channels are recorded at this structure.

Empirical Prediction of Strong Ground Motion for Subduction Zone Earthquakes

Robert R. Youngs
Geomatrix Consultants, San Francisco, California

Presented are the results of recent analyses of strong ground motion data from subduction zone earthquakes. Several new sets of attenuation relationships are presented for estimating peak horizontal accelerations and response spectral ordinates. These relationships were developed from regression analysis of recorded data augmented by numerical ground motion simulations. Attenuation relationships were developed for rock, shallow, and deep soil site classifications for both interface (plate boundary) and intraslab (Benioff) earthquakes.

The regression analyses were conducted using a *random effects* regression model, which provides an equivalent method to the two-stage regression technique. The random effects model also allows for explicit evaluation of the event-to-event variability and within event variability, providing a more complete model for the covariance matrix of the data. Numerical simulations of strong ground motion were performed to aid in interpreting the empirical data in terms of soil/rock amplifications in the near field, rate of attenuation with distance, and scaling to magnitudes greater than M 8. The numerical simulations were conducted using an extended source formulation of the band-limited-white-noise/random-vibration-theory model. Soil site motions were simulated by incorporation of one dimensional wave propagation into the model, with the soil properties modeled by the equivalent linear method.

The results of both the regression analyses and the numerical modeling studies show a lower rate of attenuation with distance for large subduction zone earthquakes compared to shallow crustal earthquakes. These results confirm results reported by many previous investigators. The shape of the attenuation curve in the distance range of 50 to 200 km is strongly magnitude dependent, possibly reflecting the effects of the great extent of the source for the largest subduction zone earthquakes.

Both the empirical data and the numerical simulations show significantly higher motions on soil than on rock sites at large distances from the source, as has been reported by previous investigators. However, as one approaches the source, the numerical simulations indicate that soil and rock ground motion levels converge, similar to near field observations from crustal earthquakes, while the empirical data suggest significant differences. Several alternative formulations for the attenuation model in the near field were applied to the data. The results of the analyses indicate that the limited near field empirical data do not provide a definitive choice for the form of near field ground motion attenuation relationships on rock.

Differences between interface and intraslab earthquakes have been attributed to either basic source differences between the two types of earthquakes or to the effect of source depth. The results of the regression analyses indicate that both effects are present in the data at a statistically significant level.

SIMULATION OF THE RECORDED RESPONSE OF UNREINFORCED (URM) INFILL BUILDINGS

J. Kariotis, T.J. Guh, G.C. Hart, J.A. Hill and N.F.G. Youssef

ABSTRACT

The Strong Motion Instrumentation Program of the California Department of Mines and Geology (CSMIP) has obtained records of the response of four buildings with unreinforced masonry (URM) infills. The response was to the Landers, Upland and Sierra Madre earthquakes. The objective of this research was to replicate by computer analysis the CSMIP records.

Three dimensional elastic computer models were prepared from data obtained from the original construction documents. The URM infills were modeled as diagonal braces in the frame. The stiffness properties of the infills were determined by a nonlinear finite element analysis.

INTRODUCTION

The Strong Instrumentation Program of the California Department of Mines and Geology (CSMIP) has instrumented buildings with unreinforced masonry infills. Four of these buildings were shaken by the Landers earthquake. Two of these buildings had been shaken by near small magnitude earthquakes, the 1990 Upland and the 1991 Sierra Madre earthquakes. These buildings are:

- A six-story commercial building in Pasadena (CSMIP Station No. 24541) that was constructed in 1906. It has a steel frame infilled with unreinforced brick masonry. The maximum acceleration at the basement level was 0.195g during the Sierra Madre earthquake and 0.04 g during the Landers earthquake.
- A six-story commercial building in Pomona (CSMIP Station No. 23544) that was constructed in 1923. It has a reinforced concrete frame with unreinforced brick masonry infills. The maximum acceleration at the basement level was 0.13g for the 1990 Upland earthquake and 0.07g for the 1992 Landers earthquake.
- A nine-story office building in Los Angeles (CSMIP Station No. 24579) that is L-shaped in plan. It was constructed in 1923 and has a reinforced concrete frame with unreinforced masonry infills. The maximum acceleration at the basement level was 0.05g during the Landers earthquake.
- A twelve-story commercial/office building in Los Angeles (CSMIP Station No. 24581) that was constructed in 1925. It has a concrete encased steel frame and unreinforced brick masonry infills. The maximum acceleration at the basement floor level was 0.04 g during the Landers earthquake.

STATEMENT OF THE PROBLEM

The data recorded by CSMIP was the response of buildings that have very significant vertical and plan irregularities. The lateral resistance was provided by the frames and the unreinforced masonry that is infilled into the frame. The masonry is multi-wythe brick laid in lime, Portland cement, and mortar. Cast stone, terra cotta and brick veneer wythes are a part of the

masonry infills. The material properties of the masonry were estimated by comparison with masonry that had been tested by the flat jack method.

The problem is to simulate the recorded response of these buildings to the motions recorded at the lowest level. The existing building is a complex assembly of materials with nonlinear behavior. The mechanical properties of the structural materials must be estimated and effects of systems such as stairs that are continuous between floors and interior partitioning, cannot be quantified. The problem is to reduce these complex buildings to a simple linear elastic model that has similar stiffness and damping characteristics.

GOAL OF THE RESEARCH

The goal of this research is to provide information for the development of standards and ordinances for earthquake hazard reduction in this class of building. The research will provide information of how to model the frame, how to include the effect of the infill on the frame and how to account for stiffness degradation the frame-infill system. Development of a procedure for conversion of the infill, in any configuration or shape, into an equivalent diagonal brace is the goal. Without procedures for the estimation of effective stiffness of these structural systems, prescription of drift limits and calculation of drift is not possible.

RESEARCH PLAN

The existing structural systems, the mass of the building and the geometry of the system was determined by review of the existing drawings. The weight and center of gravity of each story level above the base of the building was estimated. Elevations of each column-beam line and sketches of the infilled bays were prepared. The size and location of all openings within the infilled bays were noted on the elevations.

This data was developed for each of the four buildings. Concurrently, the recorded data for each building was examined and analyzed. The time-displacement histories obtained from the CSMIP records were differenced to determine the average interstory deformation caused by the ground shaking. This interstory displacement was used in the development of the equivalent strut. The records of instruments located on a common floor level that recorded parallel motions were differenced. This was converted to rotation by dividing the difference by the distance between instruments. This data was used to isolate rotational modes and to confirm that the floor is rigid in its plane. The frequency content of instrumental records was analyzed by preparation of damped spectra and by Fourier analysis. After this raw data was accumulated and analyzed, the buildings were modeled by the SAP 90 linear-elastic three-dimensional program.

The exterior elevations showing openings in the infills of the buildings were used to determine "typical" infill patterns. The parameters for establishing "typical" infills were:

- Moment of inertia and area of the confining frame members.
- Story height and length of the infilled bay.
- Location of the openings relative to the frame and number and size of the openings.

The initial compressive modulus of elasticity, the tensile cracking stress, the strain associated with peak compressive stress and the peak compressive stress were chosen by experience and/or visual evaluation of the exposed masonry. The force-displacement relationship for each of the "typical" infill panels was calculated by use of a nonlinear finite element program developed by Robert D. Ewing, Ahmad El-Mustapha and John Kariotis (FEM Version 1.08). An effective stiffness of a pair of diagonal braces within the bay of the infilled frame was substituted for the unreinforced masonry. This effective stiffness was determined by the following process:

- For each typical infill bay configuration, the confining frame and the masonry was analyzed by the nonlinear FEM.
- The force-displacement relationship of the frame and its infill was determined by incrementally displacing the assembly. This analysis determines the stiffness degradation of the system due to cracking and strain in the frame and infill.
- The confining frame was analyzed without any infill.
- The force-displacement relationships of the infilled frame and the frame alone was differenced.
- The area and modulus of elasticity of the equivalent diagonal braces was calculated to provide an effective system stiffness at the story displacement as determined by evaluation of the CSMIP displacement data.

The process of obtaining a best-fit computer replication was an iterative process. The viscous damping used in the linear-elastic model was established using the best available data. The computed periods of the linear-elastic model were compared to estimated periods extracted from the CSMIP data. Rotational periods for the SAP model and for the CSMIP data were compared. The parameters that were modified to improve the fit were the effective stiffness of the frame members, the effective stiffness of the diagonal struts that represent the infills and the percent of critical damping. These parameters are variables as the materials properties of the concrete frames, the stiffness of the beam-column connections of the steel frames and the material properties of infills are estimated, not quantified by physical testing.

ANALYSIS

The data available to the researchers consisted of the building plans, plans and elevations showing the location of all instruments, and the processed records of each of the instruments. There were conflicts between the existing construction of CSMIP Station No. 23544 in Pomona as shown on the original construction documents and observations of the exterior walls. The light well on the west begins at the second floor level rather than at the mezzanine level as shown on the drawings. There is a conflict as to the materials of the frame that extends from the main floor to the second floor level at the south end. The original drawings show that these columns are reinforced concrete. A supplemental drawing shows a structural steel girder at the second floor level supported by steel columns encased in concrete. Additions have been made to CSMIP Station No. 24541 in Pasadena. These additions tie the two wings of the U-shape together at all level.

The CSMIP Station Nos. 24579 and 23544 have reinforced concrete frames. Station No. 23455 has a severe plan irregularity below the second floor level and a lesser degree of plan irregularity from the second floor to the roof level. A mass irregularity is at the roof level. The lateral resistance at the east and

south is provided by the concrete frame and minimal infills. The percentage of the gross moment of inertia of the columns at this level that should be used as effective stiffness was investigated. Station No. 24579 is an L-shaped building that has a single story garage structure constructed in the portion of the property not occupied by the nine-story building. Reinforced concrete walls separate the occupancies. These reinforced concrete infills were analyzed by methods identical to those used for unreinforced masonry infills. The effect of changing the modulus of elasticity of the concrete frame independent from changing the effective area of the masonry strut was investigated.

The CSMIP Station No. 24541 and 24581 have structural steel frames and multi-wythe brick masonry infills. Station No. 24541 has a severe plan and stiffness irregularity below the second floor. The south and east street fronts have only frames to resist lateral displacements. The west wall below the second floor is infilled with a small window in each bay. The north end is highly perforated with openings. Above the second floor the infilled walls at the perimeter of the light well add stiffness, especially in the north-south direction. The exterior walls have more symmetry in plan above the second floor except that the east and south walls are thicker. This moves the probable rotational center of the building above the second floor in the opposite direction from the probable location below the second floor. Station No. 24581 is nearly symmetrical in plan in the north-south direction. A plan irregularity exists in the east-west direction. The floor beams are encased in concrete. The columns of both buildings are encased in brick or clay tile. The floor beams in Station No. 24541 support a clay tile arch system topped with an unreinforced concrete slab.

The infill within the steel or reinforced concrete frame resists shear distortion of the frame. Experimental testing of solid infills have shown that the behavior of the infill can be represented by a compression-only strut extending from the upper to lower corners of the bay of the frame. Experimental testing of infills with openings has shown that the presence of openings changes the effective stiffness of the infill. The effect of the infill with openings was represented by pinned-end struts placed diagonally in the frame for all opening configurations. The area in this diagonal was determined by the nonlinear finite element analysis. The nonlinear finite element model must be programmed with materials behavior and this materials behavior should be determined by physical testing. The materials properties needed for the nonlinear analysis of an infill are:

- Tensile cracking strain. This property is assumed to be isotropic.
- Initial modulus of compression.
- Strain at peak compressive stress. This should be the strain caused by cyclic loading in compression.
- Peak compressive stress.
- Mechanical and physical properties of the confining frame if structural steel.
- Properties of the concrete such as described for the masonry if the confining frame is reinforced concrete.
- Assumption of a tension stiffening model for the reinforced concrete elements.

The choice of element size used in the nonlinear analysis is critical. Small elements must be used in critical stress and strain zones adjacent to the confining frame. The reinforcement in a reinforced concrete frame may be a smeared model, that is the quantity of reinforcement is uniformly distributed

over the gross area. The steel member may be represented by flange and web or by an appropriately sized rectangle. The nonlinear analysis of infilled frames is a two-part analysis. The frame is first analyzed without infills. The second analysis is of the frame and the masonry infill. The force-displacement plot of the monotonic loading is differenced and used as the effective stiffness of the diagonal members that represent the infill. In these analyses, the relative displacement at each story level has been estimated by use of the CSMIP displacement data. This story displacement is used in conjunction with the FEM analysis to determine a secant stiffness of the system. This stiffness is assigned to a pair of struts of elastic material that are identical to that material used for the beams and columns. These analyses initially did not analyze the steel frames without infill. The area of the diagonal members was determined directly from the nonlinear analysis of the masonry and the confining steel frame. However, the dynamic analysis of CSMIP Station No. 24581 found that the stiffness of the steel frame must be deducted from the results of the nonlinear FEM analysis.

All beams that frame into the building columns were included in the model. All beam-column joints were considered fixed. This assumption was used for the structural steel systems regardless of the detailed connection. The analyses of CSMIP Station No. 24581 found that the stiffness of the steel beams in the frame must be adjusted to less than 100% to account for the flexibility of the beam-column connection. The diagonal members were given pinned-ends to eliminate any contribution to flexural stiffness. Eighty percent of the stiffness determined from the FEM analysis was used as the initial elastic stiffness. This was chosen to estimate the stiffness on reloading to a stabilized force-displacement envelope. The base of the building was taken as the top of the first floor. This assumption was made as reinforced concrete perimeter walls are below this level. All columns were considered fixed at this level. This assumption and the assumption of a fixed base building, that is no rotation of the building on the supporting soils, increased the effective stiffness of the computer model of the building over that of the existing building. There are three critical unknowns as to the dynamic response of these buildings. These are:

- Translational stiffness on the x and y axes.
- Rotational stiffness at levels of plan irregularity.
- Damping that occurred during the recorded time.

Matching of the CSMIP time-displacement records would require that all three of these critical unknowns be calculable. The translation and torsional stiffness was calculated for the computer model using "typical" infilled bays. The damping force used in the linear-elastic model was a viscous damper that functions full time during the time-history analysis. The percentage of critical damping is calculated for the structural stiffness of each mode. The dynamic damping force is related to the response velocity. The actual damping is hysteretic and does not have a damping force acting opposite to the loading force on a loading cycle. The real damping is due to nonlinear cyclic distortion of the masonry infill. The damping ratio used in these analyses was limited to five percent of critical damping.

The data recorded in the building was the response of a building founded on soils at a story height below the base elevation that was used in the linear-elastic model. The added story height and flexibility of the soils increased the recorded building period over that calculated by the linear-elastic model. It is probable that the top displacement may be unchanged by the increase in period. The basement spectra at the Pasadena and Pomona sites, as shown on tripartite

plots, has a near constant displacement (SD) branch for periods greater than about 1.5 seconds . The frequency of the rotational modes should be less affected by the added story height and soil flexibility than translational modes. All parameters that affect displacement and modal frequencies were subject to modification. However, the frequencies calculated by the SAP model should be less than that deduced from the CSMIP data.

RESULTS OF THE ELASTIC ANALYSES
CSMIP STATION NO. 23544, LANDERS EARTHQUAKE

A damping ratio of 2% of critical was used. The effective stiffness of the diagonal members was 100% of that calculated by the FEM analysis. The effective stiffness of the beams was taken as 70% of that calculated using the concrete section. Sixty percent of the stiffness of the concrete columns above the second floor and 35% of the stiffness of the concrete columns below the second floor was used to estimate the reduction in stiffness due to cracking of the concrete. A comparison of the relative displacements recorded and calculated in given in Table 4.1. The values from the CSMIP data and calculated by SAP have very good correlation in peak value. The comparison is plotted in time in Figures 1 and 2. The channels that recorded translational and rotational modes show that the SAP model over predicts the displacement in the beginning of the shaking but has better correlation from 25 seconds to 45 seconds.

CSMIP STATION NO. 23544, UPLAND EARTHQUAKE

The Upland earthquake preceded the Landers earthquake. The ground motion recorded at the base of the building during the Upland earthquake was used to excite the SAP model correlated to the Landers data. The north wall in the mezzanine floor level was damaged by the Upland earthquake. A comparison of the relative displacements recorded and calculated is given in Table 4-2. A better correlation is made with peak values than with the plots of displacement-time shown in Figures 3 and 4.

CSMIP STATION NO. 24541, LANDERS EQ.

This building has one significant translational line of resistance below the second floor. All modes with significant mass coupling are torsional. The torsional stiffness above the second floor greatly exceeds the torsional stiffness below the second floor. The stiffness of the infill panels was taken directly from the FEM analyses. No reduction in stiffness of the infill due to cyclic loading was taken. The stiffness of the structural steel frame was not deducted from the infilled system stiffness. The material properties used to model the masonry were identical to that used for the other three buildings. It is possible that the estimated materials properties exceeds those that would be determined by testing. The SAP model generally over estimated the dynamic displacement at the second floor level and under estimated the displacements at the roof. Five percent damping was used for all nodes. Six modes of response were used in the SAP model. The relative displacements shown in Table No. 4-3 have a reasonable agreement. The displacement-time record shown in Figures 5 and 6 are out of phase. The difference appears to be related to the frequency of rotational modes.

CSMIP STATION NO. 24541, SIERRA MADRE EQ.

The comparison of measured and calculated displacements is shown in Table No. 4-4. The stiffness model used for these predictions is the same as used for predicting the displacements caused by the Landers earthquake. The quality of the predictions when plotted in time vs. displacement, Figure 7 and 8, are better in phase relationship.

CSMIP STATION NO. 24579, LANDERS EQ.

The comparison of measured and calculated displacements is shown in Table No. 5. The time-history analyses used six modes with 3% of critical damping for the first 3 modes and 5% of critical damping for the nest 3 modes. The stiffness used for diagonals was 70% of the FEM results and the stiffness of the concrete frame was taken as 85% of the gross section stiffness. The plots of the time-displacements shown in Figures 9 and 10 show that the torsional response recorded in Figure 10 is out-of-phase with the calculated response at the roof level. The torsional stiffness is provided by tall slender frames at the north and west. The response shown in Figure 9 has less coupling with torsion.

CSMIP STATION NO. 24581, LANDERS EQ.

The comparison of measured and calculated displacements is shown in Table 6. The time-history analyses used six modes with 3% of critical damping for the first 3 modes and 5% for the remainder. The preliminary analyses found that the stiffness of the steel frame must be deducted from the stiffness of the infilled system. Figure 11 shows the response of the building in the longitudinal direction. The recorded response shows that the higher modes are not included in the SAP model. The response at the 12th floor level is a better correlation of recorded an calculated response. Figure No. 12 is the response of the building at an end wall in the transverse direction. The comparison at the 12th floor level show the difference in frequency between the building and the SAP model.

CONCLUSION

The elastic three-dimensional analyses successfully predicted the maximum values os the relative displacement of four buildings with URM infills. The comparative time-histories shows that the technical limitations of the elastic model to replicate nonlinear behavior limits the matching of displacement records to a small segment of time. Variables used to improve the fit of the calculated data to the recorded data included damping, reduction of the stiffness of concrete frames from uncracked stiffness, reduction of the stiffness of the equivalent diagonal braces from that determined by the nonlinear finite element analysis and reduction of the stiffness of beams in a steel frame due to flexibility of the beam-column connection. There is technical substantiation for the values used in these studies. Additional research is needed to establish most probable values of element stiffness but the methodology used in this research has been shown to be adequate.

TABLE NO. 1
COMPARISON OF DISPLACEMENTS FOR STATION NO. 23544, LANDERS EQ.

DIRECTION	FLOOR & LOCATION	CHANNEL	CSMIP DATA MAX. INCHES	SAP DATA MAX. INCHES
N-S	Mid 2nd Fl.	5	0.36	0.36
E-W	S. 2nd Fl.	9	1.33	1.38
E-W	N. 2nd Fl.	10	0.76	0.68
N-S	Mid Roof	2	0.59	0.61
E-W	S. Roof	7	1.86	2.00
E-W	N. Roof	8	1.47	1.32
N-S	W. Roof	3	0.37	0.42
N-S	W. Roof	4	0.36	0.42

TABLE NO. 2
COMPARISON OF DISPLACEMENTS FOR STATION NO. 23544, UPLAND EQ.

DIRECTION	FLOOR & LOCATION	CHANNEL	CSMIP DATA MAX. INCHES	SAP DATA MAX. INCHES
N-S	Mid 2nd Fl.	5	0.63	0.56
E-W	S. 2nd Fl.	9	1.28	1.52
E-W	N. 2nd Fl.	10	0.95	1.17
N-S	Mid Roof	2	1.09	1.05
E-W	S. Roof	7	1.83	2.05
E-W	N. Roof	8	1.90	2.08
N-S	W. Roof	3	0.68	0.71
N-S	W. Roof	4	0.70	0.71

TABLE NO. 3
COMPARISON OF DISPLACEMENTS FOR STATION NO. 24541, LANDERS EQ.

DIRECTION	FLOOR & LOCATION	CHANNEL	CSMIP DATA MAX. INCHES	SAP DATA MAX. INCHES
N-S	W. 2nd Fl.	1	0.24	0.26
N-S	E. 2nd Fl.	2	0.90	1.34
E-W	N. 2nd Fl.	11	0.80	1.05
E-W	S. 2nd Fl.	12	0.75	0.85
N-S	W. Roof	3	1.40	1.06
N-S	E. Roof	4	2.00	1.97
E-W	N.W. Roof	5	2.50	2.00
E-W	N.E. Roof	6	2.50	2.00
E-W	Mid Roof	7	2.02	1.57
E-W	S. Roof	8	1.35	1.35

TABLE NO. 4
COMPARISON OF DISPLACEMENTS FOR STATION NO. 24541, SIERRA MADRE EQ.

DIRECTION	FLOOR & LOCATION	CHANNEL	CSMIP DATA MAX. INCHES	SAP DATA MAX. INCHES
N-S	W. 2nd Fl.	1	0.20	0.20
N-S	E. 2nd Fl.	2	0.90	0.86
E-W	N. 2nd Fl.	4	0.50	0.75
E-W	S. 2nd Fl.	12	0.50	0.60
N-S	W. Roof	3	1.60	0.84
N-S	E. Roof	4	1.60	1.15
E-W	N.W. Roof	5	1.50	1.52
E-W	N.E. Roof	6	1.50	1.52
E-W	Mid Roof	7	0.98	1.02
E-W	S. Roof	8	0.80	0.91

TABLE NO. 5
COMPARISON OF DISPLACEMENTS FOR STATION NO. 24579, LANDERS EQ.

DIRECTION	FLOOR & LOCATION	CHANNEL	CSMIP DATA MAX. INCHES	SAP DATA MAX. INCHES
N-S	S.W. 2nd Fl.	8	0.18	0.16
E-W	S.W. 2nd Fl.	9	0.16	0.17
E-W	N. 5th Fl.	10	1.15	1.13
E-W	S.W. 5th Fl.	11	0.60	0.54
N-S	S.W. 5th Fl.	12	0.55	0.49
N-S	W. 5th Fl.	13	0.91	0.94
E-W	N. Roof	14	2.22	2.06
E-W	S.W. Roof	16	0.96	1.01
N-S	S.W. Roof	17	0.87	0.88
N-S	W. Roof	18	1.56	1.77

TABLE NO. 6
COMPARISON OF DISPLACEMENTS FOR STATION NO. 24581, LANDERS EQ.

DIRECTION	FLOOR & LOCATION	CHANNEL	CSMIP DATA MAX. INCHES	SAP DATA MAX. INCHES
N-S	W. Mezzanine	5	0.37	0.32
N-S	Mid Mezzanine	6	0.19	0.25
N-S	E. Mezzanine	7	0.38	0.35
E-W	Mid Mezzanine	8	0.11	0.11
N-S	Mid 4th Fl.	9	0.57	0.80
E-W	Mid 4th Fl.	10	0.60	0.42
N-S	W. 12th Fl.	11	2.56	2.25
N-S	Mid 12th Fl.	12	2.28	2.31
N-S	E. 12th Fl.	13	2.10	2.12
E-W	Mid 12th Fl.	14	2.48	2.57
N-S	Mid Roof	15	2.51	2.38
E-W	Mid Roof	16	2.57	2.63

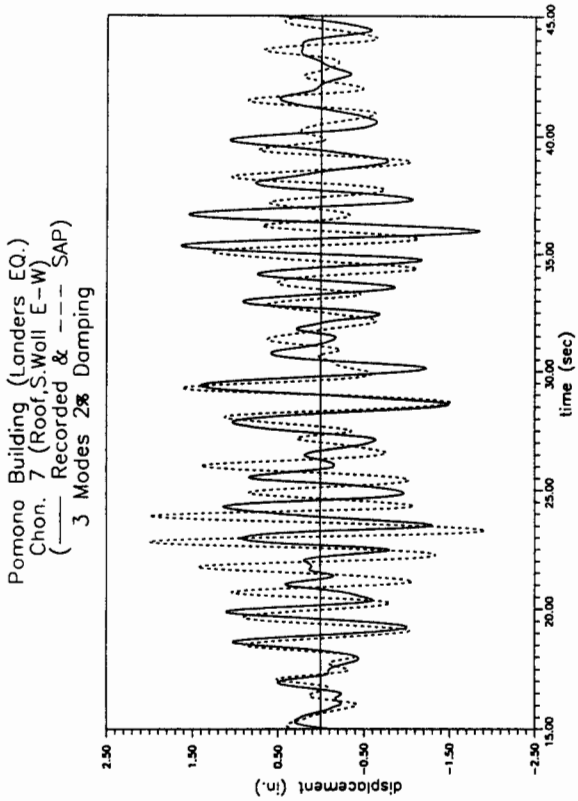

FIGURE NO. 1 - RESPONSE OF CSMIP STATION NO. 23544 AT ROOF, LANDERS EQ.

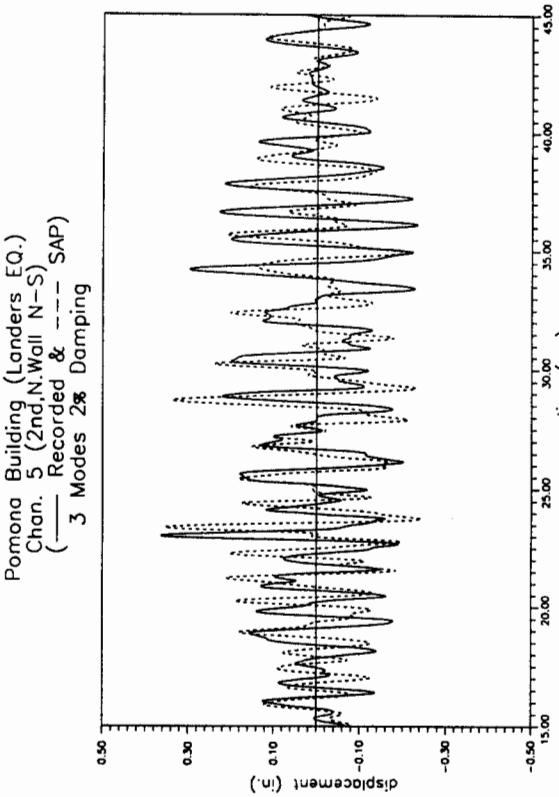

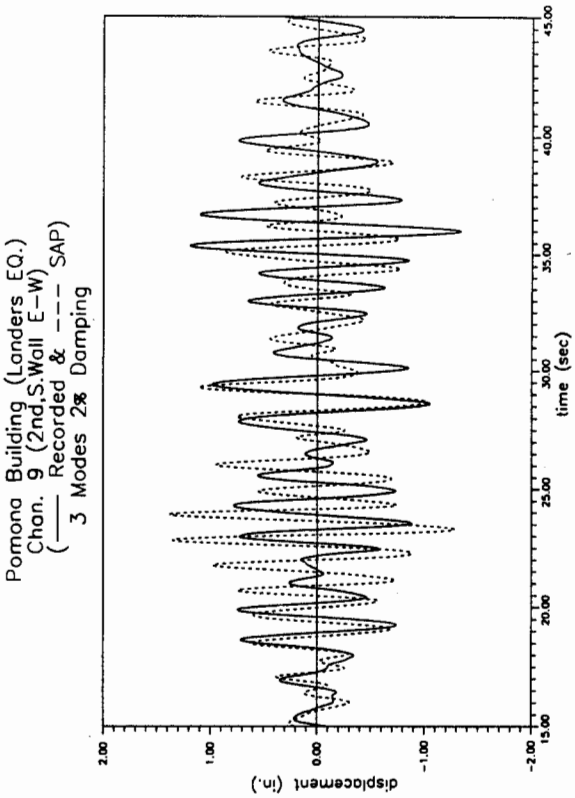

FIGURE NO. 2 - RESPONSE OF CSMIP STATION NO. 23544 AT 2nd FLOOR, LANDERS EQ.

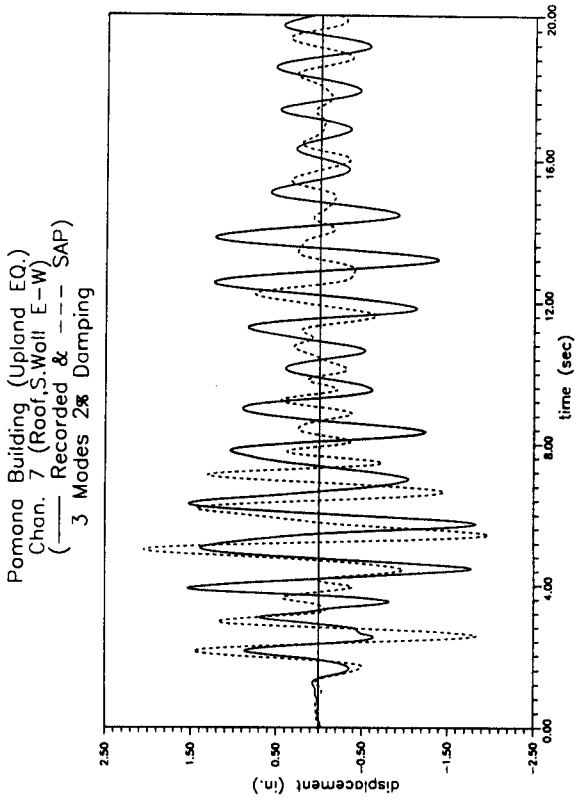

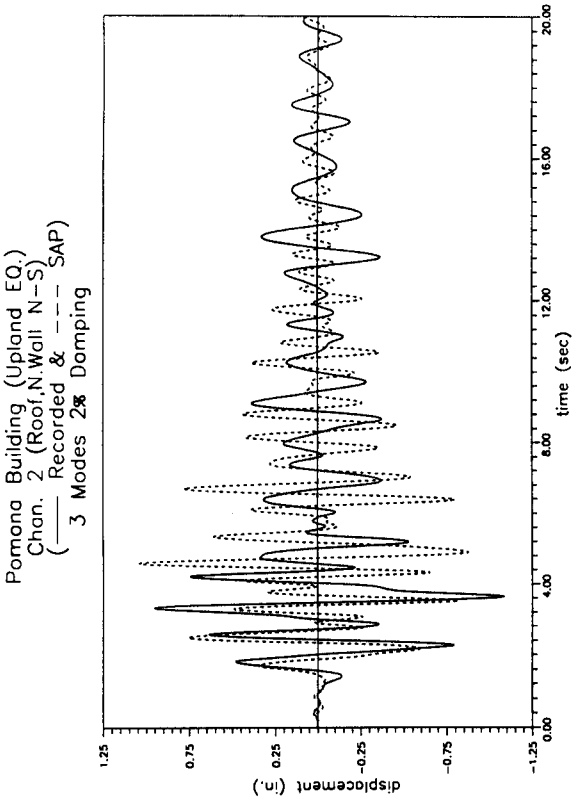

FIGURE NO. 3 - RESPONSE OF CSMIP STATION NO. 23544 AT ROOF, UPLAND EQ.

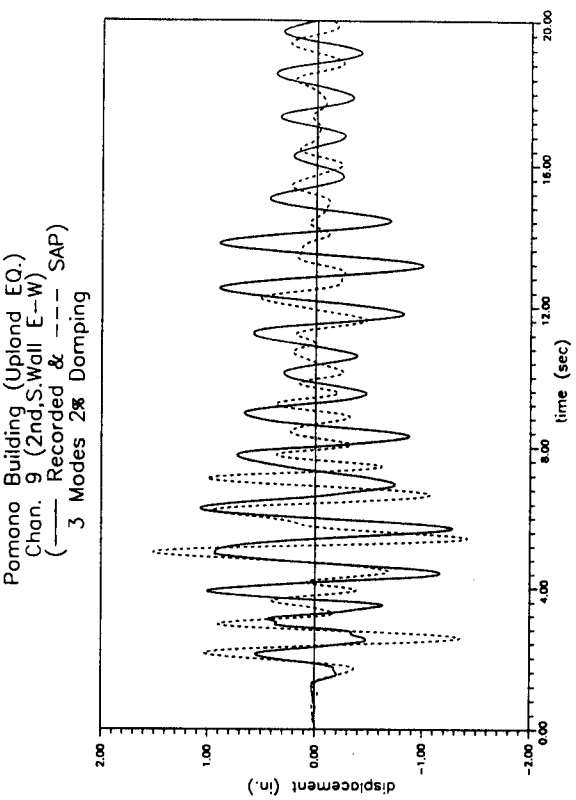

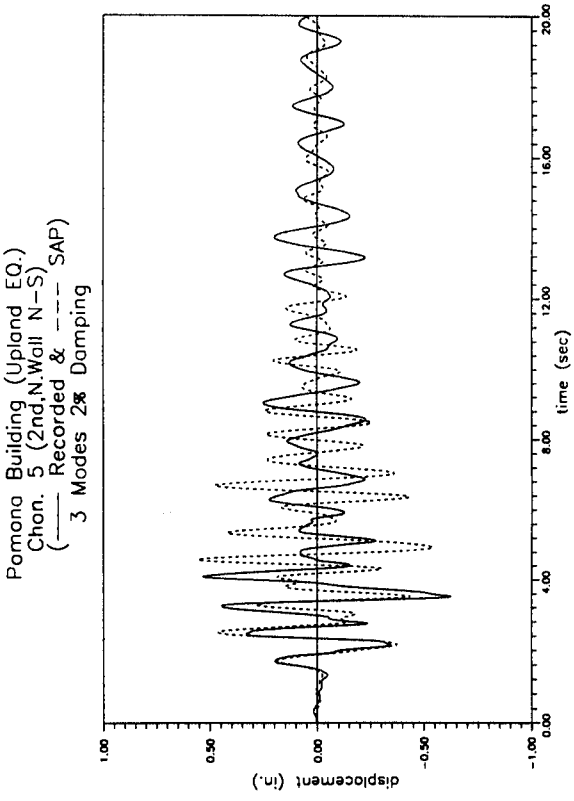

FIGURE NO. 4 - RESPONSE OF CSMIP STATION NO. 23544 AT 2nd FLOOR, UPLAND EQ.

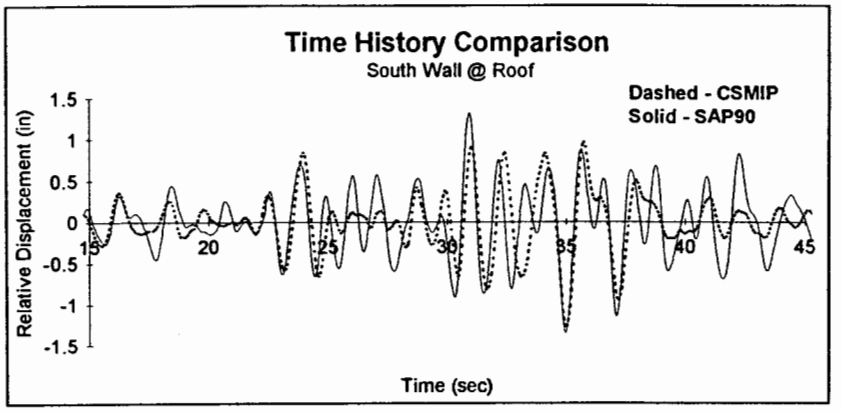

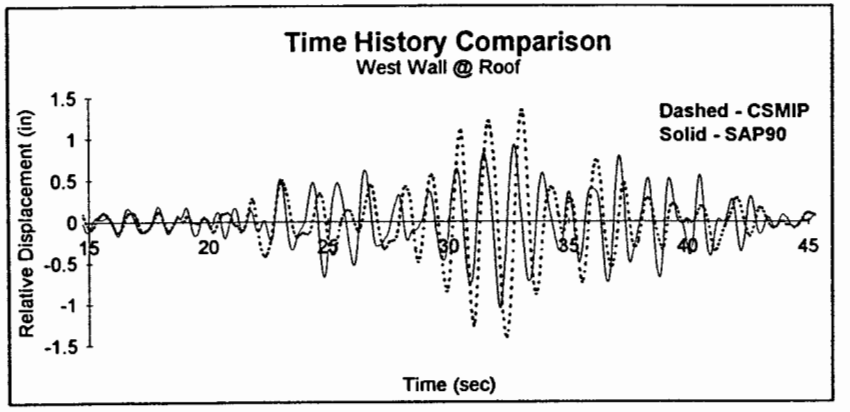

FIGURE NO. 5 - RESPONSE OF CSMIP STATION NO. 24541 AT ROOF, LANDERS EQ.

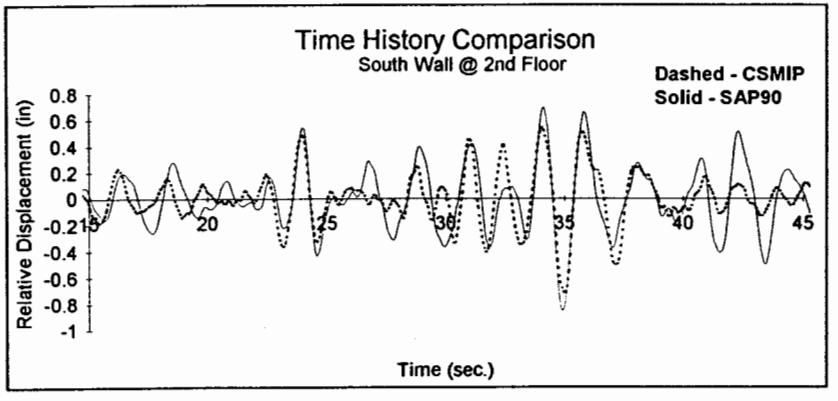

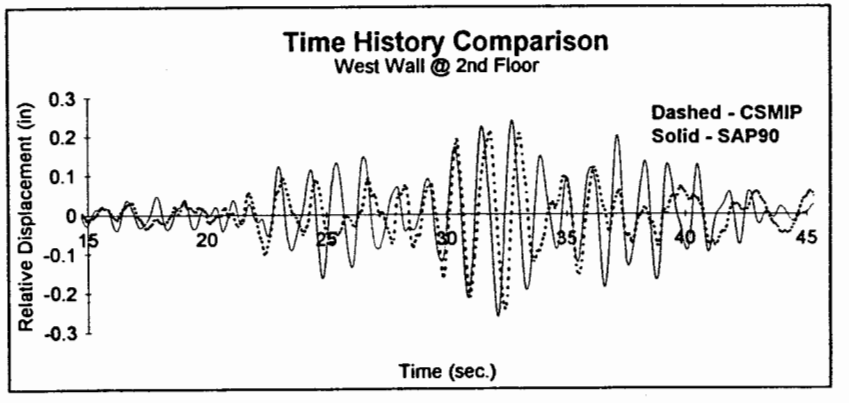

FIGURE NO. 6 - RESPONSE OF CSMIP STATION NO. 24541 AT 2nd FLOOR, LANDERS EQ.

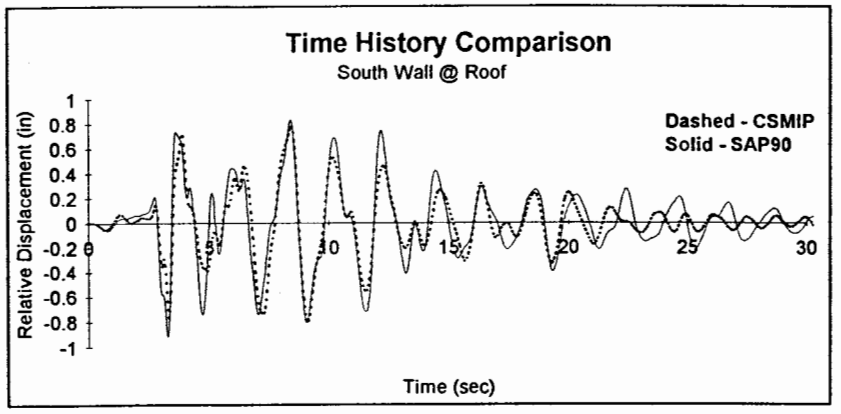

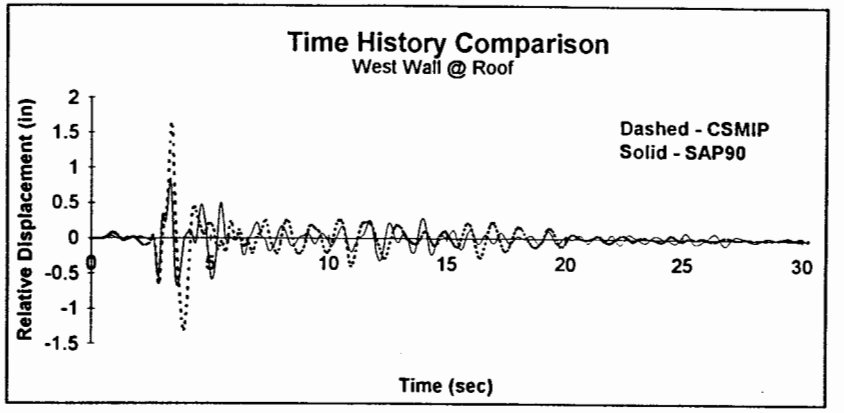

FIGURE NO. 7 - RESPONSE OF CSMIP STATION NO. 24541 AT ROOF, SIERRA MADRE EQ.

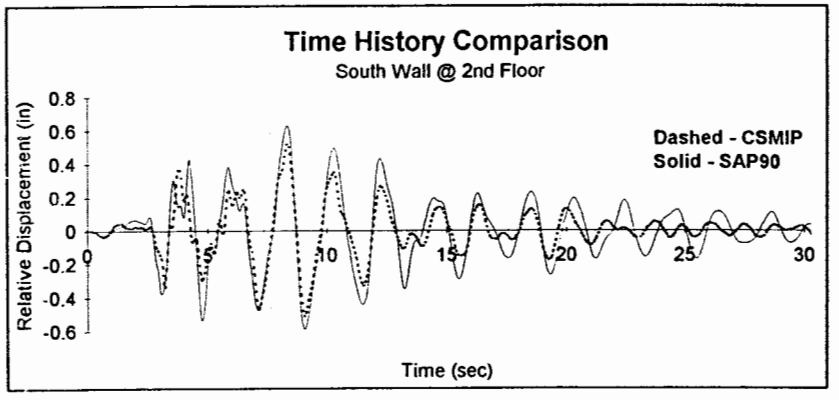

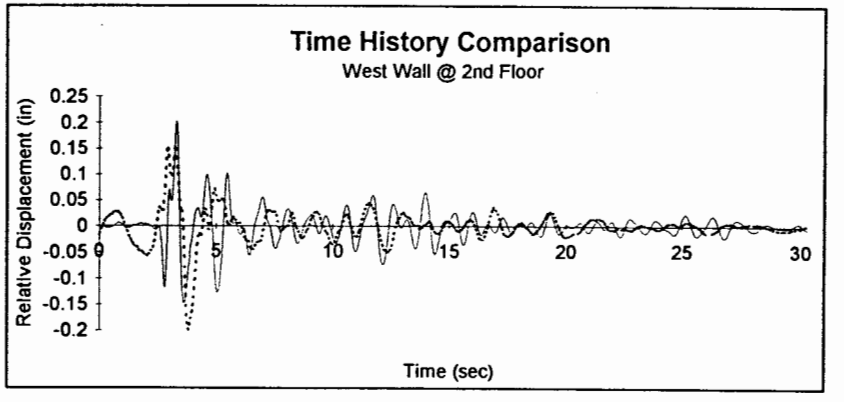

FIGURE NO. 8 - RESPONSE OF CSMIP STATION NO. 24541 AT 2nd FLOOR, SIERRA MADRE EQ.

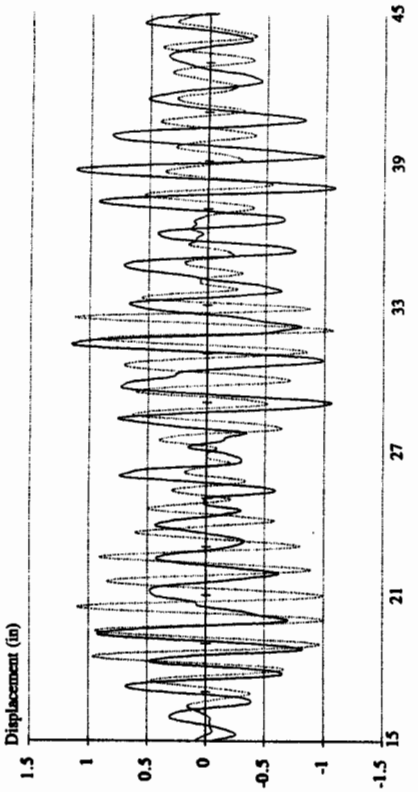

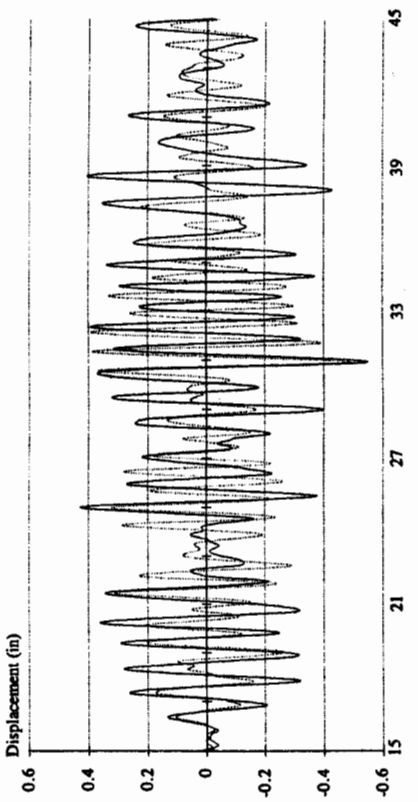

FIGURE NO. 9 - RESPONSE OF CSMIP STATION NO. 24579 AT 5th FLOOR (12) AND ROOF (17), LANDERS EQ.

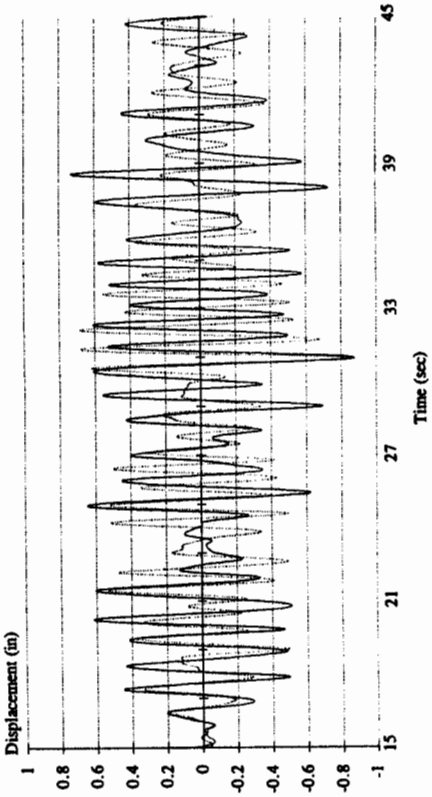

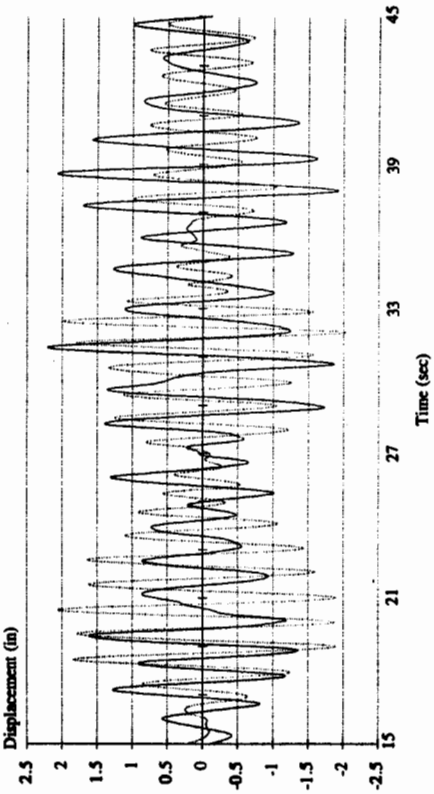

FIGURE NO. 10 - RESPONSE OF CSMIP STATION NO. 24579 AT 5th FLOOR (10) AND ROOF (14), LANDERS EQ.

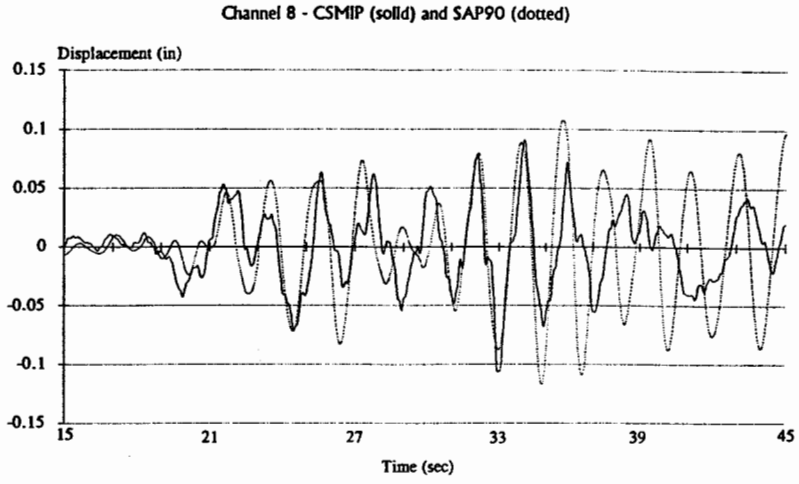

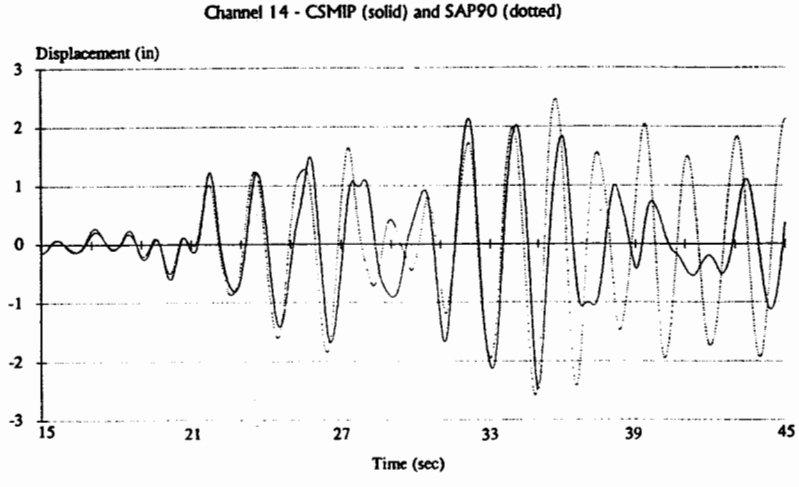

FIGURE NO. 11 - RESPONSE OF CSMIP STATION NO. 24581 AT 2nd FLOOR (8) AND 12th FLOOR (14), LANDERS EQ.

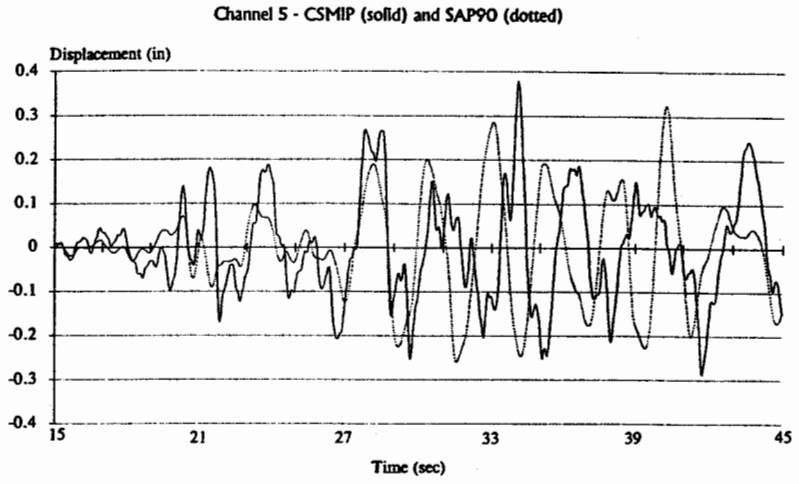

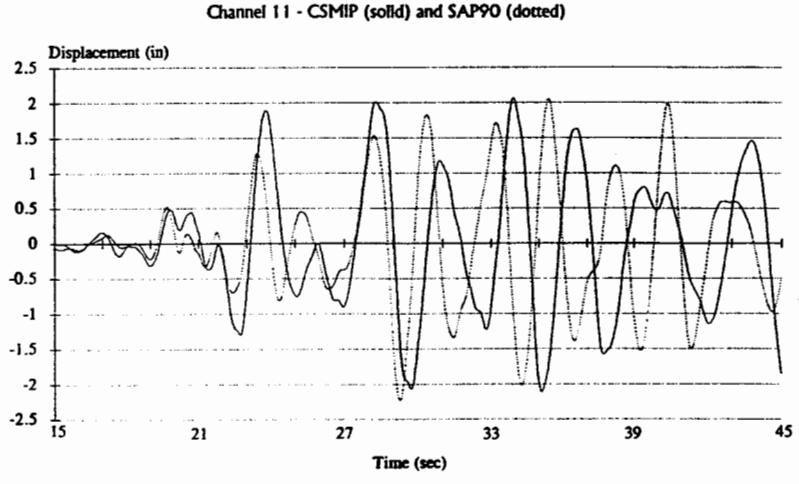

FIGURE NO. 12 - RESPONSE OF CSMIP STATION NO. 24581 AT 2nd FLOOR (5) AND 12th FLOOR (11), LANDERS EQ.

QUANTIFYING THE EFFECTS OF SOIL-STRUCTURE INTERACTION FOR USE IN BUILDING DESIGN

Chris D. Poland[1], Jeffrey R. Soulages[2], Joseph Sun[3], Lelio H. Mejia[4]

ABSTRACT

This research seeks to investigate the effects of soil-structure interaction (SSI) for regular buildings, validate current analysis techniques, and investigate the degree to which SSI contributes to the code based R factor for a variety of building and soil conditions. The research includes the analysis of strong motion records for 11 CSMIP building/free-field pairs to investigate the reduction in building response due to soil-structure interaction. The research also includes SSI analyses using the FLUSH computer program for four CSMIP buildings sites, comparison of recorded with model response, and comparison of the predicted base shear reduction using FLUSH and ATC 3-06 to the actual reduction recorded.

INTRODUCTION

The successful performance of buildings subjected to strong earthquake ground motions depends on their strength, the selected structural system and configuration, as well as the detailing and interconnection of the structural elements. Strong motion recordings taken during large earthquakes continue to show that properly designed buildings are capable of sustaining large recorded ground accelerations with little or no damage even though these motions far exceed their calculated strength. Recent experience in the Loma Prieta earthquake demonstrated that structures subjected to 30 to 40% g peak ground acceleration did not experience the kind of damage that would have been predicted using purely elastic analysis techniques.

Current seismic design provisions used in the United States include large reduction coefficients called R factors to account for this phenomena. These factors range in value from 1.5 to 12 and are used to define a suitable design base shear from an elastic response spectrum. From a structural design point of view, the key components making up the R factor include over-strength, redundancy, damping, multi-mode effects, system ductility, and soil-structure interaction (SSI). It is commonly recognized that extensive research is needed to justify and refine the arbitrarily established R values and tailor their use for new design.

It is often assumed that the motion experienced at the base of a building is the same as the free-field ground motion. This is only true if the structure is thought to be supported on soil which is rigid. For most soil conditions, the motions at the base of the building can be significantly different than in the free-field, and may even include a rocking component in addition to horizontal translational and vertical components [1]. This phenomena has been commonly termed soil-structure interaction.

---

[1]President, H.J. Degenkolb Associates, Engineers, San Francisco, CA

[2]Design Engineer, H.J. Degenkolb Associates, Engineers, San Francisco, CA

[3]Project Engineer, Woodward-Clyde Consultants, Oakland, CA

[4]Senior Associate, Woodward-Clyde Consultants, Oakland, CA

This research seeks to investigate the beneficial effects of soil-structure interaction for regular buildings, validate current analysis techniques, and investigate the degree to which it contributes to the code based R factor for a variety of building an soil conditions.

SUMMARY OF PREVIOUS WORK

Although the concept of soil-structure interaction has been in the literature for a number of years, most of the research has been centered on massive, concrete embedded structures such as nuclear reactors. The number of researchers investigating the response of conventional buildings, however, has been steadily increasing.

Seed, in his Nabor Cabrillo Lecture of 1986 [2], observed that the peak acceleration due to earthquake ground motion decreases significantly as the depth of the soil deposit increases. This was verified by records from a number of strong motion sites with downhole, vertical arrays of instruments such as the USGS instrument at Menlo Park, California, an array at Narimasu, Japan, and the EERC array at Richmond Field Station, California. As further evidence, a number of nearby pairs of buildings, each pair with one building constructed on the ground surface and one with a full basement, was compared by Seed and Lysmer [3] for peak ground accelerations during the San Fernando, California earthquake of 1971. In 7 of the 8 cases studied, the peak acceleration recorded at the base of the building with a basement was on the average about 27% less than the building founded on the ground surface. Seed neglected to add the case to the table of data presented where an increase was observed. He concluded that this reduction in pga with depth was "not a chance phenomena, but a pattern attributable to deterministic effects" [2].

Seed [2], also postulated that "inertial interaction tends to cause a slight reduction in the intensity of motions developed at the base of the structure compared with the intensity of motions developed in the free field... for most structures the effect will be small, of the order of about +10 to -20%." He based this observation not on building base shear reductions, but rather on a reduction in peak ground acceleration. This range of values for the amount of reduction due to SSI is similar to the range predicted by ATC 3-06, but has yet to be verified with a large amount of experimental data.

The effect of inertial soil-structure interaction on building response is well documented in ATC 3-06 [1], published by the Applied Technology Council in 1978 and based on the work of Valestos and others. A hand procedure based primarily on the period of the building, shear wave velocity and shear modulus of the soil, and foundation damping is discussed. In general, the ATC procedure shows that the effects due to SSI are small, on the order of +0 to -15% for most buildings. In addition, a number of limits are placed on the calculations so that the amount of reduction due to SSI is limited to -30%. For example, both the "effective" height and weight of the building are taken as 70% of the actual height or weight in the ATC 3-06 calculations. The procedure is based primarily on analytical solutions and classical mechanics and has been compared with only a few actual building records.

Fenves and Serino studied soil-structure interaction effects for the Hollywood Storage building in Los Angeles using the 1987 Whittier earthquake for their analysis [4]. They found that using a 3D finite-element model for the structure and using soil-springs to model the soil provided good results. In the conclusions, Fenves proposes, "a more detailed modelling of the foundation and soil, accounting for embedment, piles, and soil layers, may improve the correlation between the model and the recorded transfer functions, particularly in the short period range." [4]

INVESTIGATION OF REDUCED PGA WITH DEPTH

One of the basic parameters in judging the strength of earthquake ground motion is the peak ground acceleration (pga) at a free field or building site. The peak ground acceleration is the largest recorded acceleration (positive or negative) during an event at any time point in the record. Although caution should be used when comparing pga values since the values occur at different times for every record and often at very high frequencies, they are in general, a good indication of an earthquake's intensity.

Seed has found that one of the most influential parameters effecting the amount of reduction due to soil-structure interaction is depth of embedment of the structure. Seed suggested that the difference in pga between the ground and the basement can be used as a rough indication of the amount of reduction in motion due to SSI.

In Table 1, the peak ground accelerations at a number of CSMIP building sites are listed along with each corresponding free-field station. The records in the table are separated by those having basements (Table 1a) and those constructed on the ground surface (Table 1b). The data of buildings with basements is an extension of the work presented by Seed and Lysmer for the 1971 San Fernando earthquake but has a number of significant differences.

Table 1a compares peak ground acceleration values at the base of each building as compared to a nearby free field instrument whereas Seed and Lysmer used nearby pairs of buildings, one on the ground surface and one embedded. Now that the data is available, the use of free field stations is probably more appropriate since it more accurately represents the true response at the ground surface. The percent change surprisingly varies from -43.5 to +30.5%.

Seed and Lysmer used records with particularly strong shaking. On average, the ground motions they used had a pga of about 0.20g. Looking at Table 1a, a number of observations can be made. For small earthquakes, those with peak ground accelerations ≤ 0.8, the motions actually increased or stayed the same for buildings with basements (with the exception of the First Federal Savings Building in Pomona). For stronger earthquakes, Table 1a shows that buildings with basements generally show a reduction in motion, in some cases as much as 43.5% (First Federal Savings Building - Upland).

Looking at Table 1b, for buildings without basements, earthquakes with pga's ≤ 0.08 increase the motion at the base when compared to the free field (except for the 15-story Government Office building in Los Angeles and the Medical Office Building in Lancaster). Even with stronger shaking (pga ≥ 0.8), some buildings, including the 3-story Office building in San Bernadino as well as the 1-story Supermarket building in Fortuna, continue to show large increases in motion. In fact, the Imperial Valley County Services building had the largest increase in response, one of the largest ground pga values, and was the only building on the list that was severely damaged.

It is clear that the amount of reduction in peak ground acceleration is dependent on the soil conditions and the level of ground shaking experienced at a particular site. Reductions in the -40% range have occurred.

GROUND MOTION ANALYSIS

A ground motion analysis technique was developed to investigate the amount of reduction in response due to soil-structure interaction using simple tools, recorded strong motion records, and existing techniques. The analysis technique is predicated on pairs of records (building and free-field) for each earthquake to be investigated. Although CSMIP has many building instruments, only a small percentage have free-field instruments in close enough proximity to make this type of analysis. Because the response of many regular buildings is dominated by their fundamental mode of vibration, response spectra for the free field and for the building base were compared in the fundamental period range.

The first step was the determination of building period. For each building record in each principal direction, the fourier transform is taken of the time history at the roof and the time history at the base (see Figure 1). The roof spectrum is divided by the base spectrum to form a transfer function which is plotted against frequency. An example is shown in Figure 2 for the EW direction of Hollywood Storage building. The first peak is characteristically the building's fundamental frequency. This method was used by Cole et.al. in a recent CSMIP study on building periods [5].

It has been suggested that the building period will lengthen as an earthquake progresses and the building begins to yield. However, when the entire 30 to 40 second time history is used in the calculations of the transforms, this effect is lost. To accurately follow the change in building period over time, the time history was divided into a number of five second windows. The transfer function of roof/base fourier transform was computed for each time window and these were plotted together on one graph (see Figure 2). In this way, the period of the building during the time of strong ground shaking can be observed separately from the building period after the shaking has stopped and the building is vibrating harmonically. Note that the period of Hollywood Storage building started at 0.57 sec., lengthened to 0.66 sec., and then shortened to about 0.62 sec. (see Figure 2). The period used was typically the harmonic period of the structure after shaking had stopped. This was usually always close to the average period over the entire time history range.

After the building period has been determined, the response spectrum at the base of the building is plotted with the response spectrum for the properly rotated direction of the free-field on the same graph. If a line is drawn at the building fundamental period, a reduction in motion between the base and free-field curves can often be observed at or slightly above the building period (see Figure 3). This reduction can better be seen by dividing the base by the free-field response spectrums and plotting the spectral ratio. Frequencies with a spectral ratio below 1.0 show a reduction in spectral acceleration. At the building's fundamental period, this shows as a valley in the graph (see Figure 4). The results of each strong motion record investigated are shown in Table 2.

Looking at Table 2, the results for the reduction in building base motion vary considerably from a low of -40 to a high of +40%. However, a number of important observations can be made. The valley that occurs in the Hollywood Storage - EW record also appears in many of the other records with reductions that vary from -15 to -40%. However, in 9 of the 22 records studied, an increase in the response occurred. The same behavior seemed to occur for various sizes of earthquakes, soil conditions, and various types of construction. No trends are currently apparent. Also, there seems to be no correlation with the results shown in Table 1, even for the exact same building and earthquake.

SOIL-STRUCTURE INTERACTION ANALYSIS

In order to investigate the validity of current analysis techniques for conventional buildings, a number of sites were chosen for more detailed analysis. The four sites chosen, Richmond City Hall, Imperial Valley County Services building, Hollywood Storage building, and Hayward - 13-story CSUH Administration building, were selected to represent a variety of different building and soil types (see Table 2). The analysis procedure is based on the FLUSH soil-structure analysis program, using commercially available techniques and procedures.

The stick model is developed using a two-dimensional or three-dimensional full-frame SAP90 model of the building. The model is loaded with static unit loads and the displacements are computed. If the building is a stiff, shearwall building, like Richmond City Hall, the building is assumed to behave like a shear beam. The shear areas are backcalculated from the story shears and the displacements, and the moments-of-inertia are assumed to be very large. If the building is a more flexible moment frame building, like the Hayward - CSUH Admin. building, the building is assumed to act like a cantilevered frame. The shear areas and moments-of-inertia are backcalculated from the displacements and rotations at each story. The stick model is then checked against the full-frame model for proper modal behavior and matching displacements and fundamental period of vibration. Each building model is unique and care must be taken to accurately model each building as a multi-degree-of-freedom stick model.

The soil profile is developed from a geotechnical report utilizing logs of borings at the building site and shear wave profile where available. When possible, the data was based on borings that went down to bedrock. In many places however, such as the Los Angeles basin, borings stop well short of this depth. For these sites, an educated estimate of the shear wave velocity profile past the depth at which the borings stop was made.

The soil-structure interaction analysis developed for this study uses FLUSH, a SSI program developed by Lysmer et. al.[6]. The program uses a two-dimensional finite element mesh representing differing soil characteristics with depth and lateral extent, and can approximate the behavior in three-dimensions by the use of energy-dissipating dashpots in the out-of-plane direction. For buildings with basements, the basement condition was modelled as rigid. The soil finite element used in FLUSH incorporates non-linear material behavior. Each mesh was generated such that the model would be valid for frequencies up to 15 Hz. Since the motions in the soil are assumed to be vertically propagating S-waves, the influence of frictional piles, such as used for Hollywood Storage building, was neglected since they do not significantly influence the horizontal response motions.

The four buildings were analyzed in both principal directions except CSUH which is symmetric in both directions. The results of the seven soil-structure interaction analyses completed for this study are summarized in Table 3. In addition, the response spectrums for one direction of each building are plotted in Figures 5 through 8. On each graph is plotted the response spectrum for the recorded time history at the base of the building versus the corresponding response spectrum for the FLUSH analysis. Three other columns are included in Table 3 for comparison. The "Record" column shows the results of analyses of stick models using the response spectrum recorded at the base of the building as the input motion and calculating the reduction compared to the result using the free-field response spectrum as the input motion. The "ATC 3-06" column shows the amount of reduction calculated using the hand procedure in ATC 3-06. The "Other Studies" column shows the results of other SSI analyses which looked at the same buildings (Fenves and Serino [4]).

In some cases, the FLUSH procedure accurately captures the spectral shape at the base of the structure and the pga recorded at various levels in the superstructure for Hollywood Storage building, Richmond City Hall, and Hayward - CSUH Admin. building (see Figures 5, 7, and 8). However, for the Imperial Valley County Services building, the results of the FLUSH analysis are not in as good agreement with the recorded motions (see Figure 6). First, the motion at the base of the building is significantly higher than the free field motion over the entire period range. This is contrary to all other records we looked at for this study. It is unusual that the base of the building amplified the free-field motion even at very low periods (high frequency motion) which is usually not amplified by typical structures. Second, the computed building response using FLUSH is strongly influenced by the free-field control motion. The model is not able to reproduce the high spectral amplification in the period range between 0.2 to 0.5 seconds seen in the building base record. In addition, the results from the FLUSH analyses do not seem to correlate well with what is seen by the building strong-motion records.

The comparison of the results using FLUSH for Hollywood Storage building look very comparable to the results obtained by Fenves and Serino [4] (see Table 3). This suggests that for stiff, uniform sites with low to moderate levels of seismic excitation, the linear soil springs used by Fenves and Serino appear to be acceptable.

Looking at the "FLUSH" and "ATC 3-06" columns of Table 3, there appears to be reasonable correlation between the two analyses. For Richmond City Hall in the NS direction, Imperial County Services in the EW direction, and Hollywood Storage in both directions, the results are very good, within about 10% of each other. However, for Richmond City Hall in the EW direction, Hayward CSUH for both directions, and Imperial County Services in the NS direction, the hand procedure over-predicts the FLUSH analysis results. For a preliminary assessment, it appears that the ATC 3-06 hand procedures provide the right order of magnitude estimate of base shear reductions due to SSI for many sites. It is not surprising that reasonable correlation occurs between FLUSH and ATC 3-06 since both procedures are analytically based.

CONCLUSIONS

An analysis of strong motion records for 11 CSMIP building/free-field pairs to investigate the reduction in building response due to soil-structure interaction has been completed. Soil-structure interaction analyses using the FLUSH computer program for four CSMIP buildings sites, comparison of recorded with model response, and comparison of the base shear reduction using FLUSH with the results of stick models, an ATC 3-06 hand analysis, and previous analyses have also been completed. Based upon the data collected, the following observations were made:

(1) Buildings are not simple, static structures, but are complex and respond non-linearly during dynamic excitation. Soil-structure interaction is a complex phenomena and is difficult to predict. Both significant increases and significant decreases are observed.

(2) Seed and Lysmer's observations that there is a reduction of base motion expressed in terms of pga with increased depth seem to be generally true for regular buildings with basements when the pga during a strong motion event is greater than 0.1g. Unfortunately, there is little correlation between pga reductions and reductions in base shear.

(3) The building period changes with time and is difficult to pinpoint, particularly for

(3) The building period changes with time and is difficult to pinpoint, particularly for low-rise buildings. This makes the results from any analysis based on building period, and the results from our technique as well, more difficult to predict. It also make a change in the code, for example a reduction due to SSI based on building period, nearly impossible.

(4) Using the difference in recorded spectral accelerations to predict the amount of base shear reduction due to soil-structure interaction is not supported by the records studied.

(5) The FLUSH soil-structure models and procedure do not correlate well with the records studied.

(6) It is too early to propose any method to incorporate into building codes to account for soil-structure interaction. More research needs to be done utilizing the most recent CSMIP strong motion records for instrumented buildings.

(7) CSMIP should be encouraged to place free field instruments near instrumented buildings so we may obtain more data pairs and continue to investigate the effects of SSI on building response. Also, vertical instruments are needed at opposite sides of a building's base to monitor rocking in buildings where this might be anticipated.

ACKNOWLEDGEMENTS

The study as reported in this paper received principal funding from the California Strong Motion Instrumentation Program, California Department of Conservation, Division of Mines and Geology, Office of Strong Motion Studies with additional funding from Degenkolb and Woodward-Clyde. The authors wish to thank Moh Huang, Anthony Shakal, and Robert Darragh at CSMIP for their assistance in collecting the strong motion records and building drawings required for this project, and Eugene Cole & Chris Tokas at Cole, Yee Schubert & Associates for providing us a draft copy of their June 1992 report. We would also like to thank John Schneider at EPRI and Chuck Theil with CURe for providing subsurface soil information at Richmond City Hall, Bob McPeak at Interactive Resources Inc. for providing additional structural information at the same site, and Farhang Ostadan with Bechtel for his helpful suggestions.

REFERENCES

[1] Tentative Provisions for the Development of Seismic Regulations for Buildings, ATC 3-06, Applied Technology Council, Palo Alto, California, 1978.

[2] H. Bolton Seed, "Influence of Local Soil Conditions on Ground Motions and Building Damage During Earthquakes," Nabor Cabrillo Lecture, November 1986.

[3] H. B. Seed and J. Lysmer, "The Significance of Site Response on Soil-Structure Interaction Analysis of Nuclear Facilities," Proceedings 2nd ASCE Conference on Civil Engineering and Nuclear Power, Knoxville, Tennessee, Vol. II, September 1980.

[4] Gregory L. Fenves and Georgio Serino, "Evaluation of Soil-Structure Interaction in Buildings During Earthquakes," CSMIP Report 92-01, Sacramento, California, June 1992.

[5] Eugene E. Cole, Christos V. Tokas, and John F. Meehan, "Analysis of Recorded Building Data to Verify or Improve 1991 UBC Period of Vibration Formulas," CSMIP Draft Report, Sacramento California, June 1992.

[6] John Lysmer, Takekazu Udaka, Chan-Feng Tsai, and H. Bolton Seed, "FLUSH: A Computer Program for Approximate 3-D Analysis of Soil-Structure Interaction Problems," EERC 75-30, Berkeley, California, March 1979.

Buildings With Full or Partial Basements

Building	Earthquake	Maximum Acceleration		Percent change
		Base	FF	
Los Angeles - Hollywood Storage Building	Big Bear	0.03	0.03	0.0%
Pomona - First Federal Savings Building	Big Bear	0.03	0.03	0.0%
Los Angeles - 54-Story Office Building	Landers	0.04	0.04	0.0%
Los Angeles - 12-Story Commercial/Office	Landers	0.04	0.04	0.0%
Los Angeles - 52-Story Office Building	Landers	0.05	0.04	+25.0%
Los Angeles - 9-Story Office Building	Landers	0.05	0.04	+25.0%
Pomona - First Federal Savings Building	Whittier	0.05	0.07	-28.6%
Pomona - First Federal Savings Building	Landers	0.06	0.07	-14.3%
Hayward - 13-Story CSUH Admin. Building	Loma Prieta	0.09	0.08	+12.5%
Palm Springs - 4-Story Hospital	Big Bear	0.08	0.09	-11.1%
Palm Springs - 4-Story Hospital	Landers	0.06	0.09	-33.3%
Richmond - Richmond City Hall	Loma Prieta	0.12	0.13	-7.7%
Los Angeles - Hollywood Storage Building	Whittier	0.13	0.21	-38.1%
Pomona - First Federal Savings Building	Upland	0.13	0.23	-43.5%

TABLE 1a - Change in Maximum Acceleration Between Base of Building and Free Field

Buildings Constructed on Top of Ground Surface

Building	Earthquake	Maximum Acceleration		Percent change
		Base	FF	
Los Angeles - 15-Story Government Office Bldg.	Big Bear	0.03	0.04	-25.0%
Los Angeles - 15-Story Government Office Bldg.	Landers	0.03	0.04	-25.0%
Los Angeles - 17-Story Residential Building	Big Bear	0.04	0.04	0.0%
Los Angeles - 17-Story Residential Building	Landers	0.05	0.04	+25.0%
Lancaster - Medical Office Building	Whittier	0.06	0.06	0.0%
Sylmar - Olive View Medical Center	Landers	0.06	0.06	0.0%
Sylmar - Olive View Medical Center	Whittier	0.06	0.06	0.0%
Long Beach - Harbor Administration Building	Whittier	0.07	0.07	0.0%
Eureka - 5-Story Residential Building	Petrolia Aftershock #1	0.08	0.07	+14.3%
Lancaster - Medical Office Building	Landers	0.07	0.08	-12.5%
Piedmont - 3-Story School Building	Loma Prieta	0.08	0.08	0.0%
Palm Desert - 4-Story Medical Office Building	Landers	0.06	0.09	-33.3%
Palm Desert - 4-Story Medical Office Building	Big Bear	0.07	0.09	-22.2%
San Bernadino - 3-Story Office Building	Landers	0.11	0.09	+22.2%
San Bernadino - 3-Story Office Building	Big Bear	0.13	0.10	+30.0%
San Bernadino - 1-Story Commercial Building	Big Bear	0.06	0.12	-50.0%
San Bernadino - 9-Story Commercial Building	Big Bear	0.08	0.12	-33.3%
San Bernadino - 1-Story Commercial Building	Landers	0.09	0.12	-25.0%
San Bernadino - 9-Story Commercial Building	Landers	0.10	0.12	-16.7%
Fortuna - 1-Story Supermarket Building	Petrolia	0.14	0.12	+16.7%
Fortuna - 1-Story Supermarket Building	Cape Mendicino (87)	0.18	0.15	+20.0%
Eureka - 5-Story Residential Building	Petrolia	0.16	0.17	-5.9%
Fortuna - 1-Story Supermarket Building	Petrolia Aftershock #1	0.18	0.19	-5.3%
El Centro - Imperial County Services Building	Imperial Valley	0.35	0.27	+30.5%
San Jose - 3-Story Office Building	Loma Prieta	0.20	0.28	-28.6%
Hollister - 1-Story Warehouse	Loma Prieta	0.36	0.38	-5.3%

TABLE 1b - Change in Maximum Acceleration Between Base of Building and Free Field

Bldg. Name	Bldg. Type	Foundation Type	Site Geology	# Stories[1]	EQ	FF PGA	Dir	Bldg. Period	% change
Hayward - CSUH	Conc. MF	Bearing Piles	Franciscan rock	13/0	Loma Prieta	0.08	E	1.39	-20%
							N	1.39	-40%
Hollister Warehouse	Tilt-up w/ plywood roof	Spread footings	Alluvium	1/0	Loma Prieta	0.38	E	0.73	0%
							N	0.15	-15%
Piedmont Jr. High School	Conc. shearwalls	Spread footings w/ tie beams	Weathered serpentine	3/0	Loma Prieta	0.08	N	0.16	+20%
							E	0.16	-8%
Richmond City Hall	Conc. MF	Spread footings	Alluvium	3/1	Loma Prieta	0.13	S	0.29	+40%
							W	0.25	-20%
San Jose - Office Bldg.	Steel MF	Spread footings	Rock	3/0	Loma Prieta	0.28	W	0.71	-10%
							N	0.74	-13%
Lancaster - MOB	Masonry bearing walls	Conc. piers w/ grade beam	Alluvium	3/0	Whittier	0.06	E	0.12	-12%
							N	0.09	-42%
Long Beach - Harbor Admin. Bldg.	Steel MF	Bearing Piles	Deep alluvium	7/0	Whittier	0.07	N	1.20	+7%
							E	1.41	+5%
LA - Hollywood Storage Bldg.	Conc. shearwalls (EW)	Bearing Piles	Alluvium over shale & sndstone	14/ partial	Whittier	0.21	N	2.27	+6%
							E	0.60	-32%
Pomona - First Federal Savings	Conc. MF	Spread footings?	Alluvium	2/1	Whittier	0.07	W	0.27	-9%
							N	0.26	+1%
Sylmar - Olive View Medical Center	Conc. and steel shearwalls	Spread footings	Alluvium	6/0	Whittier	0.06	N	0.30	+34%
							E	0.27	+24%
Imperial Valley County Services Bldg.	Conc. shearwalls (NS)	Spread footings	Alluvium	6/0	Imperial Valley	0.27	N	0.50	+14%
							E	1.00	0%

[1]Above ground/below ground

TABLE 2 - Comparison of Percent Reductions in Response

Building Name	Direction	Percent Reduction in Base Shear			
		Record	FLUSH	ATC3-06	Other Studies*
Richmond City Hall	NS	+7%	-20%	-25%	-
	EW	-28%	-16%	-30+%	-
Imperial County Services	NS	+5%	+4%	-15%	-
	EW				-
Hollywood Storage	EW	-34%	-15%	-15%	-17%
	NS	-4%	-2%	-8%	-3%
Hayward CSUH	NS/EW	-21%	+3%	-4%	-

* Fenves and Serino, "Evaluation of Soil-Structure Interaction in Buildings During Earthquakes."

TABLE 3 - Reduction in Response Due to Soil Structure Interaction

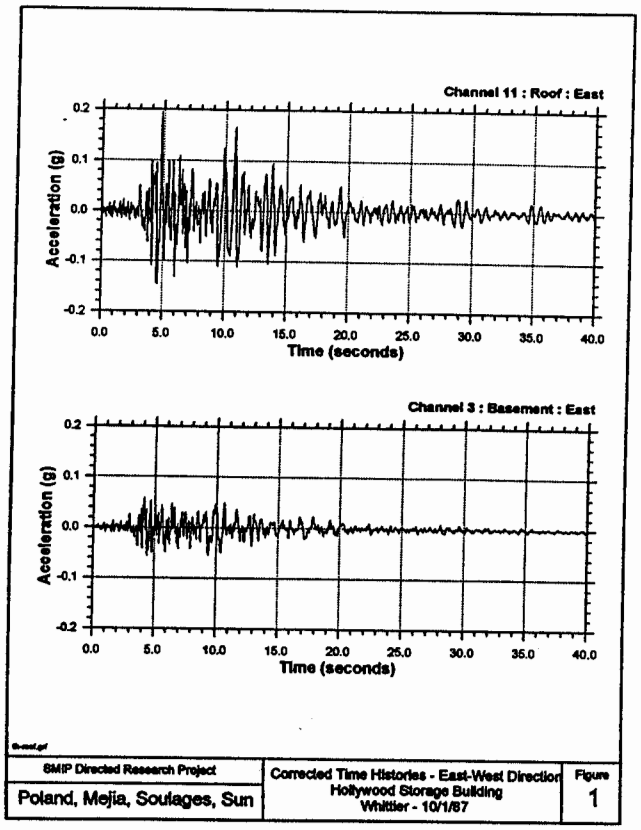
Channel 11 : Roof : East
Acceleration (g)
Time (seconds)
Channel 3 : Basement : East
Acceleration (g)
Time (seconds)
SMIP Directed Research Project
Poland, Mejia, Soulages, Sun
Corrected Time Histories - East-West Direction
Hollywood Storage Building
Whittier - 10/1/87
Figure
1

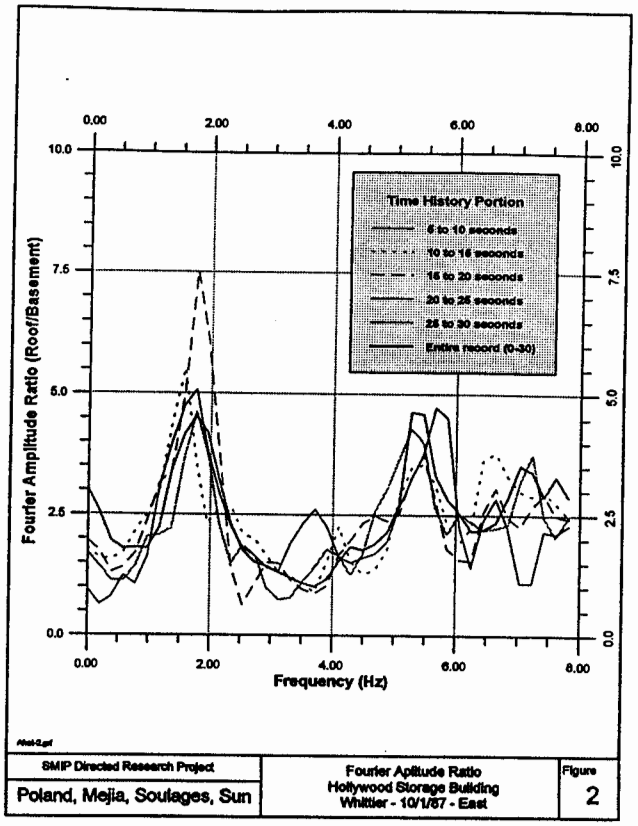
Time History Portion
6 to 10 seconds
10 to 15 seconds
15 to 20 seconds
20 to 25 seconds
25 to 30 seconds
Entire record (0-30)
Fourier Amplitude Ratio (Roof/Basement)
Frequency (Hz)
SMIP Directed Research Project
Poland, Mejia, Soulages, Sun
Fourier Aplitude Ratio
Hollywood Storage Building
Whittier - 10/1/87 - East
Figure
2

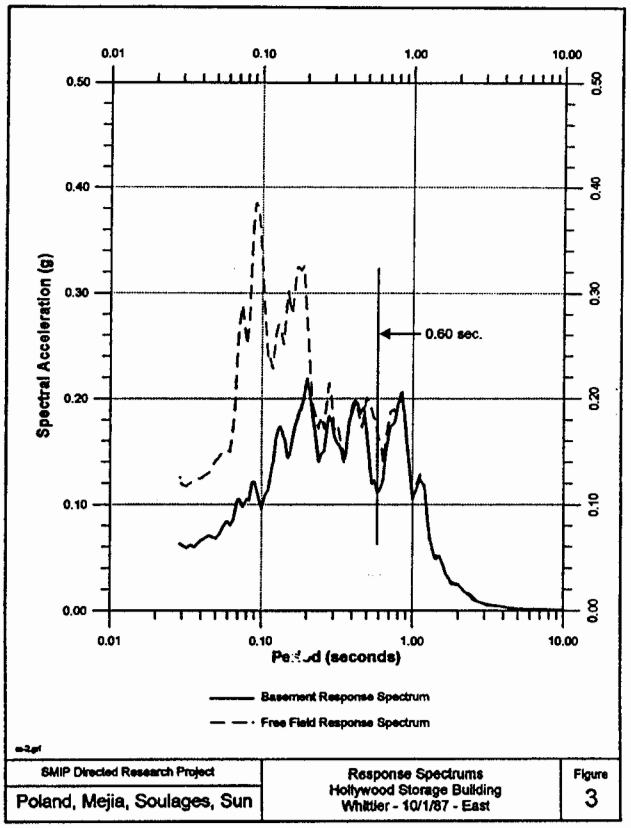
0.60 sec.
Spectral Acceleration (g)
Period (seconds)
Basement Response Spectrum
Free Field Response Spectrum
SMIP Directed Research Project
Poland, Mejia, Soulages, Sun
Response Spectrums
Hollywood Storage Building
Whittier - 10/1/87 - East
Figure
3

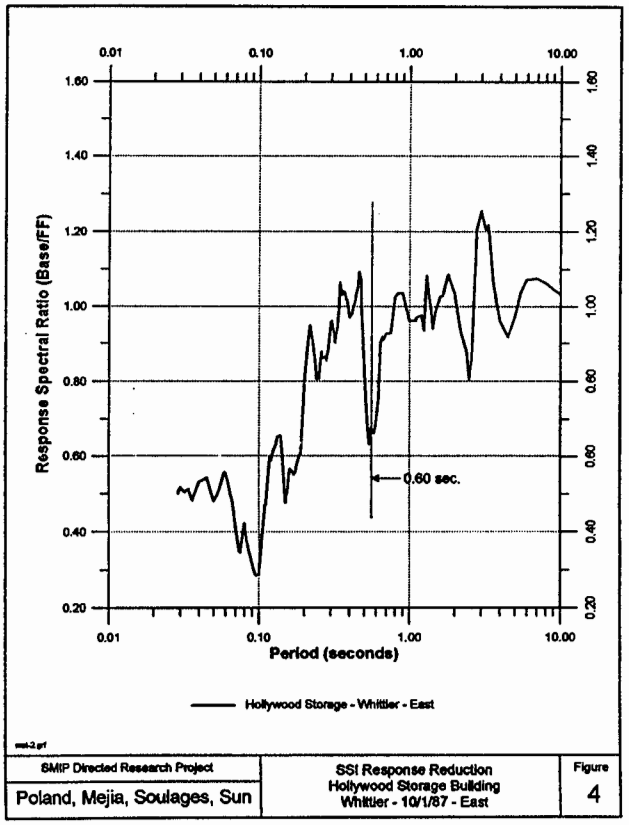
0.60 sec.
Response Spectral Ratio (Base/FF)
Period (seconds)
Hollywood Storage - Whittier - East
SMIP Directed Research Project
Poland, Mejia, Soulages, Sun
SSI Response Reduction
Hollywood Storage Building
Whittier - 10/1/87 - East
Figure
4

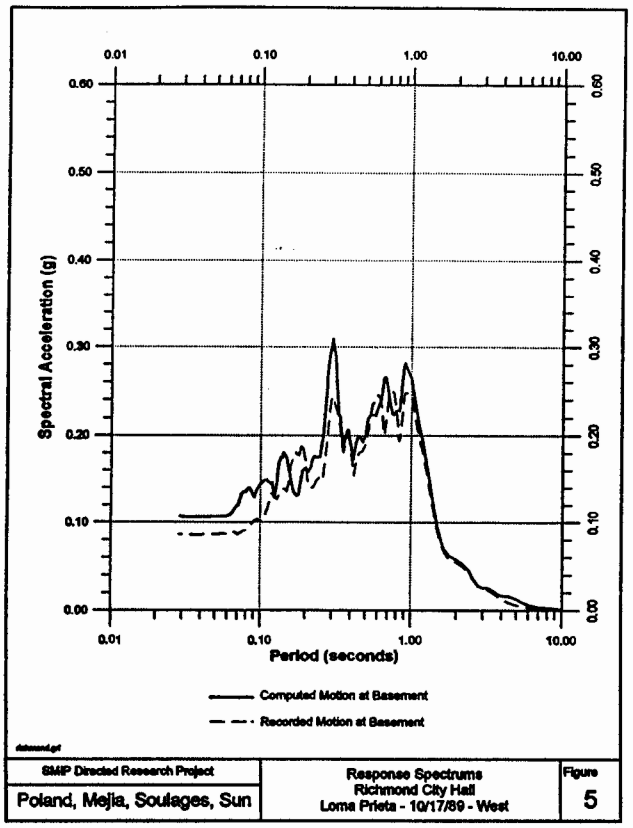
Spectral Acceleration (g)
Period (seconds)
Computed Motion at Basement
Recorded Motion at Basement
SMIP Directed Research Project
Poland, Mejia, Soulages, Sun
Response Spectrums
Richmond City Hall
Loma Prieta - 10/17/89 - West
Figure
5

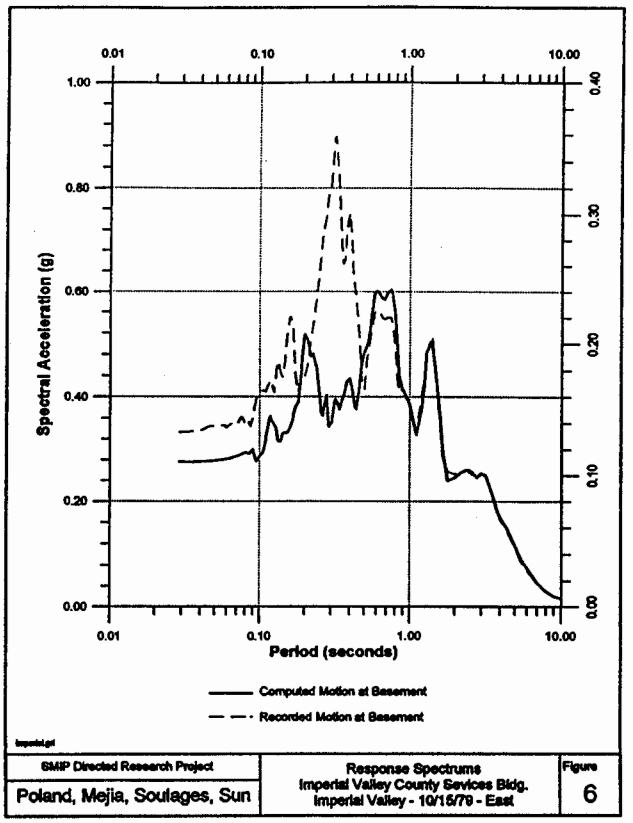
Spectral Acceleration (g)
Period (seconds)
Computed Motion at Basement
Recorded Motion at Basement
SMIP Directed Research Project
Poland, Mejia, Soulages, Sun
Response Spectrums
Imperial Valley County Sevices Bldg.
Imperial Valley - 10/15/79 - East
Figure
6

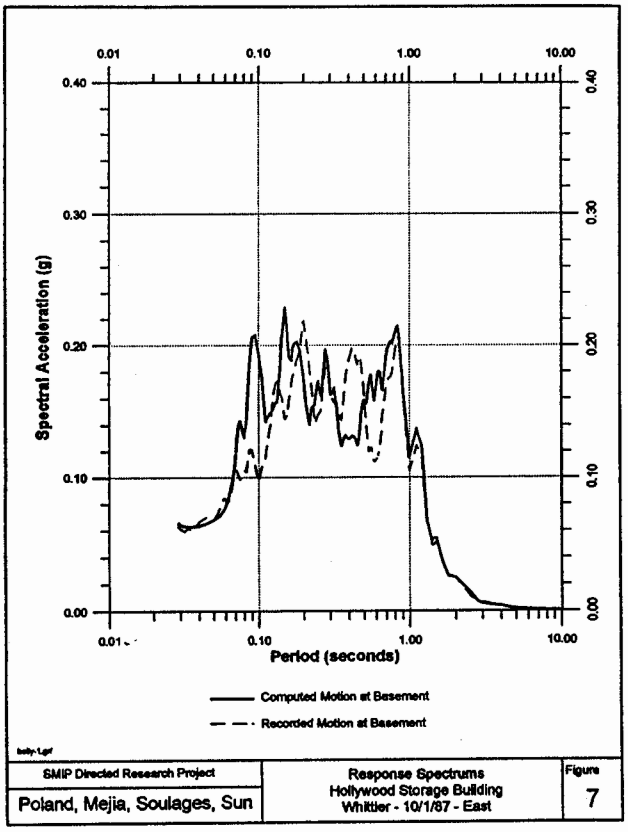
Spectral Acceleration (g)
Period (seconds)
Computed Motion at Basement
Recorded Motion at Basement
SMIP Directed Research Project
Poland, Mejia, Soulages, Sun
Response Spectrums
Hollywood Storage Building
Whittier - 10/1/87 - East
Figure
7

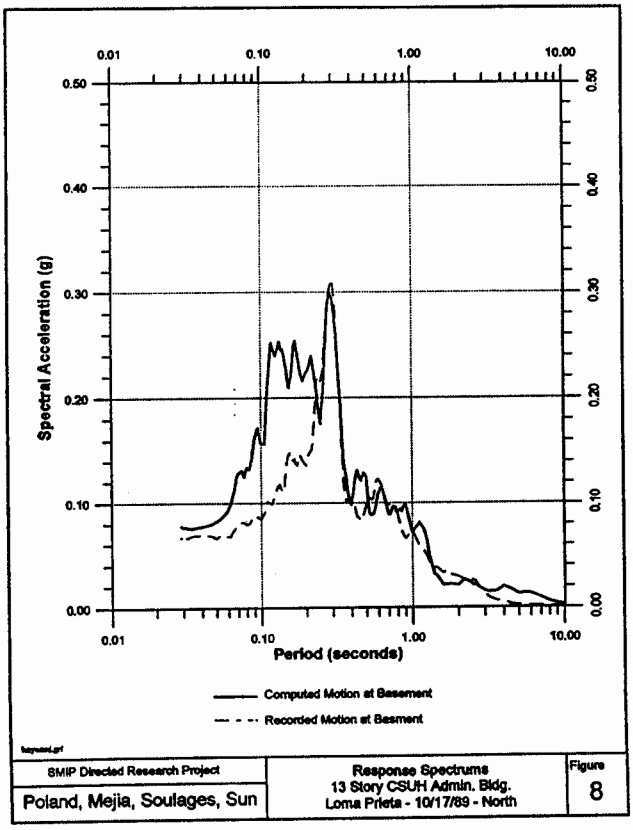
Spectral Acceleration (g)
Period (seconds)
Computed Motion at Basement
Recorded Motion at Basement
SMIP Directed Research Project
Poland, Mejia, Soulages, Sun
Response Spectrums
13 Story CSUH Admin. Bldg.
Loma Prieta - 10/17/89 - North
Figure
8

EXPECTED SEISMIC PERFORMANCE OF BUILDINGS

Prepared by

EERI Ad Hoc Committee on Seismic Performance:

William Holmes, Chair
Thalia Anagnos
Lloyd Cluff
Robert Olson
Allan Porush
Earl Schwartz

Edited By

William Holmes
Susan Tubbesing

D R A F T - February 1993

Expected Seismic Performance of Buildings

INTRODUCTION

Tens of millions of us spend much of our lives in the buildings and structures where we work, reside, worship, and go for entertainment, relaxation, or medical care. Local and state government elected officials and administrators adopt and enforce the codes and standards governing the design and construction of these buildings. Insofar as building safety is concerned, these codes are the "law of the land." The seismic design provisions of the codes are especially important to the performance of buildings in areas subject to earthquakes. We have a right to know how the buildings we occupy will perform in earthquakes.

The Earthquake Engineering Research Institute, a national professional organization dedicated to improved earthquake resistant design, prepared this document. Its purpose is to help policy-makers, code administrators, and others involved in the design, construction, and building maintenance processes understand how the seismic design provisions of the codes, knowledge and practices of our architects and engineers, and quality of construction affect the thousands of buildings of various types, sizes, and designs that we use daily. This paper attempts to establish expected levels of damage for buildings built to the 1991 Uniform Building Code (UBC 91), under various earthquake conditions.

First, we must dispel a myth: There is no "earthquake-proof" building. Although we are continuously improving our understanding of earthquakes and how buildings perform, there are limitations to building codes. Many older buildings were not built for earthquake resistance, and codes do not apply to many aspects of construction and use. As a result, we must expect losses from future earthquakes. These losses may take many forms: total or partial collapse due to shaking and ground failures, interior damage to nonstructural systems and elements, and damage to contents and equipment. While failures receive great media attention, we are heartened by the greatly improved performance of newer buildings constructed to recent building codes. But even new buildings are not immune to damage. Given the wide range of building types, site conditions, and earthquake characteristics, the performance of all building, even new ones, will not be the same. Many new buildings may suffer damage in a major earthquake, and a few should be expected to suffer serious damage.

The following sections cover the most important aspects that influence building safety. They include a discussion on earthquake causes and the accompanying shaking, fault rupture, and other ground failures. A brief summary is provided of common strategies for reducing earthquake hazards through planning, locating structures, and regulating construction. Building codes will be described in detail and the expected earthquake performance of new buildings built to the UBC 91 or older unreinforced masonry buildings retrofit to the 1991 Uniform Code for Building Conservation (UCBC) will be discussed. Initially, damage estimates have been limited to buildings in UBC Zone 4, because of the high probability of seismic events and the corresponding interest in this kind of information in this zone.

BACKGROUND

The crust of the earth, although solid and monolithic in appearance, is actually made of many individual pieces called plates. Continuous cooling and movement of the earth's molten interior forces surface plates to move, relative to each other. Some movement occurs gradually along certain plate boundaries—but most often, the plates stick together until the forces are large enough to cause sudden slippage, resulting in an earthquake. The slippage emits large amounts of energy in the form of waves that travel across the surface and through the interior of the earth, much like the waves emanating from a rock thrown into a still pond. Sometimes the slippage occurs along planes completely beneath the surface, as much as 15 miles deep, but often the boundary movement is visible, on the surface, in the form of horizontal or vertical offsets along surprisingly thin and straight lines. These offsets at the surface at plate boundaries are called surface fault ruptures.

Damage from earthquakes can be caused by the effects of surface fault rupture on structures built immediately over the fault, by (tsunami) sea waves caused by submarine ground failure, by the back and forth motion of the ground caused by the passing of waves (normally called ground shaking) or by the effects of soil failures (liquefaction or landslides) caused by the shaking. Additional damage can be caused by fires started by the shaking or by flooding from dam or reservoir failures.

Traditionally, control of construction practices through building codes has addressed only the shaking hazard. The hazards of seismic sea waves and surface fault rupture can best be reduced by planning and general avoidance of areas that are at risk. Areas prone to landslides similarly can be identified and avoided, although potential slides of small volumes may be stabilized with engineered structures. Liquefaction, the phenomena of certain wet sands turning essentially liquid when shaken, has been recognized as a potential seismic hazard for some time, but since accurate prediction is difficult, mitigation is often expensive, and the actual risk relatively undefined, code provisions in this area have been lacking. Hazards other than shaking can be mapped and should be included in the planning process. For example in California, all hazards are required to be mapped and incorporated into a community's General Plan as part of the Seismic Safety Element. Also in California, surface fault ruptures are mapped by the state as part of the Alquist-Priolo Special Studies Zones Act, designed to identify surface faults and potentially dangerous adjacent areas to each side of the fault.

Attempting to predict probable shaking at a site from a given earthquake is a complicated process and is influenced by the size of the earthquake, the distance from the source of slippage, the geology and topography of the path the wave travels between the source and the site, and the type of soil at the site. Building codes attempt to simplify this process by the use of broad zones, which influence the design criteria for seismic loading.

THE UNIFORM BUILDING CODE

The Uniform Building Code (UBC) is one of three model codes used by local and state jurisdictions throughout the United States to regulate construction of buildings. The UBC is most commonly used in the western and mid-western regions of the country including California and Utah. The UBC is updated annually and published every third year by the International Conference of Building Officials (ICBO). The principal issues that the building code addresses in its regulations are those of fire and occupant safety and structural adequacy. The regulation of the electrical, plumbing, and mechanical components of buildings are contained in separate, closely-related, companion codes.

The code's principal purpose as stated in its Administrative Chapter is:

> *"...to provide minimum standards to safeguard life or limb, health, property, and public welfare by regulating and controlling the design, construction, quality of materials, use and occupancy, location and maintenance of buildings..."* (emphasis added).

For the Uniform Building Code to be effective in meeting this purpose it must be adopted as law and enforced through effective administration by a city, county or state government. During the adoption process jurisdictions may decide to modify certain code requirements to address unique local conditions that the model code did not consider as common or universally necessary. These changes are in most cases more restrictive than those found in the standard code provisions and hence enhance the level of safety provided.

Changes to the UBC can be proposed by any interested person but are normally suggested by groups of building officials who enforce the code, or by associations representing design professionals and other construction industry associations who use the code. The process for a proposed change to become part of the code is arduous and filled with opportunities for review and challenge. As a result of this careful, deliberative code change process, major changes may take as many as 10 years to successfully complete the full cycle of development, review, approval, publication, adoption, and enforcement.

The seismic provisions of the Uniform Building Code are of primary interest in this report. The UBC contains a map that locates the boundaries of six seismic zones in the US. These zones are based on scientific studies of the intensity of ground motion and damage patterns produced in past earthquakes and the location of the fault zones where these earthquakes have occurred. The six seismic zones within the Uniform Building Code are: 0, 1, 2A, 2B, 3, and 4. Zone 0 represents minimum seismic risk with higher numbers representing increasing risk up to Zone 4, the maximum seismic risk zone. (See Figure 1) The basis for this map as well as other seismic design requirements in the UBC is subject to review and change as better information on these subjects becomes available.

FIGURE 1 1991 UNIFORM BUILDING CODE

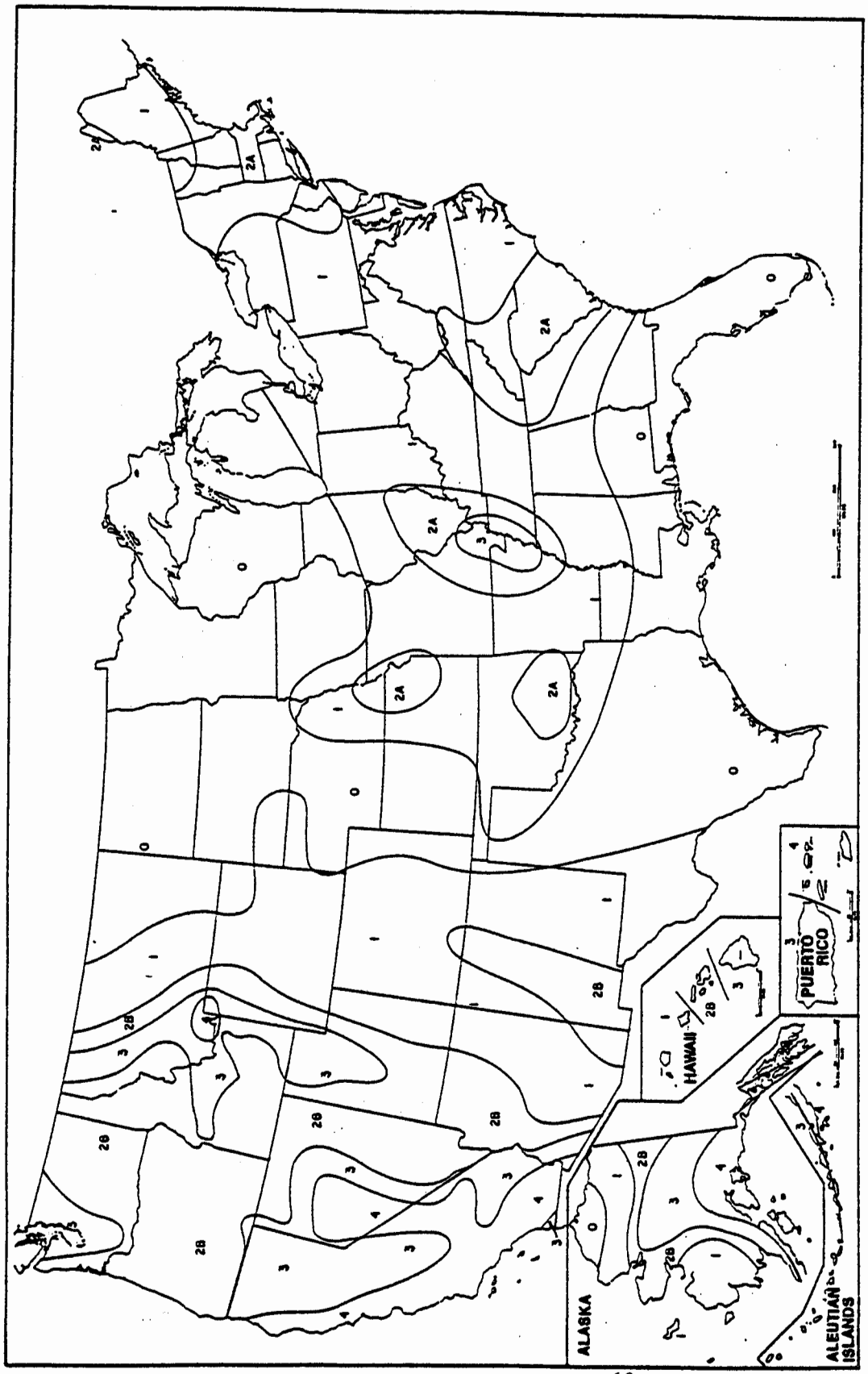

FIGURE NO. 23-2—SEISMIC ZONE MAP OF THE UNITED STATES

The seismic zone boundaries in the western U.S. have been revised twice since the 1979 edition of the UBC. Substantial changes in the zone boundaries took place in the 1988 edition partially based on the mapping prepared as a result of research conducted under the federally funded National Earthquake Hazards Reduction Program. The purpose of these changes was to provide a more accurate basis for successfully meeting the basic intent of the code. An additional seismic zone change, affecting southern Arizona, was approved in 1992.

Provisions for seismic-resistant design contained in the UBC were developed largely in response to the damage and casualties in past earthquakes. The 1933 Long Beach, 1940 Imperial Valley, 1952 Kern County, and 1971 San Fernando earthquakes made great impressions on code writers and structural engineers. The 1964 Alaska, 1979 Imperial Valley, 1985 Mexico City and 1989 Loma Prieta earthquakes also significantly influenced the thinking of the US structural engineering community regarding building performance.

In all of these earthquakes, buildings collapsed, lives were lost and injuries sustained. However, just as striking to the trained observer, and to building officials and code writers, was the observation that not all buildings collapsed. In fact, in spite of media emphasis on disastrous collapses in every one of these earthquakes, only a small minority of structures failed. And after each of these events, engineers learned valuable lessons and made changes to the building codes. Major improvements to the seismic design provisions were made in 1973 and again in 1988 to incorporate lessons that had been learned.

What has resulted from this series of landmark seismic events is a set of minimum requirements for the design of buildings that are likely to be subjected to seismic ground shaking. For the most part, the seismic design provisions were written by practicing structural engineers, who first looked at the patterns of failure and who then determined which changes in design practice would be necessary to avoid collapse. In many cases, they tried to answer the question of why one type of building failed, and another type directly across the street suffered only minor damage.

The design provisions that resulted were thus "empirical" in nature — as opposed to "rational." This means that they were developed less by the application of scientific principles, and more by judgement based on observation of what "worked" and what didn't work in structures that had been subjected to real earthquakes. The empirical provisions that were developed included requirements for providing minimum levels of strength and stiffness in a structure, and also some very prescriptive requirements governing the details of design and construction and intended to prevent collapse in the largest earthquakes.

Engineers who developed the early seismic provisions were impressed by the observation that many structures would distort, crack, yield and spall. However, as long as no weak links pulled loose or failed prematurely, the buildings, damaged though they might be, did not collapse and the occupants were usually unhurt. They observed that when controlled and distributed, this damage actually appeared to be effective in absorbing the energy of the earthquake, and thus, the damage actually helped prevent collapse and protected building occupants.

Two key conclusions can be drawn from the preceding discussion. These are as follows:

1. The primary intent of seismic design procedures contained in current building codes is to protect the life safety of building occupants.

2. Although seismic-resistant design procedures may reduce the severity of damage in small or moderate earthquakes, they do not prevent buildings from experiencing damage in large earthquakes, but actually presume damage, and indeed, rely upon it for protection of life safety

Reasonable trade-offs between initial cost of construction and damage in relatively rare earthquakes therefore have been a part of code development. The commentary to the Structural Engineers Association of California's booklet upon which the UBC provisions are based (SEAOC, 1988) gives the following expectations of seismic performance of code-designed buildings:

> *Structures designed in conformance with these Recommendations should, in general, be able to:*
>
> 1. *Resist a minor level of earthquake ground motion without damage;*
>
> 2. *Resist a moderate level of earthquake ground motion without structural damage, but possibly experience some nonstructural damage;*
>
> 3. *Resist a major level of earthquake ground motion having an intensity equal to the strongest either experienced or forecast for the building site, without collapse, but possibly with some structural as well as nonstructural damage.*

Although the goal stated above is to protect the life safety in any event that might be expected in California, the variables discussed above will occasionally combine to create a hazardous condition, even for buildings that "meet the code." Although variations in damage between apparently similar buildings are to be expected and forms an important part of an understanding of damage estimations, all variables cannot be considered in a simplified presentation of estimated damage.

The UBC addresses the design of new construction. The primary code does not specifically address the evaluation or the upgrade of older existing buildings in a comprehensive way. Exceptions to this generalization are the provisions contained in the Uniform Code for Building Conservation (ICBO 1991) that prescribe a minimum level of seismic retrofit for unreinforced masonry bearing wall construction. Similar provisions have been adopted by several cities, including Los Angeles. Few other standards exist for upgrading of older buildings.

By a wide consensus, unreinforced masonry (URM) construction, is one of the most dangerous types of construction present in our older cities. Not permitted in the most seismically active areas in California since the 1933 Long Beach earthquake, existing URM buildings, particularly in UBC Seismic Zone 4, must be considered hazardous and their occupants at great risk.

The UCBC-type provisions for the retrofit of existing unreinforced masonry buildings are less stringent requirements than are demanded for new construction, and were developed considering and balancing the expense of retrofit, the value of the existing building stock and the desired reduction in seismic risk. The code for new buildings had been described above as a minimum legal basis for design of buildings—one that provides a reasonable minimum assurance for life safety. The UCBC, therefore, should be expected to provide less than minimum assurance of life safety.

The UCBC-type URM retrofit provisions should, on a statistical basis, result in a major reduction in collapsed buildings and therefore in casualties. Studies have theorized that retrofit to UCBC provisions should reduce casualties by as much as one to two orders of magnitude (factors of 10 to 100). However, not only is there no "guarantee" of protection against damage, there is also no "guarantee" against collapse of individual retrofit URM buildings. The basis commonly used for strengthening URM buildings is thus not totally a "life safety" basis, but may legitimately be called a "risk reduction" basis.

SEISMIC PERFORMANCE ESTIMATIONS

Damage from any one earthquake in the United States has, in general, been highly variable. Buildings are usually found in many different states of damage, even in close proximity. This is because damage to any one building is dependent on many variables. The most obvious is the intensity of the shaking itself. Several factors, in turn, would be expected to affect shaking intensity, primarily the size of the earthquake (normally measured in Richter Magnitude) and the distance from the building to the portion of the fault that moved to cause the earthquake (the origin of which is called the epicenter). However, many other variables—individually or in combination—may also affect shaking as much as these two primary factors. The soil type under the building is now recognized to have a significant effect on shaking. In addition, shaking at a given site can be influenced by local geology and topography, all along the path from the earthquake source to the site.

In addition to variations in shaking itself, characteristics of structures, even of the same age, and designed using the same building code, will have a primary effect on damage levels. Combinations of structural materials (steel, concrete, wood), structural systems (braced frame, shear wall, moment frame), height, and architectural design create an endless variety of buildings; each will possess subtle differences that, when combined with the unique shaking at any one site in a given earthquake, can cause the variety of damage observed. Damage from earthquakes in other countries often leaves an impression of much more consistent damage patterns. This is often because there is far less variation in building shapes and types, and often the seismic resistance of the local construction is so far exceeded that damage is essentially complete. The Tangshan, China earthquake of 1976 destroyed thousands of very similar

unreinforced brick masonry structures, and the Armenia earthquake of 1988 similarly destroyed many poorly reinforced concrete structures. The 1985 earthquake in Mexico City also may have been perceived to create complete destruction, but, in fact, most collapses were all of a similar building type, and all were located over an ancient lake bed; low rise buildings and buildings off the lake bed were practically unaffected.

The extent of damage to buildings can also be affected by the extent of code compliance, plan review, and quality of construction.

In order to present an understandable overview of expected damage to buildings, only the size of earthquake and the approximate distance from the earthquake source will be considered. All buildings are also assumed to be located on an intermediately hard soil—not rock as found in hilly areas, nor soft, saturated soils found near bodies of water.

In order to describe the estimated effect of earthquakes on code-designed buildings with these variations, and also consider the probable variations in damage discussed above, it is necessary to define several standardized states of damage, as shown in Table 1. These descriptions of states of damage do not include detailed conditions of building elements such as columns, beams, and walls, but rather place a building in certain categories with regard to risk of death or injury and the potential for continued use or extent of repair required for the building.

Table 1 - Proposed Damage States

A	No Damage -- could be shifted contents. Only incidental hazard.
B	Minor Damage to nonstructural elements. Building may be temporarily closed but could probably be reopened after minor cleanup in less than 1 week. * Only incidental hazard.
C	Primarily nonstructural damage; also could be minor but non-threatening structural damage; building probably closed for 2-12 weeks. Times are difficult to assign because they are largely dependent on the size of building; remote chance of life threatening situation from nonstructural elements.
D	Extensive structural and nonstructural damage. Long term closure should be expected, either due to amount of repair work or uncertainty on economic feasibility of repair. Localized, life threatening situations would be common.
E	Complete collapse or damage that is not economically repairable. Life threatening situations in every building of this category.

*Times are difficult to assign because they are largely dependent on the size of building.

Damage State A represents essentially no damage, although some amount of internal disruption could always occur due to planters, office furniture, bookshelves, or other items that are free to shift around during shaking. Although essentially no injuries would be expected in these buildings, there is always a remote possibility that shaking objects could shift or topple in such a way as to cause an "incidental" hazard. It would be expected that these buildings could be reused immediately.

Damage State B would include the shifted contents discussed in State A, but in addition some permanent building elements such as ceilings, lighting fixtures, or partitions may be slightly damaged. Damage may require clean-up and minor repair to the extent that the building cannot be normally used immediately. Only incidental hazard to occupants could be expected.

Buildings in Damage State C would suffer more extensive damage to internal elements, and may also have minor structural damage such as cracks in concrete or masonry walls. However, the building would not be considered in any danger of structural failure, but a slight risk of injury would be presented by fallen ceilings, light fixtures, or other equipment. The damage would be sufficient to require repair, and the building could be partially or completely closed by the Building Department pending repairs. Partial closure would be expected in any case while repairs and clean-up are completed. Photographs 1 and 2 show the type of damage that may be characteristic in State C.

Damage to structural elements of the building such as walls, columns and beams would be expected in Damage State D. Buildings may be leaning or certain floor levels may be out-of-plumb. Internal elements may be damaged beyond repair. These buildings would be closed by the building department until structural repairs are completed. Occupants or passersby may have been injured or killed by falling debris. Owners of buildings that have been damaged this severely often must wait for engineering and economic studies to be completed to determine if it is economically justifiable to repair the building or whether to simply demolish it. See Photographs 3 and 4.

Damage State E includes both collapsed buildings and those that are so severely damaged that repair is clearly uneconomical. Life-threatening situations caused by falling internal elements or collapsing floors would occur in every building in this category. Damage state E is shown in Photographs 5 and 6. Because of the many controls placed in the code for new buildings aimed directly at preventing collapse, this damage state is expected to occur only rarely.

The number of buildings in each damage state will vary with the intensity of shaking. The intensity of shaking, in turn, is primarily dependent on the size of the earthquake and the distance from the fault which has slipped. A subjective measurement used by earthquake engineers that describes the shaking intensity in any particular area is the Modified Mercalli Intensity (MMI) scale as shown in Table 2. As can be seen, MMI levels are indicated by Roman numerals and are determined by what damage the shaking has caused. The standard MMI levels were set by investigation and comparison of similar patterns in many earthquakes. Richter magnitude, on the other hand, is a characteristic of the earthquake itself and does not vary from place to place. Studies of the patterns of MMI on past earthquakes allow engineers to estimate what MMI might be expected at various distances from future earthquakes of

PHOTOGRAPHS 1 AND 2

DAMAGE STATE C

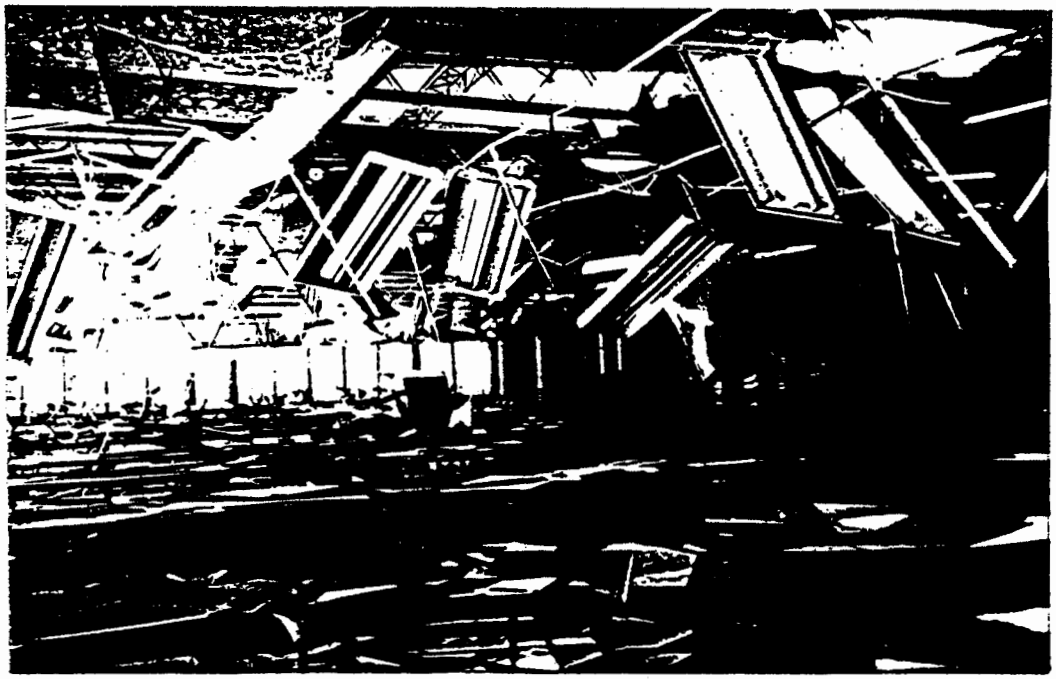

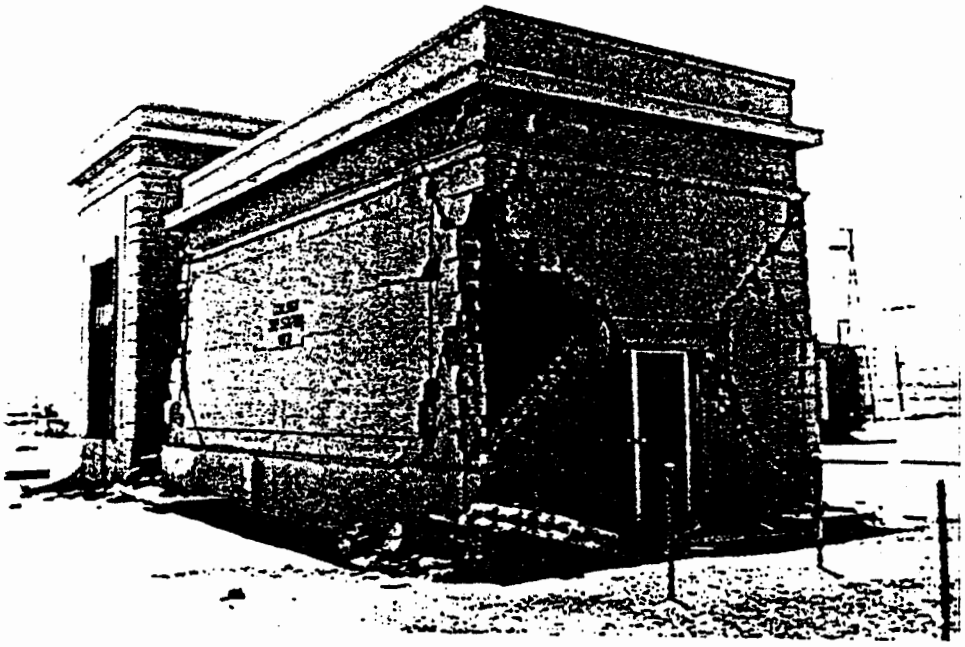

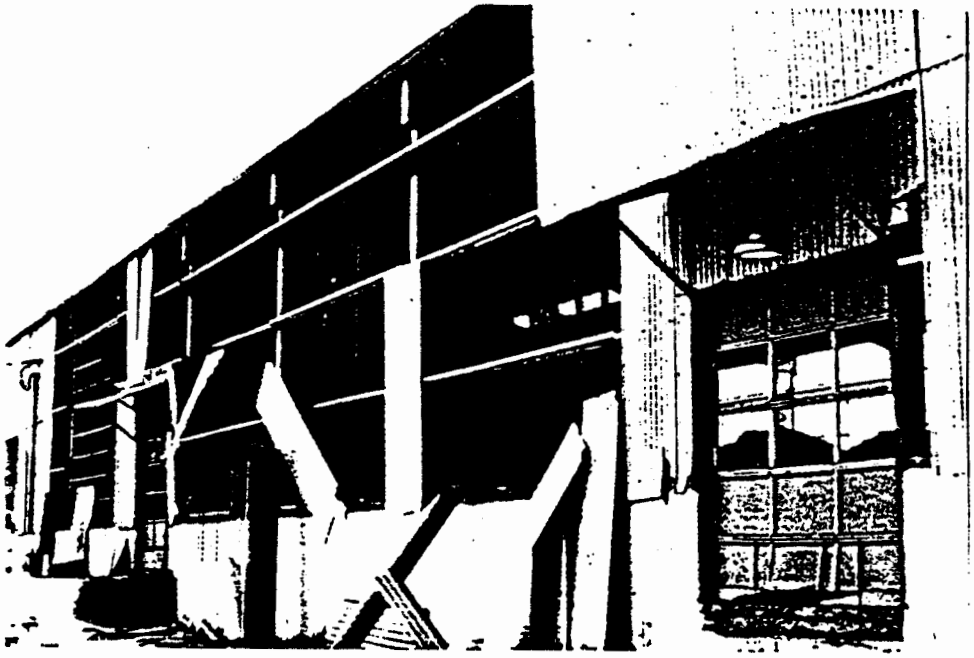

PHOTOGRAPHS 3 AND 4
DAMAGE STATE D

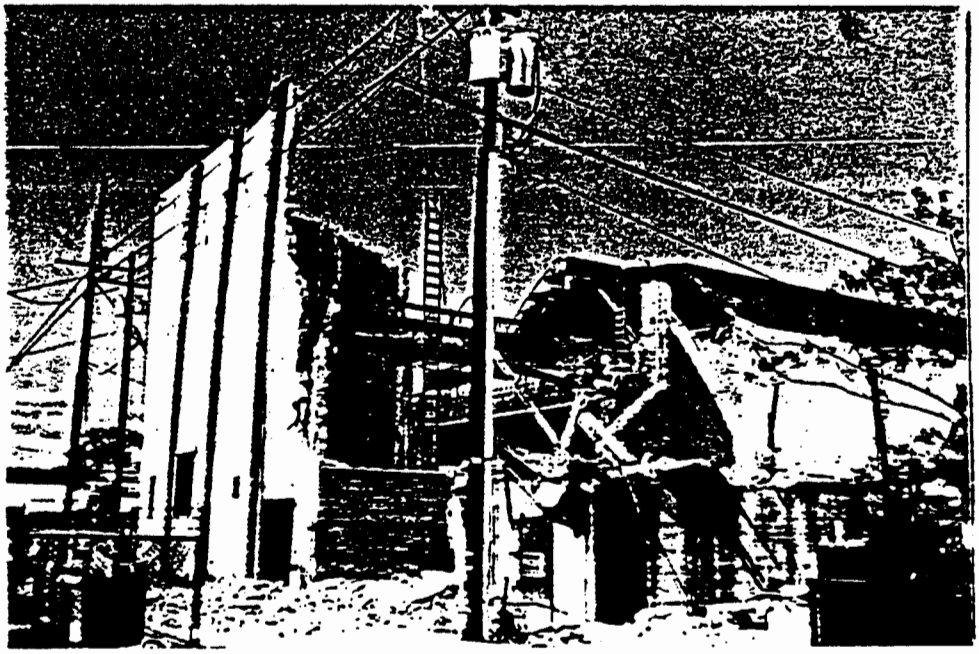

PHOTOGRAPHS 5 AND 6
DAMAGE STATE E

TABLE 2

MODIFIED MERCALLI INTENSITY SCALE

The severity of an earthquake is described by the Modified Mercalli Intensity scale introduced in 1931 by American seismologists Harry Wood and Frank Neumann. They established 12 categories of intensity. The following is a condensed version:

I	Not felt except by a very few under favorable circumstances.
II	Felt only by a few persons at rest, especially on the upper floors of buildings. Suspended objects may swing.
III	Felt quite noticeably indoors, especially on upper floors of buildings, but not necessarily recognized as an earthquake. Standing cars may rock slightly. Vibration similar to that of a passing truck.
IV	If during the day, felt indoors by many, outdoors by few. If at night, few awakened. Dishes, windows, and doors rattle, walls creak. A sensation such as a heavy truck striking the building. Standing cars rock noticeably.
V	Felt by nearly everyone, many awakened. Some dishes and windows broken, some plaster cracked, unstable objects overturned. Disturbance of trees, poles, and other tall objects. Pendulum clocks may stop.
VI	Felt by all, many people run outdoors. Fallen plaster, minor chimney damage. Movement of moderately heavy furniture.
VII	Everybody runs outdoors. Damage negligible in buildings of good design and construction, slight to moderate in well-built ordinary structures, considerable in poorly built or badly designed structures. Some chimneys broken. Noticed by persons driving cars.
VIII	Damage slight in specially designed structures, considerable in ordinary substantial buildings. Panel walls thrown out of frame structures. Chimneys, factory stacks, monuments, walls, and columns fall. Heavy furniture overturned and damaged. Changes in well water. Sand and mud ejected in small amounts. Persons driving cars are disturbed.
IX	Damage considerable in specially designed structures, well-designed frame structures thrown out of plumb, great damage in substantial buildings, which suffer partial collapse. Buildings shifted off foundations, ground noticeably cracked, underground pipes broken.
X	Some well-built wooden structures destroyed, most masonry structures destroyed, foundations ruined, ground badly cracked. Rails bent. Considerable landslides from steep slopes and river banks. Water splashed over banks. Shifted sand and mud.
XI	Few, if any, masonry structures remain standing. Bridges destroyed. Broad fissures in ground. Underground pipes out of service. Earth slumps and landslips in soft ground. Rails bent greatly.
XII	Total damage. Waves seen on ground surfaces. Lines of sight and level are distorted. Objects thrown into the air.

Wood, H.O., and Neumann, Frank, 1931, Modified Mercalli Intensity scale of 1931: Bulletin of the Seismological Society of America, v. 20, p. 277-283.

different sizes. Figure 2, for example, shows the shaking intensities that occurred for a magnitude 7.1 earthquake on the San Andreas fault in Northern California in 1989. If a certain MMI is expected for firm soil in a given area, the presence of soft soils at a site could increase the intensity by an entire MMI level, or more.

Table 3 relates damage expected for buildings designed in accordance to the 1991 UBC for various shaking intensities. Also shown in the table are examples of Richter magnitudes and distances which might produce the given MMI on sites of moderate and firm ground. The values shown in the table are percentages of buildings that are expected to be in each damage state, assuming all building in the area are designed in accordance with the 1991 UBC. Because of the variations in damage between building and structural types and lack of data upon which to base precise numbers, the values are given in ranges. However, Table 3 should provide a rough picture of the damage patterns for various conditions.

TABLE 3

Expected Damage to Buildings (in percent of buildings) Designed in Accordance with the 1991 UBC

			DAMAGE STATE				
MMI	EQ Size in Richter Magnitude		A	B	C	D	E
	6.0-6.5	7.5-8.0					
	Distance						
VII	30 mi.	50 mi.	60-90	10-40	1-5	< 1	0
VIII	3 mi.	40 mi.	35-60	35-45	10-30	1-5	0-1
IX	1 mi.	30 mi.	25-40	25-40	20-40	3-10	0-2
- X	-----	3 mi.	7-25	7-25	40-70	10-30	0-5

Table 4 presents similar information for unreinforced masonry buildings originally built between about 1870 and 1935 and seismically strengthened in accordance with the requirement for such buildings in the Uniform Code for Building Conservation. It will be noted that damage to these URM buildings is projected to be considerably higher than for new buildings. The benefit to retrofit cost relationships considered in the development of this code, as well as the inherent unknown quality of these older buildings accounts for these differences.

FIGURE 2

Preliminary Map Showing the Distribution of Modified Mercalli Intensity for the 1989 Loma Prieta Earthquake

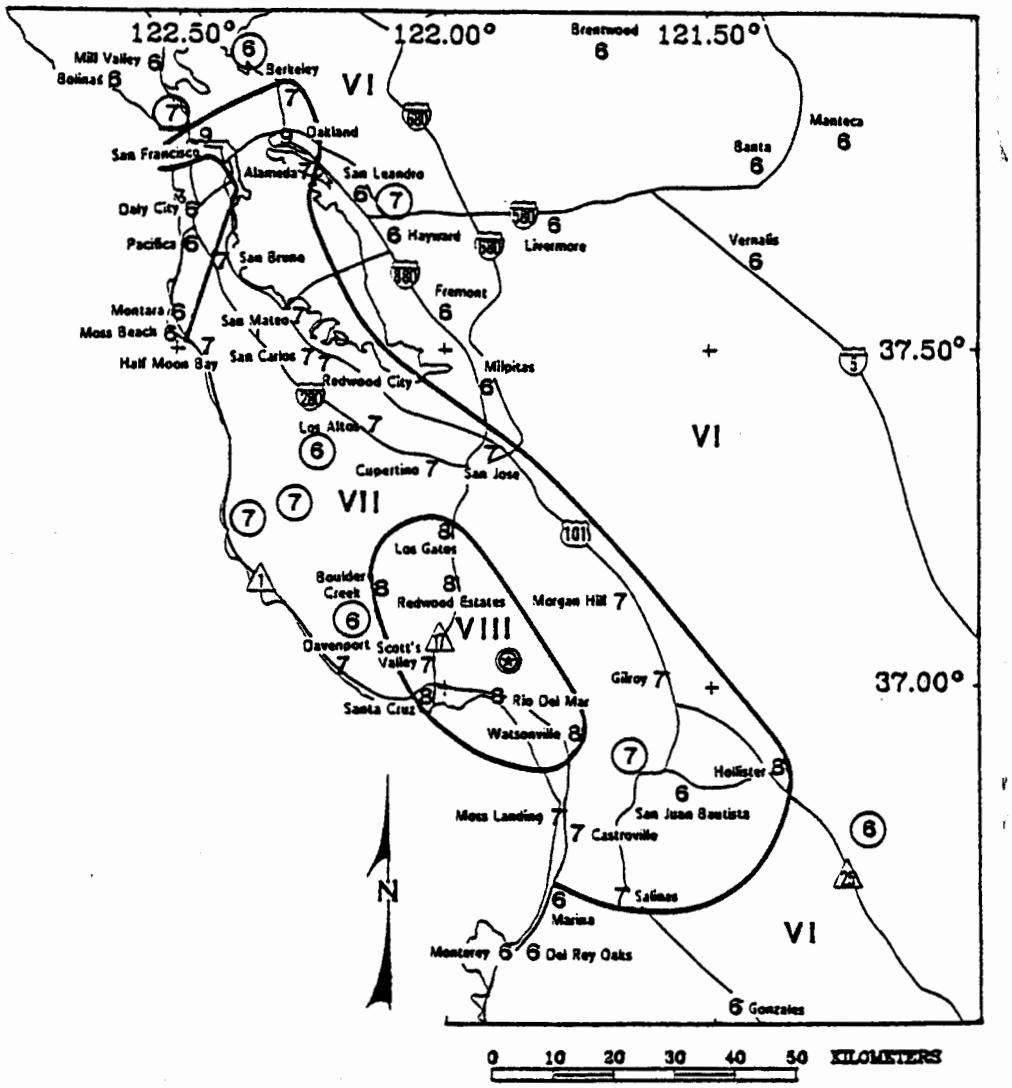

Roman numerals represent the intensity level between isoseismal lines. Location of the earthquake epicenter is shown by the circled star. Numbers enclosed in circles have been added since original publication. (Pflaker and Galloway, 1989)

TABLE 4

Retrofitted URM

Expected Damage to Buildings (in percent of buildings)
Retrofitted in Accordance with the 1991 UCBC

MMI	EQ Size in Richter Magnitude		DAMAGE STATE A	B	C	D	E
	6.0-6.5	7.5-8.0					
	Distance						
VII	30 mi.	50 mi.	50	30	15	5	< 1
VIII	3 mi.	40 mi.	20	20	25	30	5
IX	1 mi.	30 mi.	3	7	30	50	10
X	-----	3 mi.	< 1	5	15	60	20

Earthquakes occur infrequently, and detailed damage statistics are expensive to collect. The estimates given here are based on the best judgement of a group of structural engineers experienced in earthquake investigations and in writing building codes. An ad hoc group was formed at the request of the Earthquake Engineering Research Institute by the Structural Engineers Association of California (SEAOC) for the purpose of estimating building performance for use in this publication. The original raw data generated by the SEAOC group were combined and slightly modified by EERI for ease of presentation. The damage estimates shown in Tables 3 and 4 do not represent an official position of the Structural Engineers Association of California. The raw data originally proposed by the SEAOC group by building type are given in Appendix A.

APPENDIX

The development of accurate damage statistics for buildings constructed to the 1991 UBC or retrofitted to the 1991 UCBC is a very difficult task. Few of these buildings have been subjected to earthquakes, and even less have experienced earthquakes of moderate or large magnitude. Thus there is insufficient damage data available to perform meaningful statistical analyses. Furthermore, most of the data that has been collected is descriptive of the type of damage without any quantification of the level of damage. Often available damage data omits essential information such as structural type, year of construction, and site location. Thus most of the available damage data have deficiencies that preclude their use in any meaningful analysis.

In light of the above mentioned problems, the EERI Committee on Seismic Performance solicited expert opinion with respect to damage statistics for eight building types when subjected to different levels of ground shaking. The experts consisted of 7 experienced structural engineers who met for a one day workshop to gain consensus on their opinions. The experts were contacted with the help of SEAOC. Their names are found in Table A1. The experts were given background information before the workshop, such as the purpose of the resulting white paper, damage probability matrices from ATC-13, and limited descriptions of damage states, building types and earthquake size.

Table A1 - Experts Solicited for Damage Statistics

Eugene Cole
Ronald Gallagher
Edwin Johnson
Melvyn Mark
Donald Strand
Thomas Wosser
Nabih Youssef

The experts were asked to describe damage using the five damage states, A through E, described earlier in this document. However, the experts felt that it was difficult to distinguish between states A and B, and thus they combined these two damage states in developing their consensus opinion. The descriptions of the damage states as modified by the experts are listed in Table A2. The consensus opinions of the experts without modification are found in Tables A3 through A10 shown below.

Several modifications to the expert opinion were made in formulating the ranges of expected damage to buildings found in Tables 3 and 4 of the text. Keeping in mind that the statistics developed by the experts are rough estimates, the EERI Committee on Seismic Performance felt that the modifications would not affect the credibility of the results.

First, the damage statistics for all buildings designed to the 1991 UBC (Table A3-A9) were combined. The ranges in Table 3 of the text consist of using the lowest and highest values of Tables A3 to A9. Secondly, the combined damage states A and B were separated. In most cases it was assumed that half of the buildings would be in state A and half in state B. However, for low-rise wood frame structures subjected to less intense shaking, it was felt that a significant portion of these buildings would end up in State A. Thirdly, UBC 91 buildings, damage statistics for MMI VII were generated by combining the expert opinion

with the judgment of the EERI committee. Finally, damage states A and B were separated for retrofitted URM buildings using the judgment of the EERI committee...

Table A2 - Descriptions of Damage States as Modified by Experts

Damage State	Description	Damage
A & B	No damage or minor damage to nonstructural elements. Only incidental hazard.	<1%
C	Primarily nonstructural damage; also could be minor non-threatening structural damage. Remote chance of life threatening situation from structural elements	<5%
D	Extensive structural and nonstructural damage. Localized, life threatening situations would be common.	<30%
E	Complete collapse or damage that is not economically repairable. Life threatening situations in every building of this category	100%

Tables A3-A10 - Percent of Buildings Damaged vs. MMI

(A3) High-rise moment frame ('91 UBC)

Damage Category	Percent of Buildings (%) VIII	IX	X
A & B	90	70	50
C	10	30	40
D	1	3	10
E	<1	<1	<1

(A4) Mid-rise moment frame ('91 UBC)

Damage Category	Percent of Buildings (%) VIII	IX	X
A & B	70	50	15
C	30	40	70
D	2	5	15
E	<1	<1	<2

(A5) Mid-rise concrete shear walls ('91 UBC)

Damage Category	Percent of Buildings (%) VIII	IX	X
A & B	90	70	40
C	10	30	50
D	2	5	10
E	<1	<1	<1

(A6) Low-rise steel frame ('91 UBC)

Damage Category	Percent of Buildings (%) VIII	IX	X
A & B	90	50	20
C	10	40	60
D	1	5	20
E	<1	<1	<1

(A7) Tilt-up and low-rise concrete block ('91 UBC)

Damage Category	Percent of Buildings (%) VIII	IX	X
A & B	75	60	25
C	20	30	40
D	5	10	30
E	1	2	5

(A8) Low-rise wood frame ('91 UBC)

Damage Category	Percent of Buildings (%) VIII	IX	X
A & B	90	75	50
C	10	20	40
D	1	5	10
E	<1	<1	<1

(A9) Mid-rise reinforced masonry ('91 UBC)

Damage Category	Percent of Buildings (%) VIII	IX	X
A & B	80	60	25
C	15	30	50
D	5	10	20
E	1	2	<5

(A10) Retrofitted URM ('91 UCBC)

Damage Category	Percent of Buildings (%) VII	VIII	IX	X
A & B	80	40	10	5
C	15	25	30	15
D	5	30	50	60
E	<1	5	10	20

ANALYSIS OF RECORDS FROM FOUR BASE-ISOLATED BUILDINGS DURING THE 1992 LANDERS EARTHQUAKE

M.J. Huang, P.K. Malhotra and A.F. Shakal

California Strong Motion Instrumentation Program
Division of Mines and Geology
California Department of Conservation

ABSTRACT

Strong-motion records were obtained from four base-isolated buildings during the 1992 Landers earthquake. The buildings are 2, 5, 8, and 9 stories in height. The distances from these buildings to the Landers earthquake range from 106 to 163 km. The peak accelerations at the foundation level of the buildings were between 0.04 g and 0.11 g. The acceleration responses of the buildings were as high as 0.19 g at the roof.

For each building, the drifts between the roof and the base of the superstructure and the relative displacements across the isolators were derived from the Landers earthquake records. The results show that the 2-story building had negligible drift and its structure above the isolator responded almost like a rigid body during the Landers earthquake. On the other hand, the superstructure drifts for the other three buildings were not negligible. The deformations of the isolators for these four buildings range from 0.8 to 1.6 cm, which are much smaller than the design values (25 to 40 cm), and the fundamental periods are slightly longer than the fixed-base periods.

INTRODUCTION

Four instrumented base-isolated buildings in California are part of the strong motion network of the California Strong Motion Instrumentation Program (CSMIP) in the Division of Mines and Geology of the California Department of Conservation. All four buildings have experienced low levels of earthquake ground shaking. The locations of these four buildings and the epicenters of three recent earthquakes are shown in Figure 1. The most significant earthquake recorded at these building is the magnitude 7.5 Landers earthquake of June 28, 1992. The distances of the buildings to the Landers epicenter range from 106 to 163 km. Although the peak accelerations in the Landers earthquake are similar to those recorded from other earthquakes, the duration of shaking is much longer than in any of the other records obtained at these buildings.

The Landers strong-motion records are analyzed and presented in this paper. A comparison is made between the responses of these four base-isolated buildings to the Landers earthquake. The responses compared include the periods of vibration, the displacements across the isolator bearings, and the drifts of the superstructures.

DESCRIPTION AND INSTRUMENTATION OF BUILDINGS

1) Rancho Cucamonga - 4-story Law & Justice Building. The San Bernardino County Law and Justice building in Rancho Cucamonga is a 5-story structure and is the first building constructed using a base-isolation system in the United States. The building is 414 by 110 feet in plan and 74 feet in height from the basement to the roof. The lateral force-resisting system of the superstructure consists of 4-story braced steel frames in the upper four stories and concrete shear walls in the basement. The structure is isolated by elastomeric bearings placed on the foundation under each of the 98 columns. More detailed information on the base isolation system used in this building is given in Tarics et al. (1984).

   The Law and Justice Building was instrumented by CSMIP in 1985 with 16 accelerometers in the building and 3 at a reference free-field site. The locations of the accelerometers are shown schematically in Figure 2. Since 1985, low-level strong-motion records from seven earthquakes have been obtained at this building. The first records from the 1985 Redlands earthquake were discussed in Huang et al. (1986). The closest earthquake is the magnitude 5.5 Upland earthquake and the farthest earthquake is the magnitude 7.5 Landers earthquake.

2) Los Angeles - 2-story Fire Command and Control Building. The Los Angeles County Fire Department's Fire Command and Control Building is a base-isolated 2-story structure which has a plan dimension of 188 by 84 feet. The lateral force-resisting system consists of perimeter braced steel frames supported by isolation bearings under all 32 columns. The isolators have a restraint system to control the uplift and the horizontal displacement across the bearings. Detailed information on the building is given in Bachman et al. (1990) and Anderson (1990).

   The Fire Command and Control Building was instrumented by CSMIP in 1990 with 16 sensors in the building and 3 at a reference free-field site. The locations of the sensors are shown schematically in Figure 4.

3) Los Angeles - 7-story University Hospital. The USC University Hospital is a 7-story steel braced frame building with a 1-story basement. The floor plan is quite irregular and has two wings connected by a narrow section. The seismic isolation system consists of 68 lead-rubber isolators and 81 elastomeric isolators. Most of the lead-rubber isolators are located under the perimeter frame. Detailed information on the building is given in Asher et al. (1990).

   The University Hospital was instrumented with assistance from CSMIP in 1991. The locations of the 24 accelerometers in the building and three at a reference free-field site are shown in Figure 6.

4) Seal Beach - 8-story Office Building. The Seal Beach Office Building is a 8-story non-ductile concrete frame structure. The building was built in 1967 and was seismically strengthened in 1990 by installing isolators at the ground floor level and adding new exterior frames with supporting foundation. The 26 interior and four corner columns have one isolator

per column. The remaining 24 exterior columns have two isolators each. Detailed information on the building is given in Hart et al. (1990) and Sveinsson et al. (1990).

The Seal Beach Office Building was instrumented by CSMIP before and after the seismic strengthening was completed in 1991. The locations of the 22 accelerometers in the building and 9 outside the building are shown in Figure 8.

RECORDED STRONG-MOTION DATA

Accelerations

Strong-motion records obtained from four base-isolated buildings are summarized in Table 1. Peak accelerations recorded at the foundation level (below the isolators), the base level (above the isolators) and the roof level are listed in the table. The 1991 Sierra Madre, the 1992 Landers and the 1992 Big Bear earthquakes were recorded at all four buildings. In addition to these three earthquakes, the Rancho Cucamonga building recorded four earlier earthquakes.

The acceleration records obtained from four base-isolated buildings during the 1992 Landers earthquake are included in the CSMIP data report by Shakal et al. (1992). Portions of the acceleration records from selected sensors in the transverse direction are shown in Figure 3 for the Rancho Cucamonga Building and Figure 5 for the Fire Command Building. Similarly, Figure 7 shows records for the University Hospital and Figure 9 for the Seal Beach Office Building.

Comparison of the acceleration across the isolators for each building shows that relatively high frequency horizontal motions were filtered out by the isolators. Significant amplifications of the motions from the base of the superstructure to the roof can be seen in all except in the Fire Command Building. As shown in Figure 5, the motions at the roof, the 2nd floor level and the base of the Fire Command Building are almost identical, which indicates that the building superstructure responded like a rigid body above the isolators.

Differencing the records from a pair of parallel horizontal sensors on the same floor allows estimation of the torsional motion at the floor. The results show that significant torsional motions occurred at the Rancho Cucamonga Building. On the other hand, rigid body rotation of the entire superstructure above the isolators, which does not cause torsional deformation of the superstructure, is significant for the Fire Command Building.

Relative Displacements

To show the drift of the superstructure, the computed displacements of the upper floors relative to the base (above the isolators) are plotted in Figures 10 through 13. The deformation of the isolators for each building is shown by the displacement of the base relative to the foundation, also plotted in these figures. The deformation of the isolators ranges from 0.8 to 1.6 cm, which is much smaller than the design value that ranges from 25 to 40 cm. As

shown in Figure 11, the superstructure of the Fire Command Building had negligible drift and most deformation occurred at the isolators. The same results are also seen in the Sierra Madre earthquake record for this building.

Profiles of the maximum displacement at each floor level relative to the foundation are plotted in Figure 14. The deformations of the isolators during the Landers earthquake are about the same for all four buildings. The superstructure of the Fire Command Building responded as a rigid body although the isolator deformations were much smaller than the design values.

The hysteretic response of the isolators at the Fire Command Building can be investigated from the lateral force versus relative displacement diagram. Since the building responded as a rigid body, the lateral force (or the base shear) experienced by the isolator is proportional to the acceleration recorded by Sensor 9, directly above the isolator. The relative displacement across the isolator, computed from the motions recorded by Sensors 9 and 6, is shown in Figure 11. The hysteresis loops corresponding to small motions, from 17 to 20 seconds, and large motions, from 29 to 32 seconds, are shown in Figure 15. The reduction of the stiffness of the isolator at large response can be seen in this figure. The equivalent viscous damping ratio calculated from the loop is about 10%.

Periods of Vibration

Periods of the fundamental mode are estimated from the records and are compared with the periods for the fixed-base structure (without isolators) and the design periods for the entire structure with isolators in Table 2. The periods during earthquakes were estimated from the portions of the records where the maximum response occurred. The fixed-base periods were obtained from either ambient measurements or computer modelling by the design engineers. As shown in Table 2, the vibration periods during the Landers earthquake are only slightly larger than the fixed-base periods. This is expected since the deformations of the isolators were much smaller than the design values.

SUMMARY

The records obtained at four base-isolated buildings during the 1992 Landers earthquake provide valuable information on the response of four different base-isolated structural systems to low-level shaking. Although the motions were of low amplitude, the 2-story Fire Command and Control Building responded as the designer expected for a stronger shaking. The design assumptions and numerical modelling for these buildings can be verified by using and analyzing these records in greater detail. The complete results of processing the records from these buildings during the Landers earthquake are available on floppy disks and in a report by Darragh et al. (1993).

REFERENCES

Anderson, T., 1990, "Seismic Isolation Design and Construction Practice," Proceedings of Fourth U.S. National Conference on Earthquake Engineering, 1990, Palm Springs, Vol. 3, pp. 519-528.

Asher, J., Van Volkinburg, D., Mayes, R., Kelly, T., Sveinsson, B. and Hussain, S., 1990, "Seismic Isolation Design of the USC University Hospital," Proceedings of Fourth U.S. National Conference on Earthquake Engineering, 1990, Palm Springs, Vol. 3, pp. 529-538.

Bachman, R., Gomez, M. and Chang, K., 1990, "Verification Analysis of the Base Isolated Los Angeles County Fire Command and Control Facility," Proceedings of Fourth U.S. National Conference on Earthquake Engineering, 1990, Palm Springs, Vol. 3, pp. 539-548.

Darragh, R., Cao, T., Huang, M. and Shakal, A., 1993, "Processed CSMIP Strong-Motion Records from Base-Isolated Buildings for the Landers, California Earthquake of 28 June 1992," California Strong Motion Instrumentation Program, Report No. OSMS 93-02, in preparation.

Hart, G., Gates, W., Drag, D., Wallace, W., Mehrain, M. and Elmlinger, J., 1990, "Seismic Strengthening of a Tall Building Incorporating Base Isolation," Proceedings of Fourth U.S. National Conference on Earthquake Engineering, 1990, Palm Springs, Vol. 3, pp. 333-342.

Huang, M., Shakal, A. and Ragsdale, J., 1986, "Recorded Motion of a Base-Isolated Building during the 1985 Redlands Earthquake," Proceedings of ATC-17 Seminar and Workshop on Base Isolation and Passive Energy Dissipation, 1986, San Francisco, pp. 93-102.

Shakal, A., Huang, M., Cao, T., Sherburne, R., Sydnor, R., Fung, P., Malhotra, P., Cramer, C., Su, F., Darragh, R. and Wample, J., 1992, "CSMIP Strong-Motion Records from the Landers, California Earthquake of 28 June 1992," California Strong Motion Instrumentation Program, Report No. OSMS 92-09, August 1992.

Sveinsson, B., Ewing, R., Mayes, R., Hart, G. and Elhassan, R., 1990, "Seismic Isolation Analysis of an Existing Eight-Story Building," Proceedings of Fourth U.S. National Conference on Earthquake Engineering, 1990, Palm Springs, Vol. 3, pp. 589-598.

Tarics, A., Way, D. and Kelly, J., 1984, "The Implementation of Base Isolation for Foothill Communities Law and Justice Center," Report to the National Science Foundation and the County of San Bernardino, 1984.

Table 1 - Strong-Motion Records Obtained From Base-Isolated Buildings

Name of Building	Type of Superstructure	Max. Horiz. Accel.(g) Foundation	Base	Roof	Earthquake	Epicentral Distance(km)
Rancho Cucamonga - 4-story Law & Justice Center (CSMIP Sta. No. 23497)	Braced steel frame (19 sensors)	0.03	0.02	0.03	10/02/86 Redlands M=4.8	30
		0.02	0.02	0.05	07/08/86 Palm Springs M=5.9	90
		0.03	0.03	0.06	10/01/87 Whittier M=5.9	47
		0.14	0.05	0.16	02/28/90 Upland M=5.5	12
		0.03	0.04	0.08	06/28/91 Sierra Madre M=5.8	43
		0.11	0.10	0.19	06/28/92 Landers M=7.4	106
		0.06	0.05	0.07	06/28/92 Big Bear M=6.4	70
Los Angeles - 2-story Fire Command/Control Bldg. (CSMIP Sta. No. 24580)	Braced steel frame (19 sensors)	0.08	0.09	0.11	06/28/91 Sierra Madre M=5.8	28
		0.05	0.08	0.12	06/28/92 Landers M=7.4	161
		0.05	0.05	0.05	06/28/92 Big Bear M=6.4	125
Los Angeles - 7-story University Hospital (CSMIP Sta. No. 24605)	Braced steel frame (27 sensors)	0.09	0.05	0.09	06/28/91 Sierra Madre M=5.8	29
		0.04	0.09	0.09	06/28/92 Landers M=7.4	163
		0.05	0.03	0.06	06/28/92 Big Bear M=6.4	127
Seal Beach - 8-story Office Bldg. (CSMIP Sta. No. 14578)	Concrete moment frame (31 sensors)	0.02	0.02	0.03	06/28/91 Sierra Madre M=5.8	57
		0.04	0.09	0.09	06/28/92 Landers M=7.4	160
		0.04	0.05	0.08	06/28/92 Big Bear M=6.4	126

Table 2 - Fundamental Periods of Base-Isolated Buildings

Name of Building	Periods (in seconds) of the Fundamental Mode Transverse	Longitudinal	Torsional
Rancho Cucamonga - 4-story Law & Justice Center			
Without Isolators (fixed base)	0.57	0.61	0.49
1990 Upland	0.75	0.74	---
1992 Landers	0.73	0.76	---
With Isolators (design)	2.00	2.00	---
Los Angeles - 2-story Fire Command/Control Bldg.			
Without Isolators (fixed base)	0.36	0.32	0.13
1991 Sierra Madre	0.91	0.86	---
1992 Landers	1.05	1.00	1.05
With Isolators (design)	2.17	2.17	1.85
Los Angeles - 7-story University Hospital			
Without Isolators (fixed base)	1.0	1.0	---
1992 Landers	1.28	1.24	---
With Isolators (design)	2.21	2.30	1.92
Seal Beach - 8-story Office Bldg.			
Without Isolators (fixed base)	1.1	1.1	---
1992 Landers	1.48	1.36	---
With Isolators (design)	2.75	2.75	---

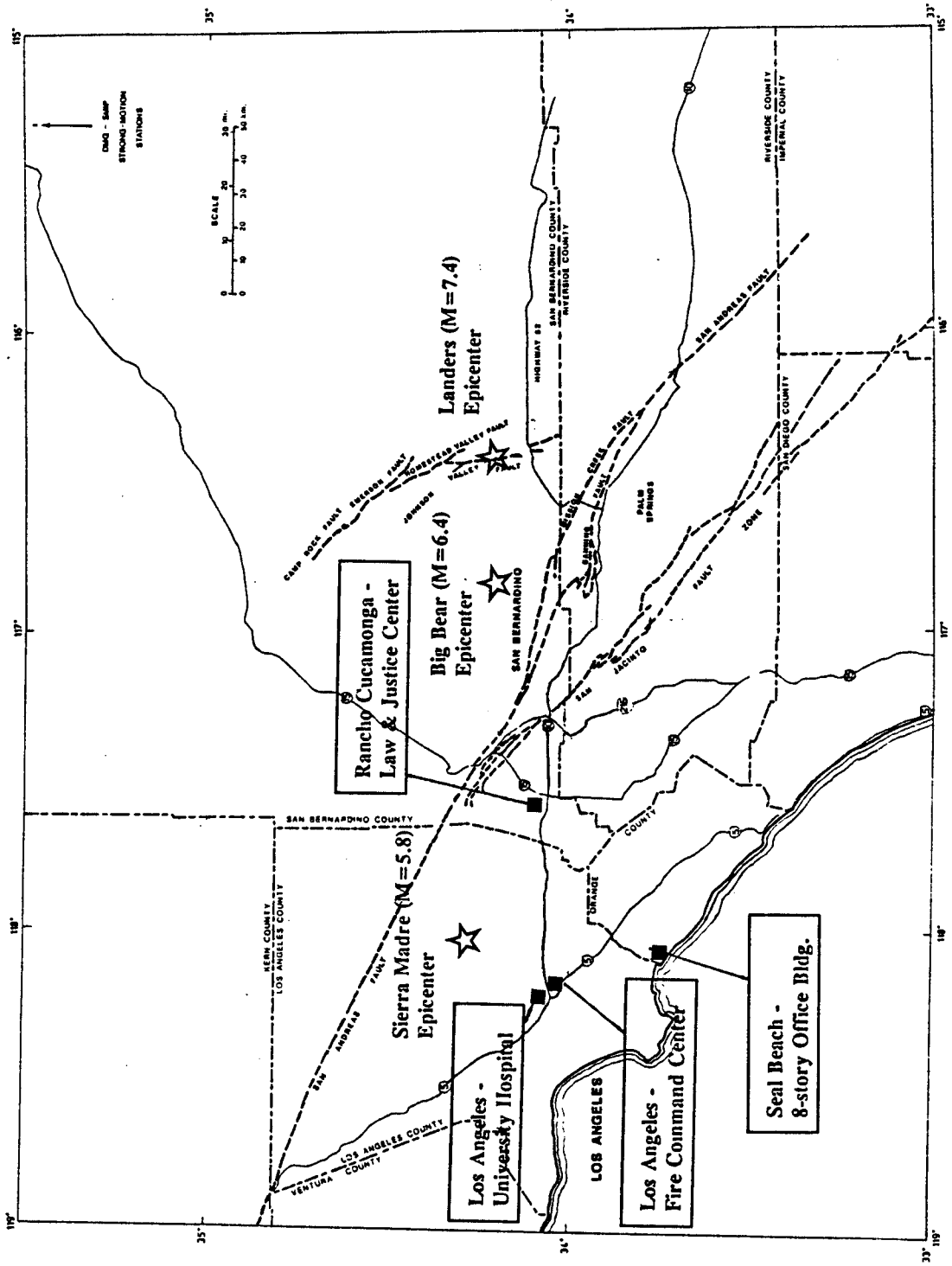

Fig. 1. Map showing locations of four base-isolated buildings and the epicenters of the 1992 Landers, the 1992 Big Bear and the 1991 Sierra Madre earthquakes. These three earthquakes were recorded at all four buildings.

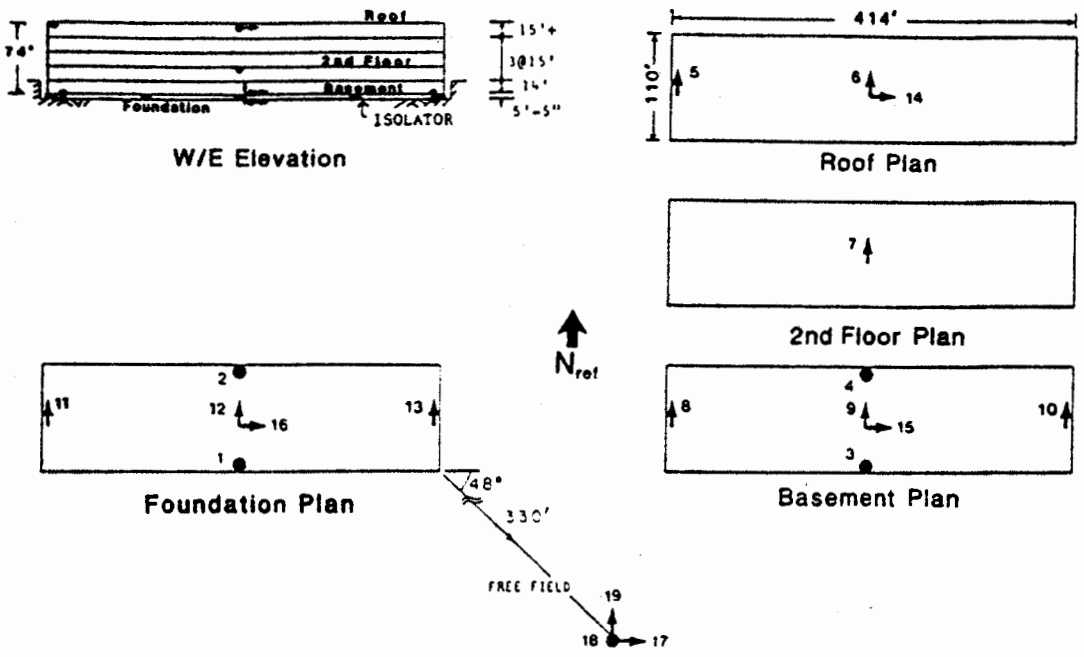

Fig. 2. Locations of accelerometers in San Bernardino County's Rancho Cucamonga Law and Justice Building.

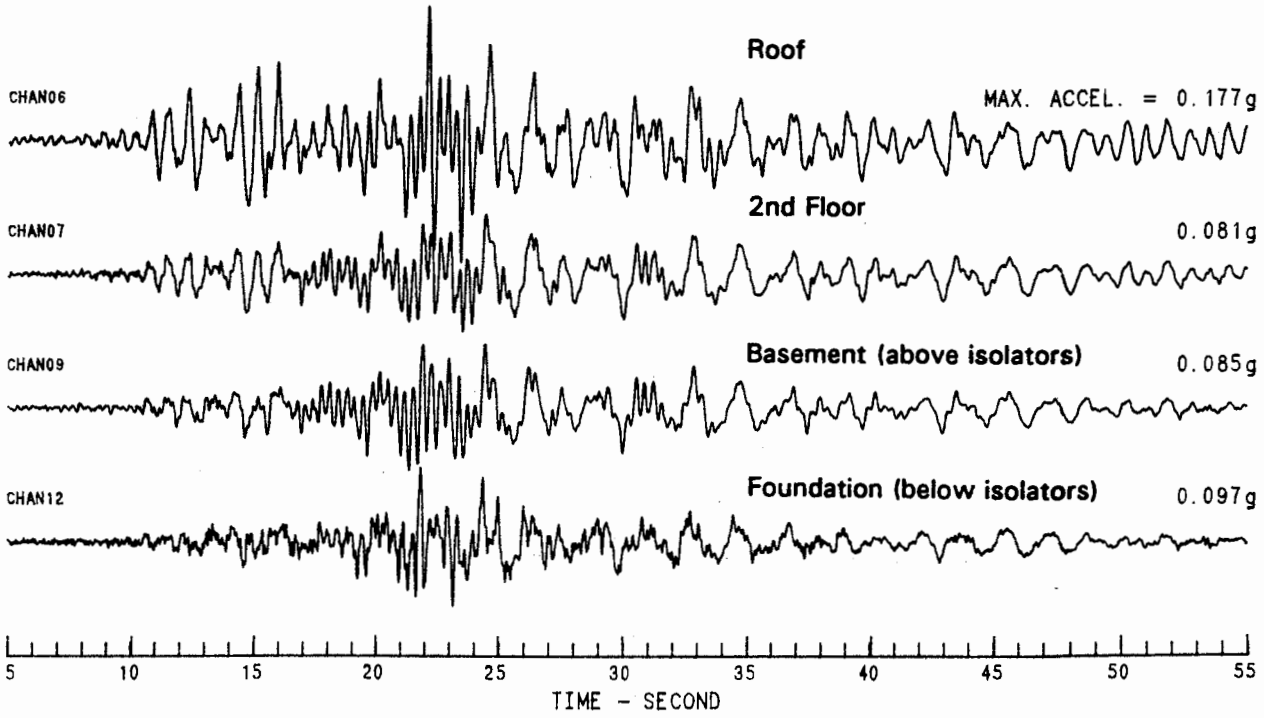

Fig. 3. Acceleration records in the transverse direction obtained at the Rancho Cucamonga Law & Justice Bldg. during the 1992 Landers earthquake.

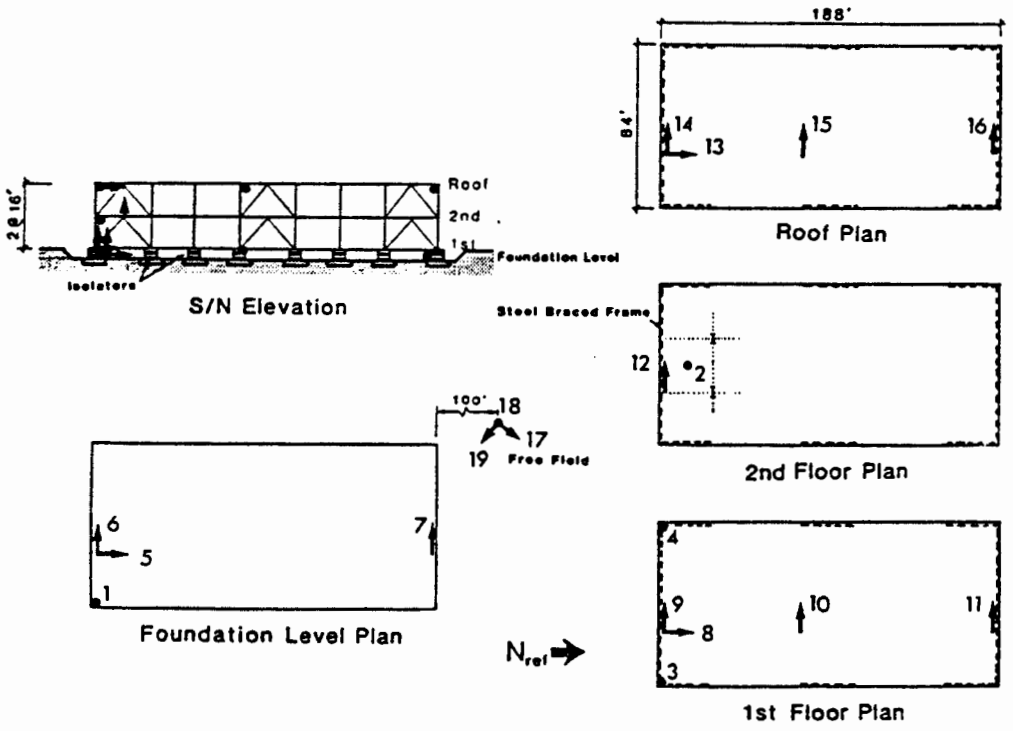

Fig. 4. Locations of accelerometers in the Los Angeles County Fire Control and Command Building.

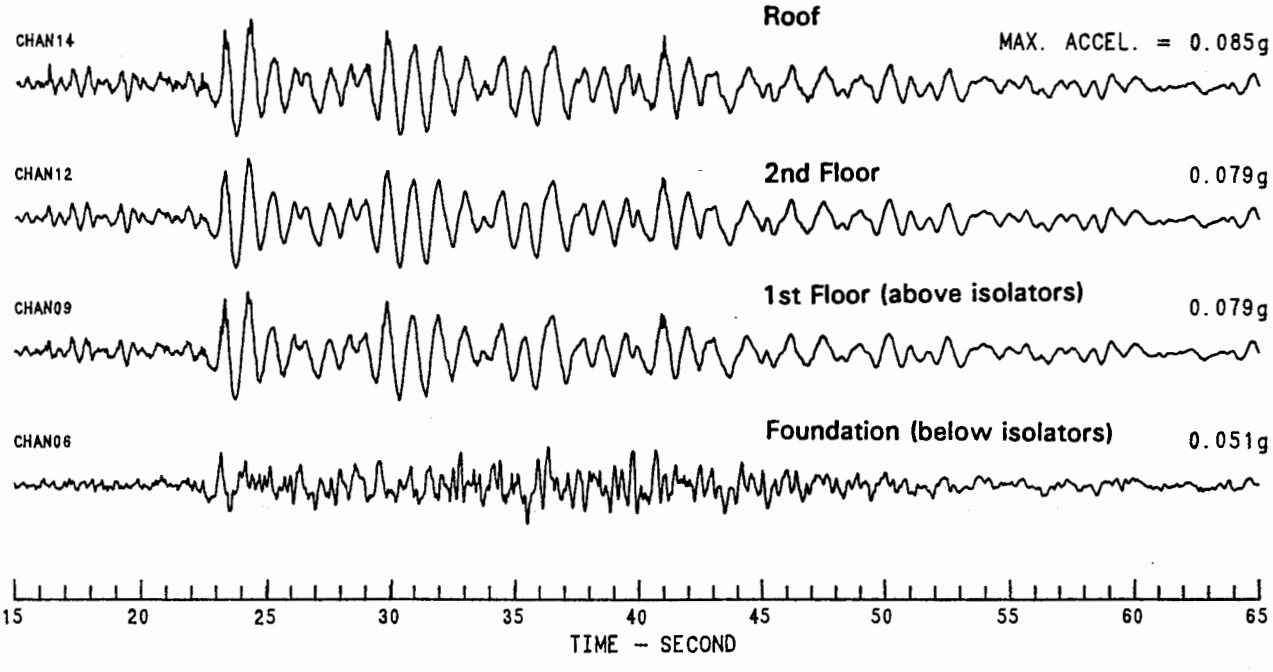

Fig. 5. Acceleration records in the transverse direction obtained at the Los Angeles County Fire Command Bldg. during the 1992 Landers earthquake.

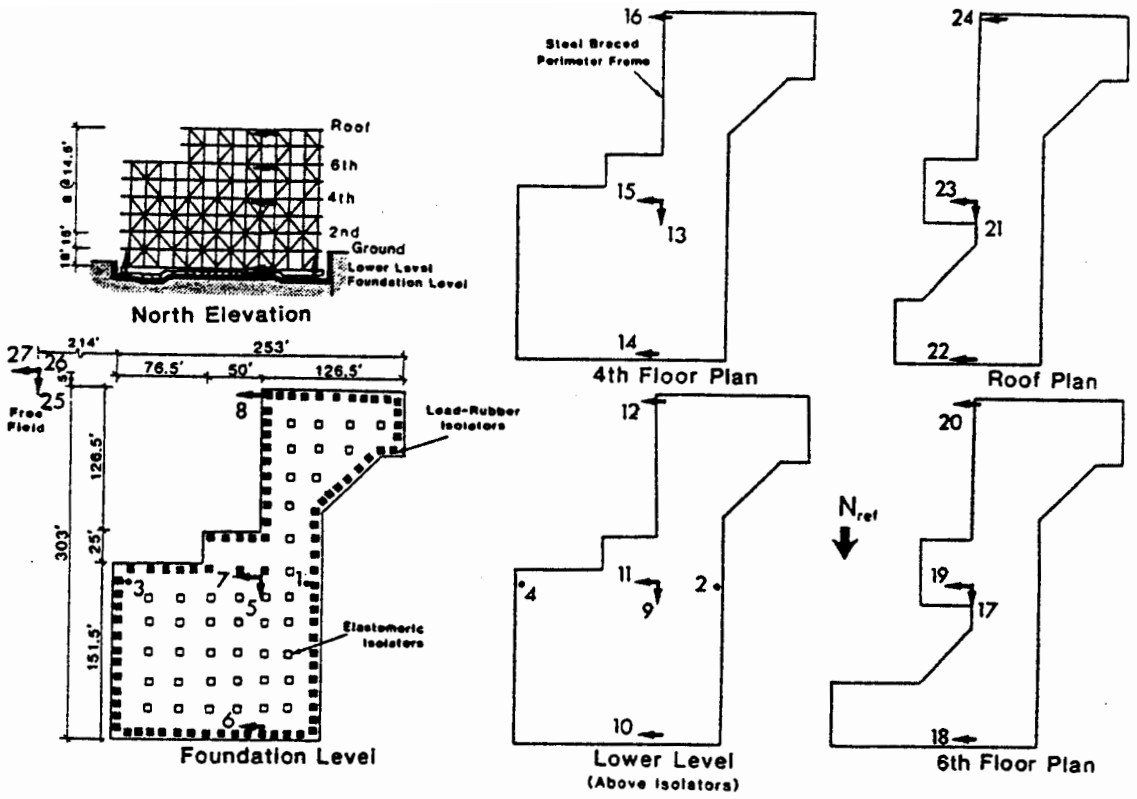

Fig. 6. Locations of accelerometers in the Los Angeles University Hospital Building.

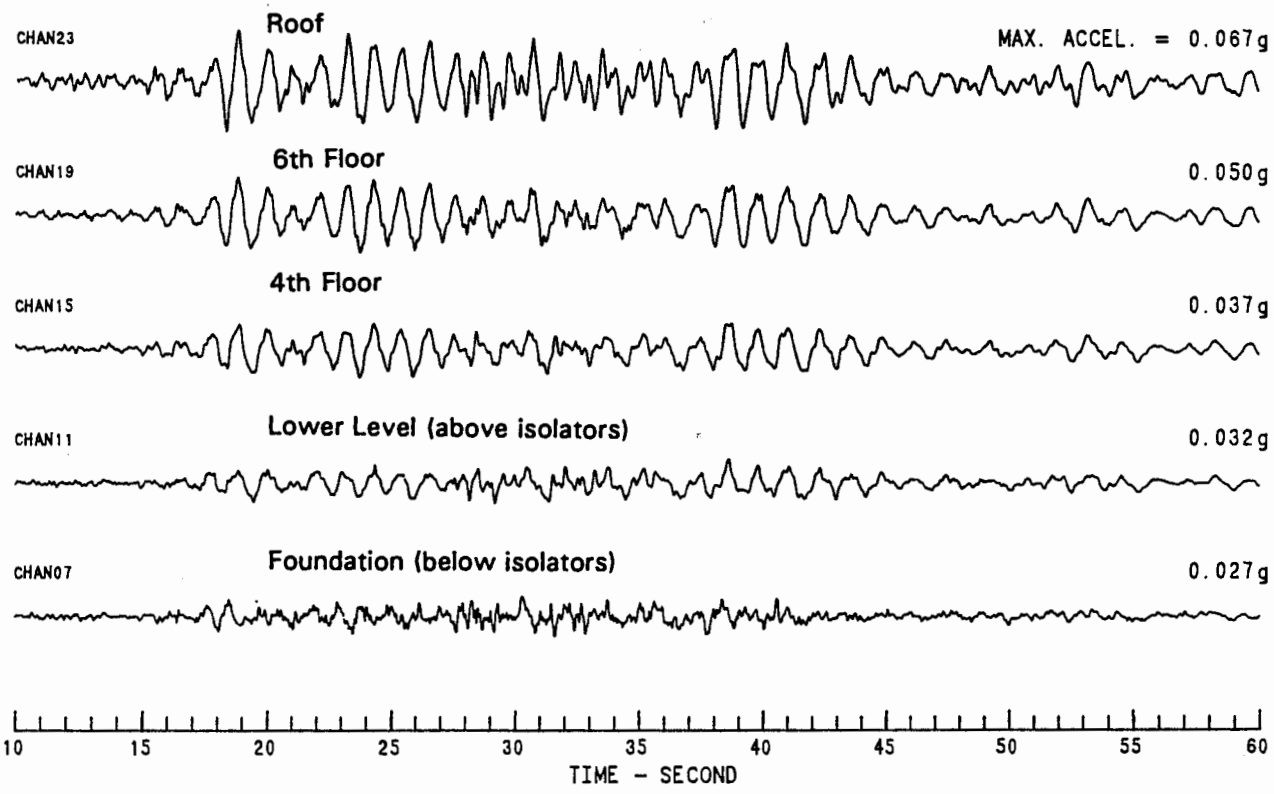

Fig. 7. Acceleration records in the transverse direction obtained at the Los Angeles University Hospital Bldg. during the 1992 Landers earthquake.

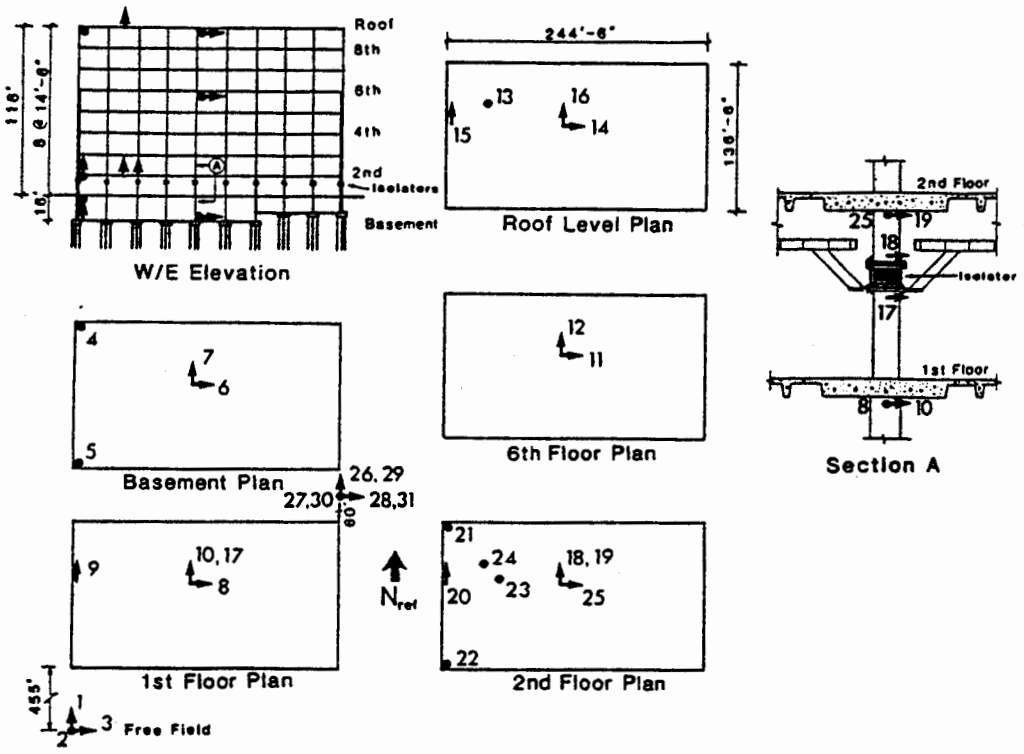

Fig. 8. Locations of accelerometers in the Seal Beach Office Building.

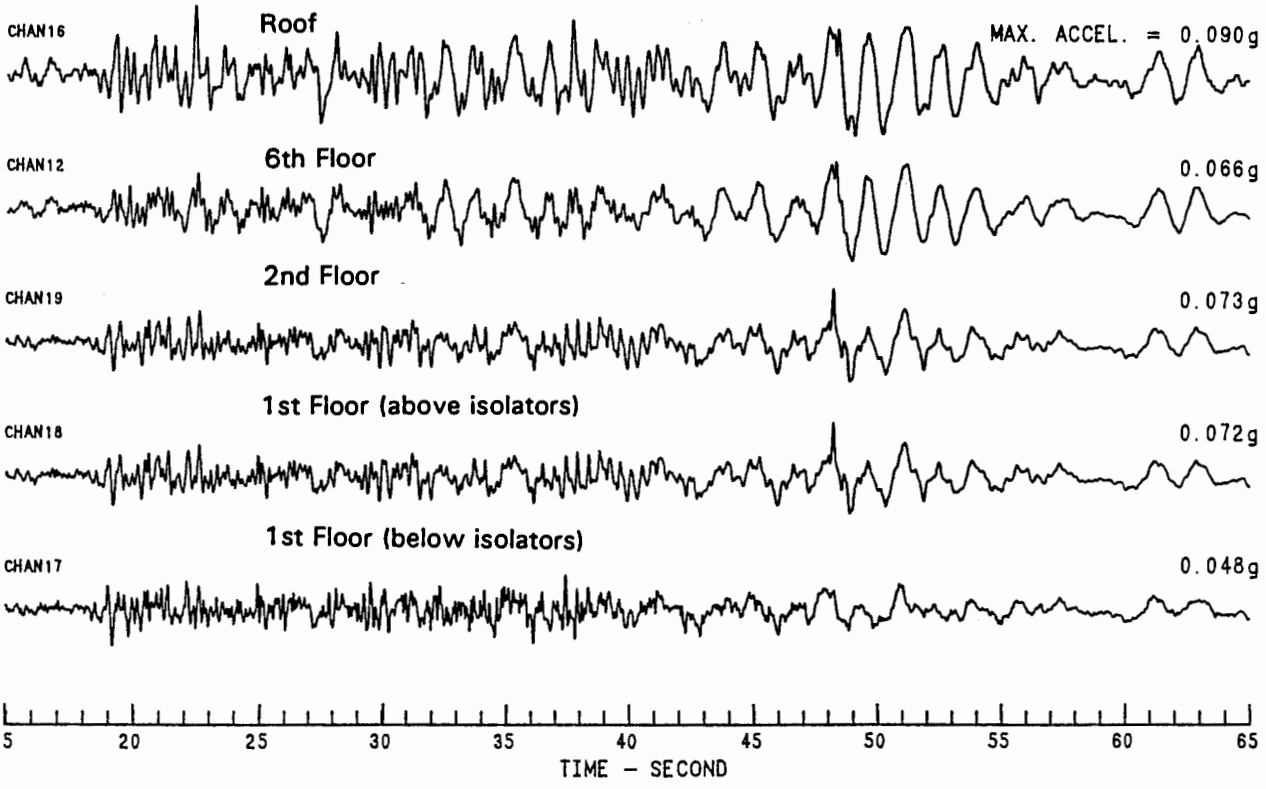

Fig. 9. Acceleration records in the transverse direction obtained at the Seal Beach Office Bldg. during the 1992 Landers earthquake.

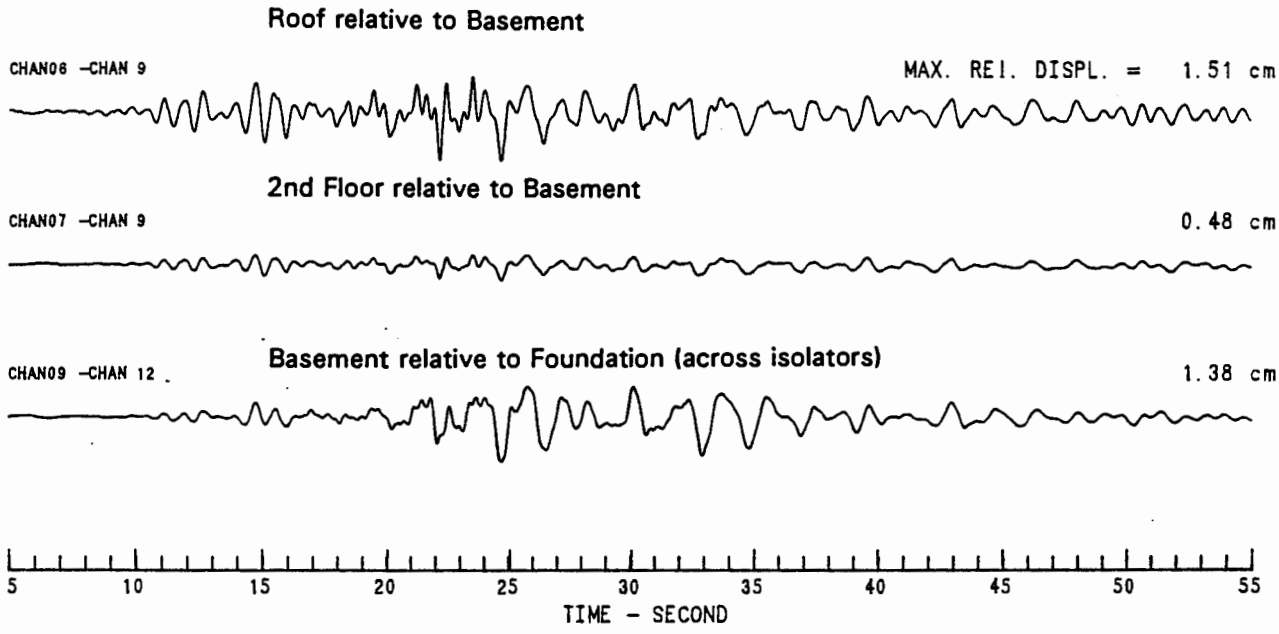

Fig. 10. Relative displacements in the transverse direction at the Rancho Cucamonga Law & Justice Bldg. during the 1992 Landers earthquake.

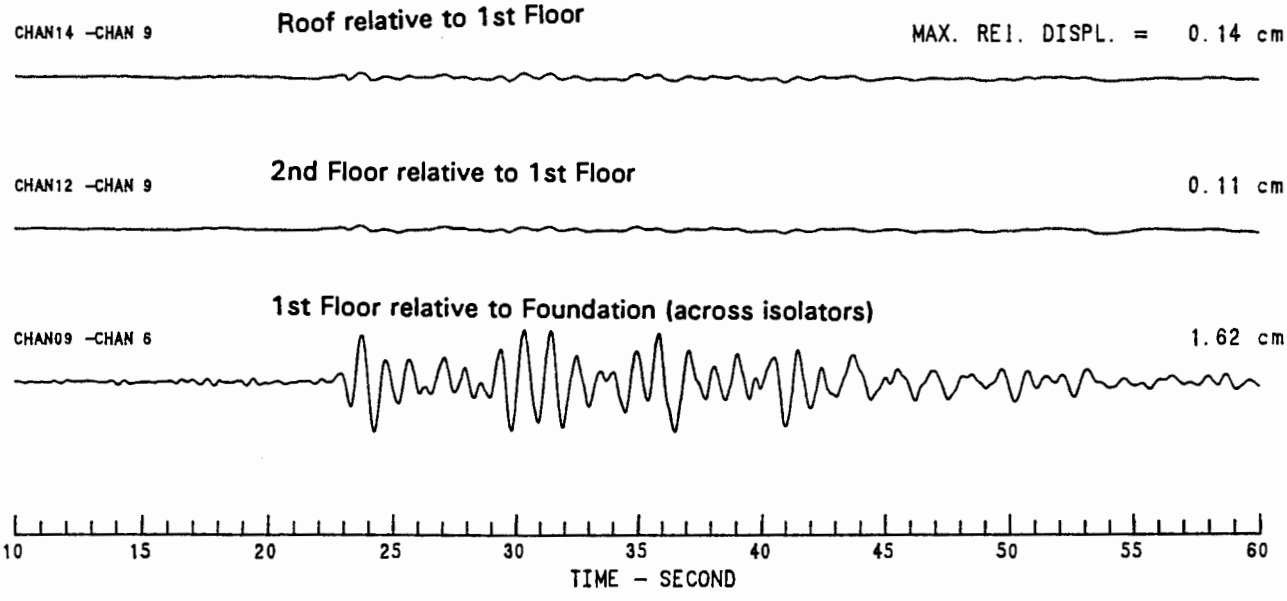

Fig. 11. Relative displacements in the transverse direction at the Los Angeles County Fire Command Bldg. during the 1992 Landers earthquake.

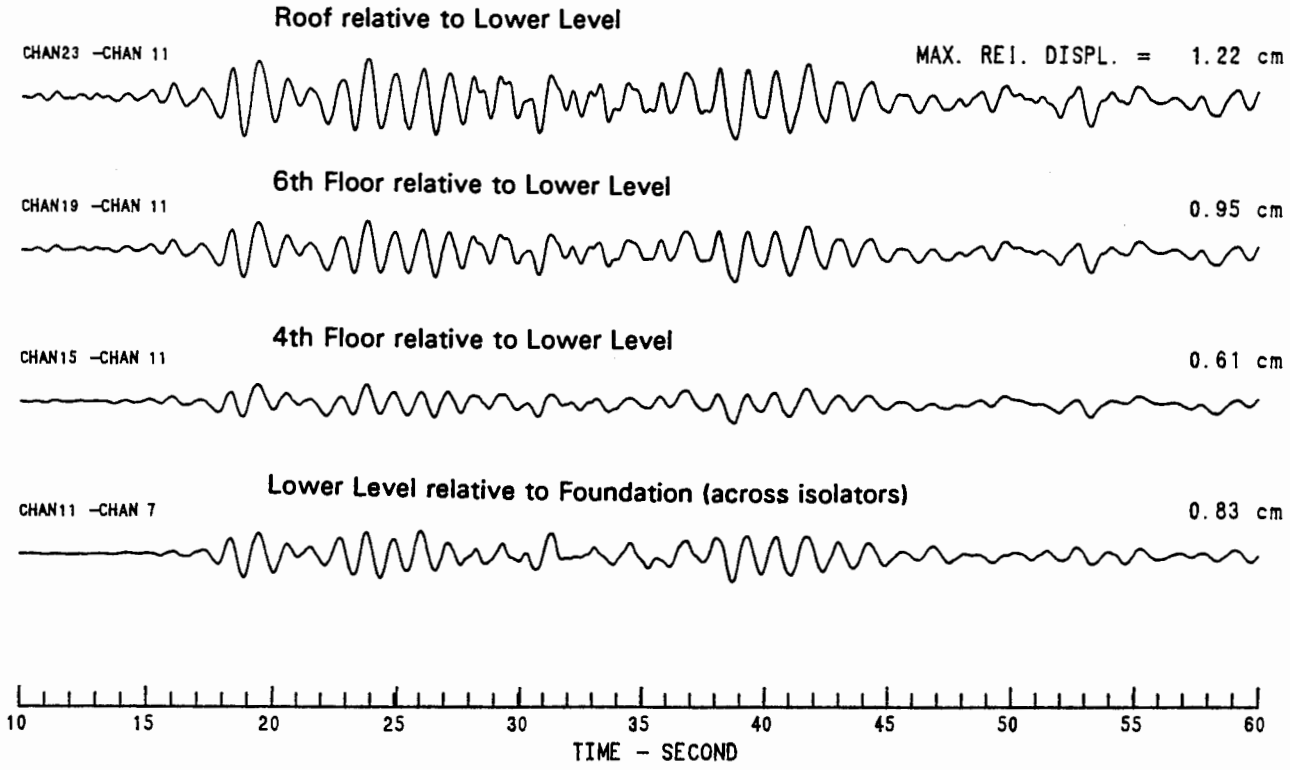

Fig. 12. Relative displacements in the transverse direction at the Los Angeles University Hospital Bldg. during the 1992 Landers earthquake.

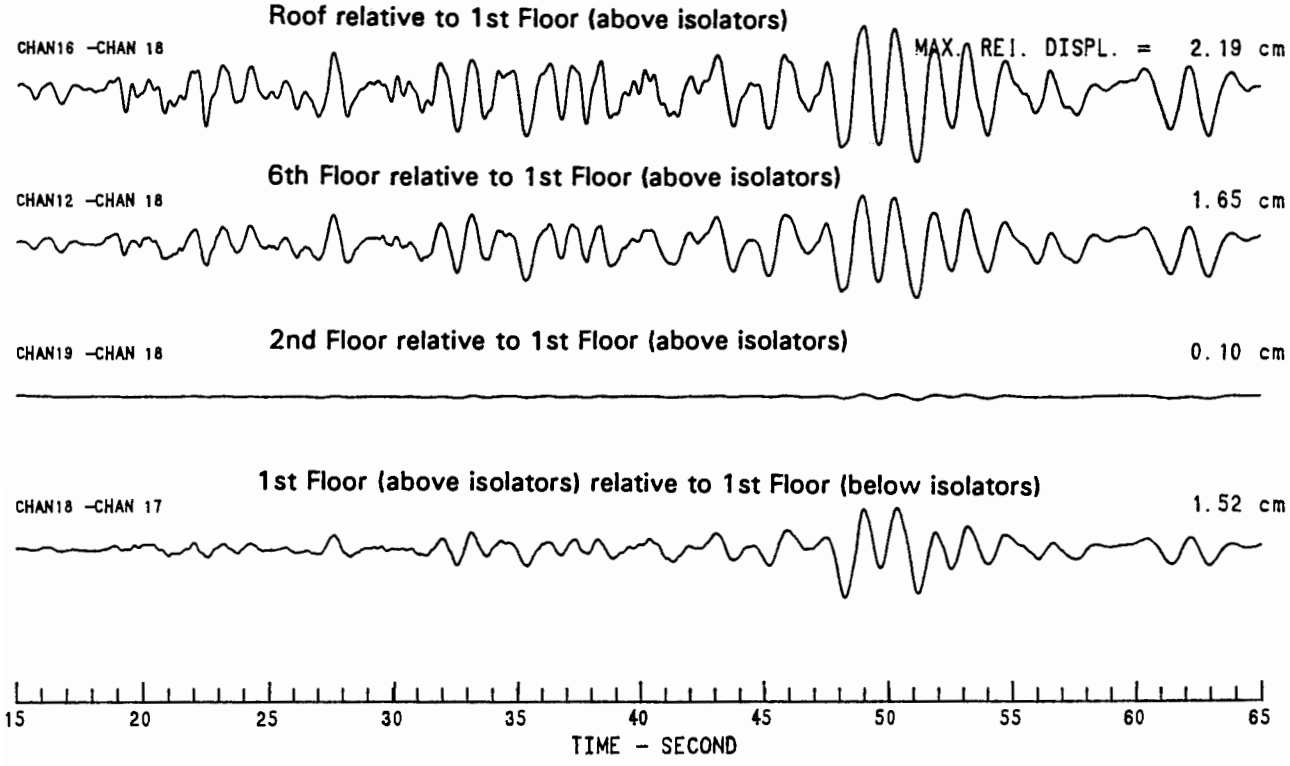

Fig. 13. Relative displacements in the transverse direction at the Seal Beach Office Bldg. during the 1992 Landers earthquake.

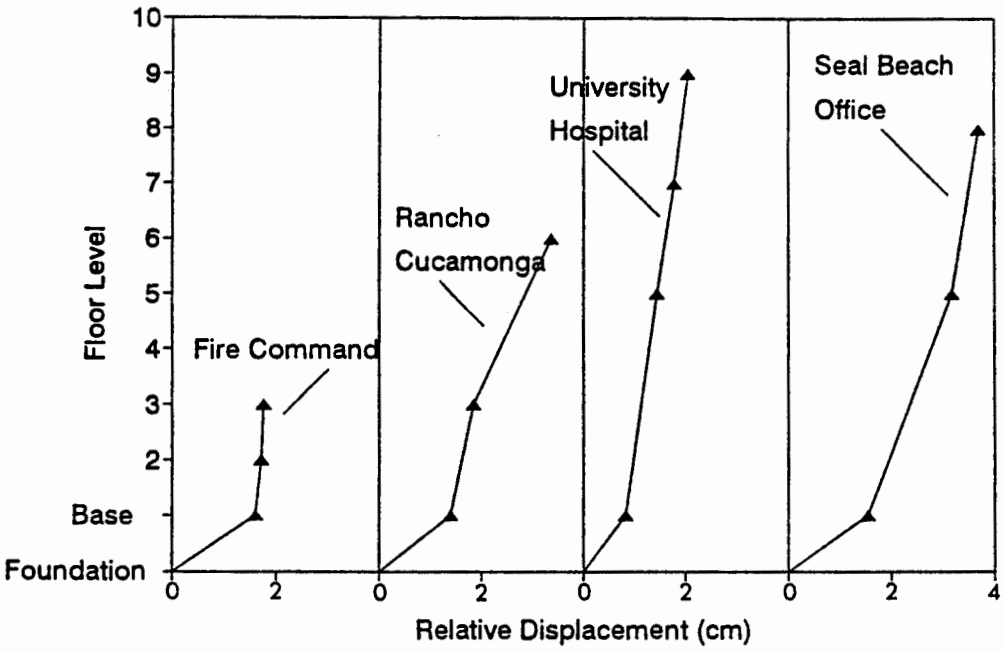

Fig. 14. Profiles of displacements relative to the foundation (below isolators) in the transverse direction at four base-isolated buildings during the 1992 Landers earthquake.

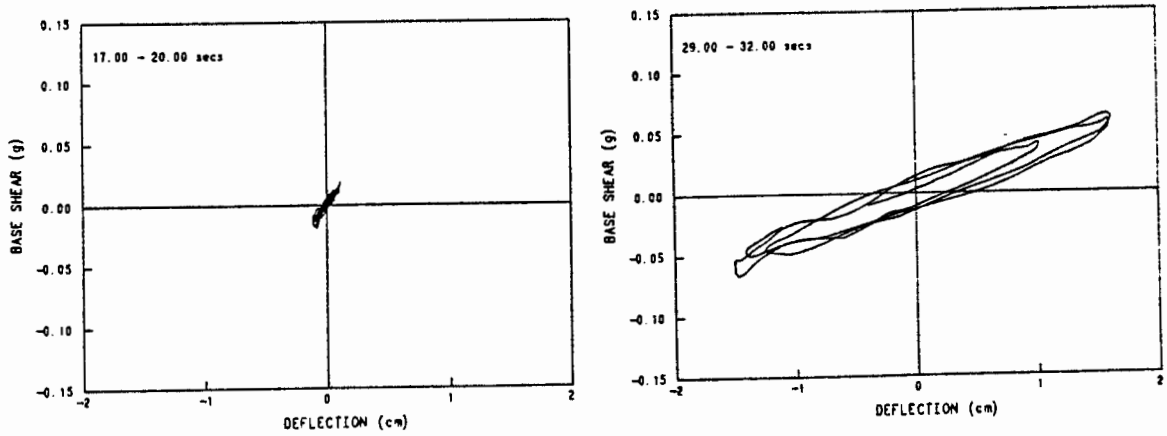

Fig. 15. Hysteresis loops for the isolators at the Los Angeles County Fire Command Bldg. derived from the motions in the transverse direction recorded by sensors 9 and 6 during the Landers earthquake. Loops for time from 17 to 20 and from 29 to 32 seconds are shown.

DYNAMIC RESPONSE ANALYSES OF COGSWELL DAM DURING THE 1991 SIERRA MADRE AND 1987 WHITTIER NARROWS EARTHQUAKES

R. W. Boulanger [1], J. D. Bray [2], S. M. Merry [3] and L. H. Mejia [3]

ABSTRACT

The recorded strong motions at Cogswell Dam during the 1991 Sierra Madre and 1987 Whittier Narrows earthquakes provide a valuable opportunity to investigate and evaluate the accuracy and reliability of conventional geotechnical procedures for evaluation of the dynamic response characteristics of rockfill dams and dams with highly three-dimensional geometries. The Sierra Madre Earthquake (M_L = 5.8) produced a significantly stronger level of shaking than the more distant 1987 Whittier Narrows Earthquake (M_L = 5.9) and thus the recorded accelerograms provide an excellent opportunity to investigate the dynamic properties of the rockfill over the imposed range of earthquake loads.

INTRODUCTION

Cogswell Dam, formerly San Gabriel Dam No. 2, is a 280-foot high concrete-faced, dumped rockfill dam founded on bedrock in a narrow notch-shaped canyon (Fig. 1). The dam is located approximately 20 miles north of Whittier, California, in the San Gabriel Mountains on the West Fork of the San Gabriel River and is owned and operated by the Los Angeles County Flood Control District (LACFCD). The dam retains Cogswell Reservoir, with a capacity of 8850 acre-feet, for the purposes of flood control and water conservation. The spillway and outlet works are both located on the right abutment. Construction of the dam and related facilities was partially completed in April, 1934, and fully completed in 1948 when the permanent concrete facing was installed.

The dam was recently shaken by two significant earthquakes - the 1987 Whittier Narrows and 1991 Sierra Madre earthquakes. The epicenter of the 1987 Whittier Narrows Earthquake (M_L=5.9) was 18 miles southwest of the dam and the epicenter of the 1991 Sierra Madre Earthquake (M_L=5.8) was 2.3 miles northwest of the dam. Maximum horizontal accelerations at the crest of the dam were about 0.15 g and 0.49 g for these two events, respectively. Records of the earthquake motions were obtained by seismographs located at the center and right side of the dam crest, and on the right abutment above the dam crest.

These recorded motions provide an excellent opportunity to: (1) investigate the accuracy of two- and three-dimensional dynamic response analyses for predicting the response of highly three-dimensional dams; and (2) complement the limited data available on dynamic properties of rockfill materials by back-calculating the dynamic properties of the rockfill over a range of earthquake-induced shear strains. This paper presents the findings of the two-dimensional analyses and describes the three-dimensional analyses in progress.

---

[1] Department of Civil Engineering, University of California at Davis

[2] Department of Civil Engineering, University of California at Berkeley

[3] Woodward-Clyde Consultants, Oakland, California

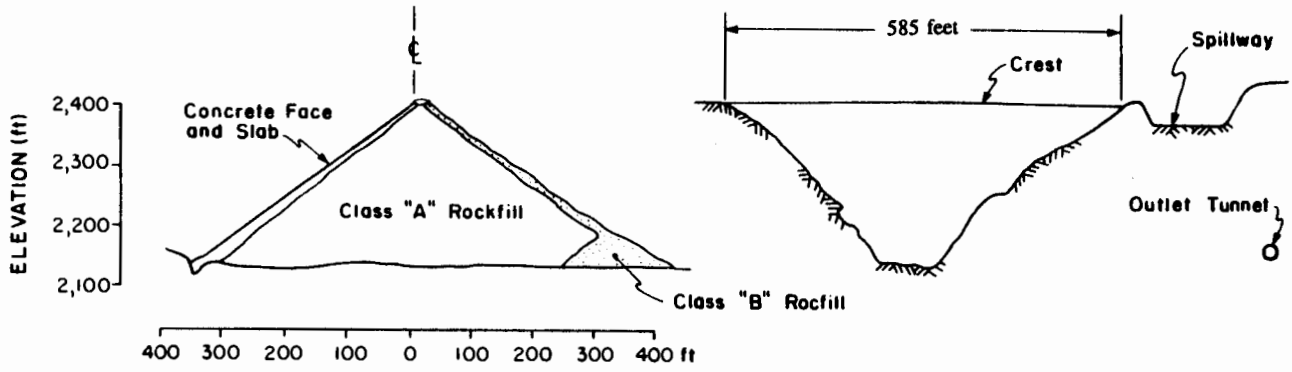

Fig. 1. Transverse and longitudinal cross-sections of Cogswell Dam

EMBANKMENT AND FOUNDATION MATERIALS

Information and data on the embankment and foundation materials were obtained from previous engineering studies, safety reviews, and construction records for the dam as maintained in the files of the Division of Safety of Dams, State of California. Recent summaries of these data are contained in reports by the Los Angeles County Flood Control District (1980) and the State of California (1986).

Cogswell Dam was constructed as a largely homogenous dumped-rockfill dam with an upstream concrete facing slab and concrete cutoff wall. Three classes of rockfill were specified in construction of the dam, as shown in Fig. 1. Class "A" rockfill comprises the main body of the dam and was a well graded mixture with the following specifications by weight: 40% from quarry chips to 1,000 lbs; 30% between 1,000 lbs and 3,000 lbs; 30% between 3,000 lbs and 14,000 lbs; and no more than 3% quarry dust. Class "B" rockfill was used to place both a 50-foot high downstream toe and a downstream facing layer varying from 8 feet thick at the crest to 12 feet thick at the toe. Class "B" rockfill was a heavier specification, with one-half to exceed 14,000 lbs in weight. Class "C" rockfill was used to place an upstream facing layer varying from 6 feet thick at the crest to 15 feet thick at the toe. Class "C" rockfill ranged from quarry chips to 14,000 lbs and was to be derrick placed to the maximum possible density.

All rockfill material consisted of granitic rock obtained from a quarry located in Devil's Canyon, which is approximately 1.5 miles upstream of the left abutment. The quarried rock was to be sound, hard, durable, and unaffected by air and moisture. Quality control tests indicated an average compressive strength of 6,629 psi, an average unit weight of 174.7 pcf, and a 5.04% breakdown by a Rock Drop test developed for the project.

The main body of the embankment was placed by dry dumping of 25-foot lifts with no compaction or sluicing. The conventional practice of sluicing the rockfill was omitted due to the scarcity of water at the dam site. Following completion of the entire rockfill section in the Fall of 1933, construction began on the concrete facing with the intention of completing this work by the Spring of 1934. Heavy rains in December 1933 through March 1934 wetted the fill and led to large settlements which disrupted the facing already constructed and caused significant deformations of the dam. During one particularly severe rainstorm of December 31, 1933 the crest of the dam settled approximately 5.8 feet, and throughout the following four

months of rain, the total settlement of the crest was as much as 13.6 feet. This led to a need to reshape the dam and reconstruct the upstream facing. A temporary timber facing was constructed and left in place for about 10 years until settlements had essentially ceased, at which time it was replaced by a reinforced concrete panel facing.

The foundation rock of Cogswell Dam is predominantly light-colored (augen) gneiss intruded by numerous dikes of andesite porphyry and hornblende amphibolite and dike-like masses of granophyric granite. Surficial weathering has reduced exposed portions of these rocks to relatively incompetent materials. During construction preparation of the dam foundation, the weakest rock was removed. The rocks within the prepared dam foundation are described as significantly jointed and sheared, moderately to strongly weathered, moderately hard, and moderately strong.

OBSERVED RESPONSE OF COGSWELL DAM

Instrumentation data for the dam includes piezometer data, drainage system discharge data, survey monument data, and strong-motion accelerograph data. The piezometer and drainage system discharge data indicate no significant effects as a result of the Whittier Narrows or Sierra Madre earthquakes. However, the reservoir was nearly empty for silt removal at the time of the Sierra Madre Earthquake and was only at about elevation 2266 feet (139 feet below the crest) at the time of the Whittier Narrows Earthquake. Survey monument data indicates that deformations of the crest of the dam were insignificant as a result of the Whittier Narrows Earthquake and attained maximum values of 1.61-inch vertically and 0.63-inch horizontally (downstream) as a result of the Sierra Madre Earthquake.

The Sierra Madre Earthquake was initially reported to have only caused minor transverse hairline cracks in the crest pavement and cracks along vertical joints in the parapet wall at three locations. Subsequent detailed inspections indicated that the earthquake caused cracking of the upstream concrete facing near its juncture with the concrete cutoff walls along both abutments. The observed zones of cracking ranged from 2 to 8 feet wide and extended from just below the parapet wall to about 35 feet down (vertically) on the right abutment and 15 feet down on the left abutment. Maximum crack widths of 0.5 inch were reported while more typical crack widths were less than about 0.25 inch. The Whittier Narrows Earthquake was not reported to have caused any damage to the dam.

A total of 3 strong motion accelerographs were installed at three locations on and near the dam as shown in Fig. 2. It should be noted that the accelerographs were temporarily removed during recent construction of a reinforced concrete parapet wall along the dam crest and upon re-installation (prior to the Sierra Madre Earthquake), were renumbered differently from the time of the Whittier Narrows Earthquake. At each location, motions were recorded in three orthogonal directions: transverse to the dam's axis, parallel to the dam's axis, and vertical. This paper will concentrate on the transverse motions as these are the motions generally considered to be of primary engineering interest. The acceleration time histories for the motions transverse to the dam's axis are presented in Fig. 3 for the Whittier Narrows and Sierra Madre earthquakes, respectively. The corresponding response spectra are shown in Figs. 4 and 6, and the corresponding Fourier amplification ratios between the center crest and abutment recordings are shown in Figs. 5 and 7. A summary of recorded motion characteristics during these events is provided in Table 1.

The two earthquakes excited Cogswell Dam at significantly different levels. The Whittier Narrows Earthquake produced transverse peak ground accelerations at the right abutment, right crest and center crest of 0.06 g, 0.10 g, and 0.15 g, respectively. Conversely, the Sierra Madre Earthquake produced higher transverse peak ground accelerations at these locations of 0.26 g, 0.32 g and 0.42 g, respectively. The observed crest to abutment amplification ratio for the Whittier narrows event was roughly 2.4; whereas, for

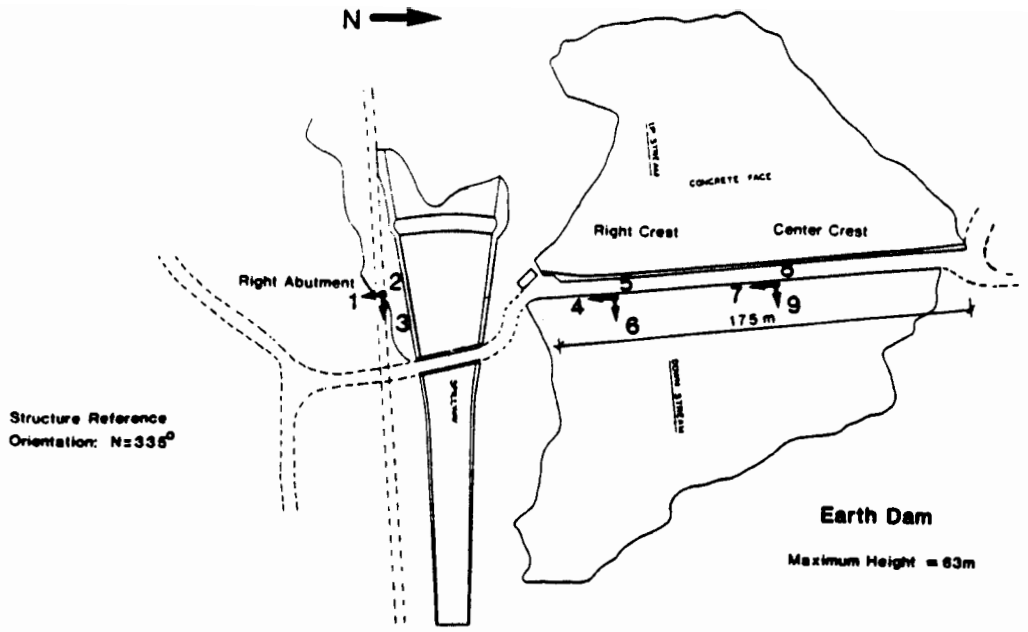

Fig. 2. Plan View of Cogswell Dam Showing Sensor Locations (CSMIP Station No. 23210)

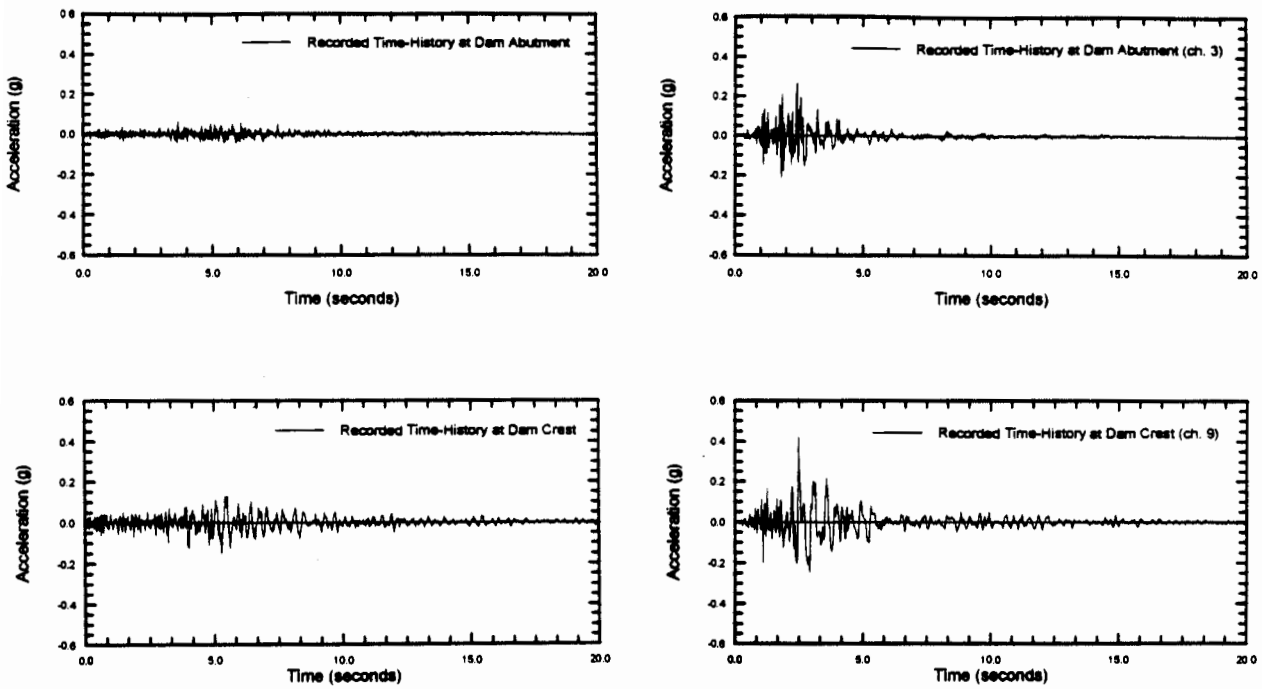

(a) Whittier Narrows Earthquake (b) Sierra Madre Earthquake

Fig. 3. Recorded Transverse Acceleration Time Histories

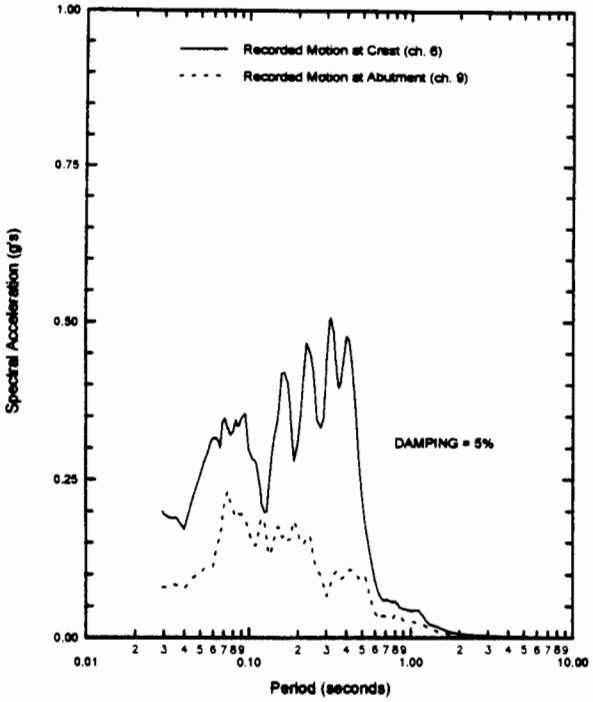

Fig. 4. Recorded Response Spectra: Whittier Narrow Earthquake

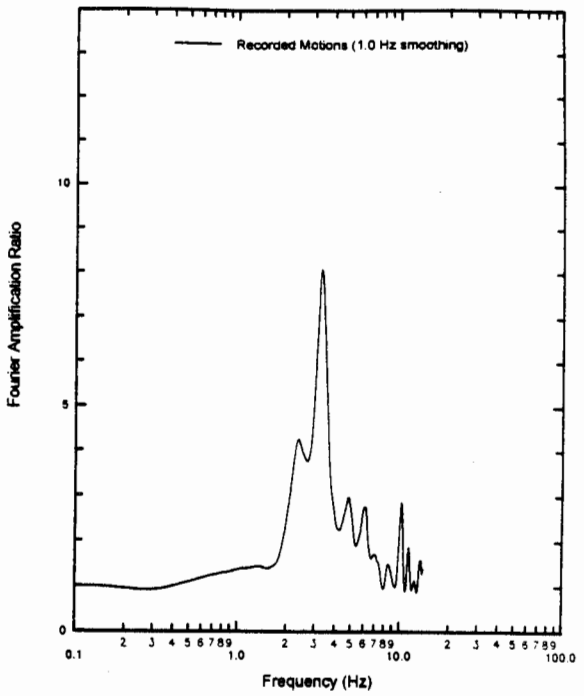

Fig. 5. Fourier Amplification Ratios: Whittier Narrow Earthquake

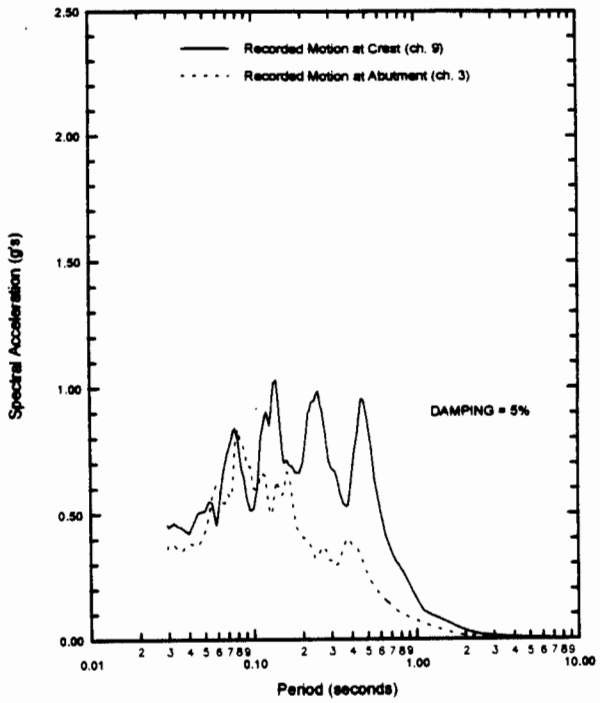

Fig. 6. Recorded Response Spectra: Sierra Madre Earthquake

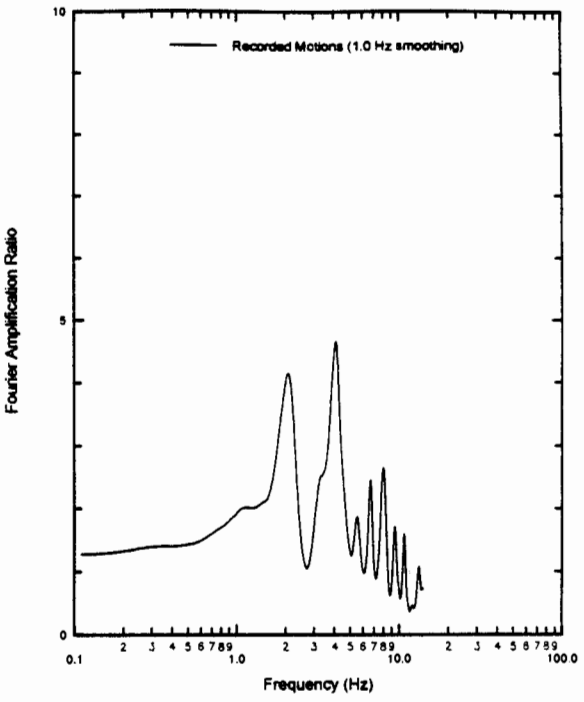

Fig. 7. Fourier Amplification Ratios: Sierra Madre Earthquake

TABLE 1. Characteristics of Earthquake Motions

Accelerograph	Component	Whittier Narrows			Sierra Madre		
		Peak Ground Accel.(1) (g)	Max. Spectral Accel.(1) (g)	Period at Max. Spectral Accel. (sec)	Peak Ground Accel.(1) (g)	Max. Spectral Accel.(1) (g)	Period at Max. Spectral Accel. (sec)
Abutment	Transverse	0.064	0.200	0.075	0.264	0.838	0.080
Right Crest	Transverse	0.100	0.367	0.190	0.318	1.082	0.227
Center Crest	Transverse	0.151	0.507	0.320	0.421	1.031	0.138
Abutment	Longitudinal	0.061	0.175	0.225	0.302	0.980	0.250
Right Crest	Longtiduinal	0.087	0.391	0.325	0.376	1.775	0.420
Center Crest	Longitudinal	0.137	0.385	0.320	0.486	1.647	0.435
Abutment	Vertical	0.06	--	--	0.227	--	--
Right Crest	Vertical	0.11	--	--	0.386	--	--
Center Crest	Vertical	0.14	--	--	0.484	--	--

(1)After baseline and instrument correction of accelerogram records.

the Sierra Madre event this ratio was 1.6. This decrease in the crest to abutment amplification ratio resulting from stronger earthquake shaking agrees with the findings of previous case studies (e.g., Harder 1991).

Three approaches were taken to evaluate the observed 3-D fundamental period of the dam during these earthquake events. For the Whittier Narrows Earthquake, the dam's fundamental period was estimated to be between 0.37 and 0.42 seconds based on: (1) the response spectra calculated for select sections of the crest accelerogram representing the initial period of decay of strong shaking suggested that the motion's predominant period was about 0.37 seconds; and (2) Fourier amplification ratios from the abutment to crest (Fig. 5) indicated that the recorded motion's predominant period was about 0.42 seconds.

For the Sierra Madre Earthquake, the dam's fundamental period was estimated to be between 0.45 and 0.48 seconds based on: (1) the response spectra calculated for select sections of the crest accelerogram representing the initial period of decay of strong shaking suggested that the motion's predominant period was about 0.45 seconds; and (2) Fourier amplification ratios from the abutment to crest (Fig. 5) indicated that the recorded motion's predominant period was about 0.48 seconds. Since the rockfill's stiffness degrades under stronger earthquake excitation, the fundamental period of Cogswell Dam is higher for the Sierra Madre Earthquake.

FINITE ELEMENT MODELS

Analyses of the initial static stresses in the dam (required for determining dynamic properties) were performed using the finite element method (FEM) program SSCOMPPC (Boulanger et al. 1991). SSCOMPPC employs the Duncan et al. (1980) hyperbolic soil model to represent the nonlinear stress-dependant stress-strain and volumetric strain response of the rockfill. The finite element mesh for the two-dimensional analyses of the maximum cross-section through the dam is shown in Fig. 8.

The two-dimensional (2-D) dynamic FEM analyses were performed using the computer program FLUSH (Lysmer et al. 1975). FLUSH is a 2-D FEM program for the dynamic response analysis of earth structures using the method of complex response to solve the equations of motion of a soil-structure system in the frequency domain. The nonlinear dynamic behavior of soils is modeled using the equivalent-linear method as proposed by Seed and Idriss (1970). After node and element renumbering, the same finite element mesh used for the initial static stress analyses was utilized for the 2-D dynamic response analyses.

The three-dimensional (3-D) dynamic FEM analyses were performed using a modified version of the computer program TLUSH (Kagawa et al. 1981). The original TLUSH program was developed to run on the now obsolete CDC 7600 main frame computer. Considerable effort has been put forth to develop a PC-compatible version of TLUSH which is currently being validated. The fully 3-D program TLUSH is similar to FLUSH in that it uses the method of complex response in the frequency domain and models soil behavior by the equivalent-linear method. The finite element mesh for the 3-D dynamic response analyses as shown in Fig. 9 has the same maximum cross-sectional geometry as in the 2-D mesh. A full mesh was used due to several asymmetrical features in the dam.

DYNAMIC ROCKFILL PROPERTIES

The dynamic properties of rockfill materials are not well documented or understood. It is customary to assume that rockfill behaves similar to cohesionless soils such as gravels or sands in terms of modulus degradation and damping characteristics. Thus, the dynamic shear modulus degradation relationships (G/G_{max} vs. shear strain relationship) and the damping ratio versus shear strain relationships as recommended by Seed et al. (1984) for gravelly soils were utilized to model the rockfill. It then remains to select a value for the parameter K_{2max} which establishes the maximum shear modulus (G_{max}) as:

$$G_{max} = 1000\ K_{2max}\ (\sigma_m')^{1/2} \qquad (1)$$

where G_{max} and the mean effective confining stress (σ_m') are in units of psf. The value of σ_m' was taken as the average of the three principal stresses, of which two are obtained from the initial static stress analyses described in the next section. Since the 2-D static stress analyses do not provide the intermediate principal stress (σ_2'), it was estimated for each element as:

$$\sigma_2' = 0.35\ (\sigma_1' + \sigma_3') \geq \sigma_3' \qquad (2)$$

The value of K_{2max} for the Class "B" and "C" rockfill zones were taken as 1/3 greater than the value assigned to the body of the dam (Class "A") in all analyses; and thus, only the value for the body of the dam is referred to hereafter. A Poisson's ratio of 0.35 was used for the rockfill.

INITIAL STATIC STRESS ANALYSES

The initial static stress analyses were performed in steps to incrementally model the placement of the rockfill and the subsequent loads produced against the upstream face by the reservoir (elevation set to the value reported at the time of each earthquake). Parameter studies showed that the calculated mean confining stresses were not sensitive to the model parameters, which is reasonable given the homogenous cross-section of the dam. The results of the 2-D static stress analysis were then corrected to account for the effects of canyon shape using data presented by Lefebvre and Duncan (1971). For a triangular shaped canyon, Lefebvre and Duncan showed that a dam with a crest length (L) to height (H) ratio of 2:1, a 2-D analysis of the maximum cross-section can overestimate the static stresses in the lower third of the dam by

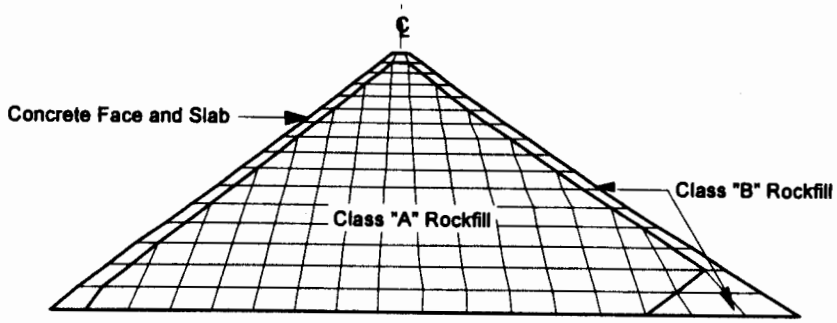

Fig. 8. Two-Dimensional FEM Mesh

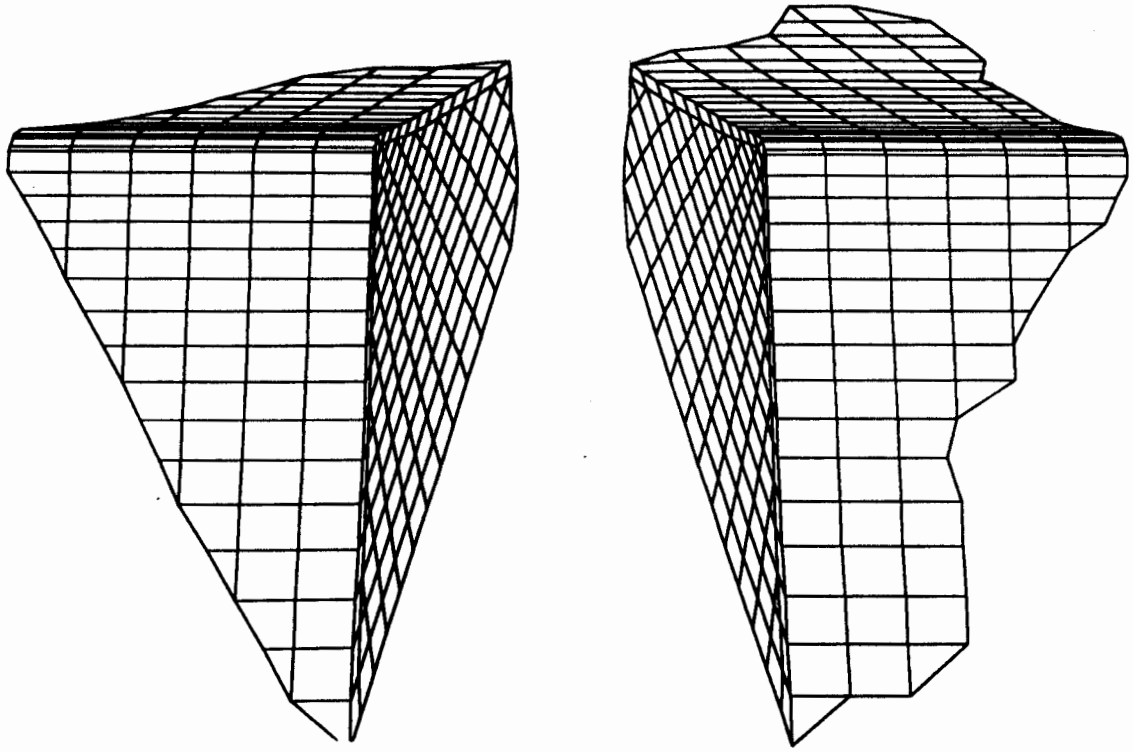

Fig. 9. Three-Dimensional FEM Mesh

as much as 40%. Consequently, the mean confining stresses obtained from the 2-D analyses were reduced by an amount that varied linearly with elevation from 0% at the lower 1/3-point of the dam to 30% at the base of the dam. Since the same maximum cross-sectional mesh geometry was used for all three FEM analyses, the calculated mean confining stresses corresponded directly to individual elements in the 2-D dynamic mesh and were projected longitudinally into the 3-D dynamic mesh.

TWO-DIMENSIONAL DYNAMIC RESPONSE ANALYSES

The 2-D dynamic response of the dam was computed using the recorded transverse abutment motions as the input motion to the rigid base. A maximum frequency of 12 Hz was used in the analyses. Analyses were performed with values for the soil model parameter K_{2max} of 60, 80, 100, 120, and 140. Additional sensitivity analyses included the use of an upper bound relationship for the damping ratio versus shear strain relationship. The computed response of the dam was compared to the recorded response in terms of acceleration response spectra, Fourier amplification ratios, and acceleration time histories at the dam crest. The results of selected analyses are summarized in Table 2. The response spectra and Fourier amplification ratios calculated for a K_{2max} value of 100 and both earthquake motions are presented in Figs. 10 through 13.

In general, the 2-D dynamic response analyses were not able to capture a couple of aspects of the recorded responses. The calculated Fourier amplification ratios exhibit their greatest value at their longest period, which corresponds to the first mode of vibration for the 2-D model and progressively smaller amplification ratios at higher modes of vibration. In contrast, the Fourier amplification ratios for the recorded motions exhibit a lower peak ratio at their first mode of vibration than is produced at the second mode of vibration. The difference in Fourier amplification ratios is reflected in the differences between the calculated and recorded acceleration response spectra. The calculated response spectra generally overpredict the recorded response spectra and do not accurately reproduce the same "shape" because the 2-D model is amplifying the input motions in a significantly different way than the recorded motions indicate was the case. The use of the upper bound damping relationship did improve the agreement between the calculated and recorded motions in terms of the magnitude of response but did not improve the general shape of the response spectra or Fourier amplification ratios.

THREE-DIMENSIONAL DYNAMIC RESPONSE ANALYSES

The 3-D dynamic response analyses are currently in progress and thus only preliminary results are currently available; each analysis requires about 1 day to run on a PC and 2 to 3 days on the VAX and thus the parameter studies are time consuming. The 3-D dynamic response of the dam is also being computed using the recorded transverse abutment motions as the input motion to the rigid base.

The 3-D dynamic response analyses appear to be able to capture some of the principal features of the recorded dam response better than was achieved with the 2-D response analyses. For example, the calculated Fourier amplification ratios exhibit the same trend of a lower amplification ratio at the first mode of vibration with a greater amplification ratio for the second mode.

The fundamental period of a dam calculated by 2-D response analyses is expected to differ significantly from values recorded for highly 3-D dam geometries. Mejia and Seed (1983) proposed a relationship between the fundamental frequency of a 3-D dam in a V-shaped or rectangular-shaped canyon versus an infinitely long dam with the same maximum cross-section and properties. For a dam with a L/H ratio of 2.1:1 in a V-shaped canyon, their relationship suggests that a 2-D response analysis using the true material properties should calculate a fundamental period which is about 1.65 times greater than the recorded

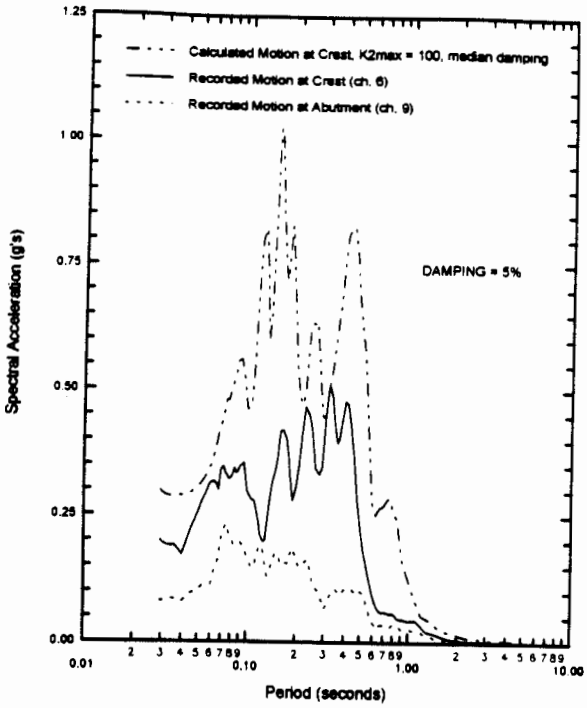

Fig. 10. Calculated 2-D Dynamic Response Spectra: Whittier Narrows Earthquake

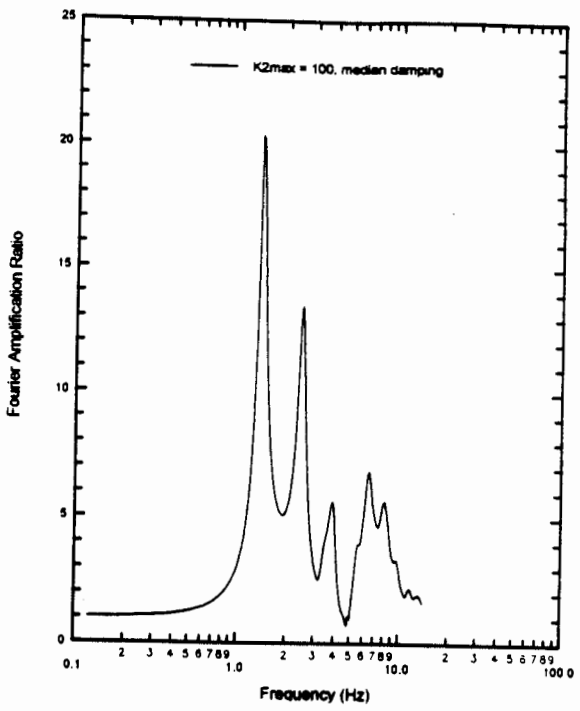

Fig. 11. Calculated 2-D Fourier Amplification Ratios: Whittier Narrows Earthquake

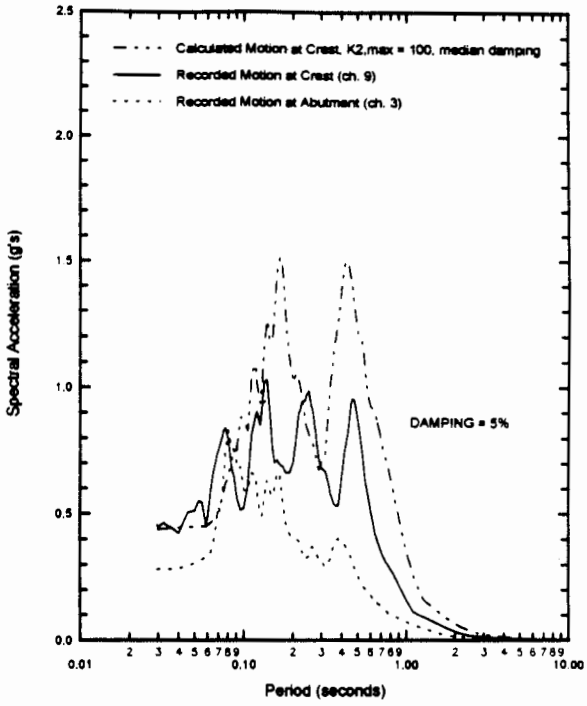

Fig. 12. Calculated 2-D Dynamic Response Spectra: Sierra Madre Earthquake

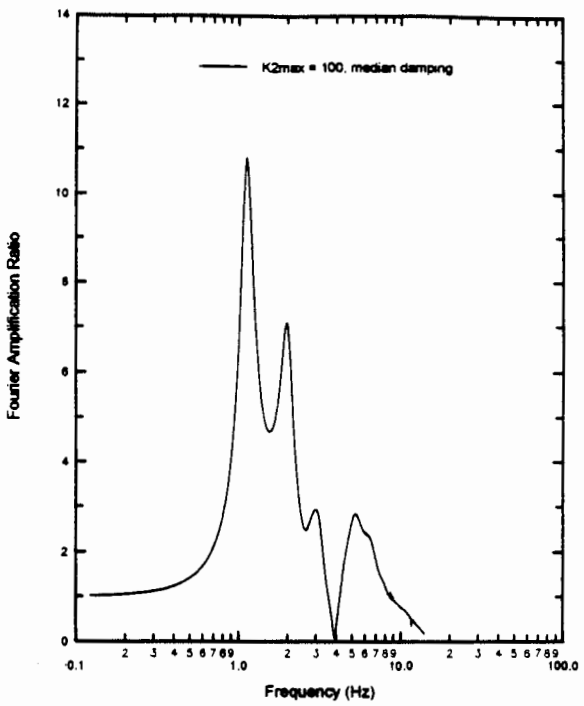

Fig. 13. Calculated 2-D Fourier Amplification Ratios: Sierra Madre Earthquake

TABLE 2(a). Results of 2-D Dynamic Response Analyses for Whittier Narrows Earthquake

$k_{2,max}$	Modulus Degradation Relationship	Damping Relationship	Average Effective Shear Strain (%) (range)	G/G_{max}	Fraction of Critical Damping (%)	Fundamental Period[1] (sec)	Max. Crest Accel. (g)	Response Spectra at Crest: Max. Spectral Accel. (g)	Response Spectra at Crest: Period at Max. Spectral Accel. (s)
60	Gravel	Median	0.013 (0.010-0.020)	0.51	6.71	0.98	0.20	0.75	0.19
80	Gravel	Median	0.012 (0.009-0.017)	0.52	6.47	0.84	0.21	0.88	0.18
100	Gravel	Median	0.010 (0.005-0.015)	0.56	5.85	0.73	0.27	1.03	0.15
100	Gravel	Upper-Bound	0.007 (0.004-0.011)	0.60	5.10	0.71	0.19	0.63	0.44
120	Gravel	Median	0.008 (0.005-0.012)	0.59	5.36	0.65	0.29	1.11	0.36
140	Gravel	Median	0.008 (0.006-0.011)	0.59	5.32	0.60	0.26	1.06	0.12
Recorded	N/A	N/A	N/A	N/A	N/A	0.37-0.42	0.15	0.51	0.32

TABLE 2(b). Results of 2-D Dynamic Response Analyses for Sierra Madre Earthquake

$k_{2,max}$	Modulus Degradation Relationship	Damping Relationship	Average Effective Shear Strain (%) (range)	G/G_{max}	Fraction of Critical Damping (%)	Fundamental Period[1] (sec)	Max. Crest Accel. (g)	Response Spectra at Crest: Max. Spectral Accel. (g)	Response Spectra at Crest: Period at Max. Spectral Accel. (s)
60	Gravel	Median	0.042 (0.030-0.058)	0.33	11.4	1.21	0.35	0.86	0.28
80	Gravel	Median	0.037 (0.026-0.054)	0.35	10.9	1.02	0.42	1.26	0.38
100	Gravel	Median	0.033 (0.024-0.052)	0.37	10.4	0.89	0.44	1.51	0.17
100	Gravel	Upper-Bound	0.027 (0.021-0.034)	0.40	9.5	0.87	0.36	1.18	0.42
120	Gravel	Median	0.032 (0.020-0.052)	0.37	10.2	0.80	0.56	1.96	0.42
140	Gravel	Median	0.033 (0.020-0.055)	0.37	10.3	0.73	0.68	2.30	0.42
Recorded	N/A	N/A	N/A	N/A	N/A	0.45-0.48	0.42	1.03	0.14

[1]Period for maximum amplification at dam crest from amplification function between crest and base of model.

fundamental period. For these preliminary 2-D and 3-D analyses of Cogswell dam, a comparison of the results for a K_{2max} value of 100 suggests that the ratio of the 2-D to 3-D calculated fundamental periods is about 2.0. The difference may be attributable to a greater stiffening effect produced by the somewhat asymmetric geometry of the canyon walls, and this possibility will be explore further as the 3-D analyses progress.

SEISMICALLY-INDUCED PERMANENT DEFORMATION ANALYSES

The presently available engineering methodologies for estimating seismically-induced permanent deformations in rockfill dams are not well refined and need to be viewed with considerable engineering judgement. It is interesting, however, to perform a deformation analysis using the parameters adopted in previous engineering studies of the dam prior to the Sierra Madre Earthquake. As part of a geotechnical investigation of Cogswell Dam, the LACFCD (1980) estimated that the pseudostatic yield acceleration for potential slip surfaces through the dam is 0.21 g. For the Sierra Madre Earthquake, the maximum average acceleration (k_{max}) for potential sliding masses is estimated to be about 0.3 g based on the recorded motions and the relationships between peak crest accelerations and maximum average accelerations presented by Makdisi and Seed (1978). Thus, the ratio of k_y/k_{max} was 0.5 for which the Makdisi-Seed (1978) procedure for estimating dam and embankment earthquake-induced deformations predicts permanent deformations for a M = 6.5 earthquake to be less than 1.5 inches. Since the 1991 Sierra Madre event was only a M_L = 5.8 event, the predicted seismically-induced permanent deformations would be less than 1 inch. A Newmark (1965) double-integration of the recorded crest acceleration-time history scaled to a peak acceleration of 0.3 g was also performed. This approach predicted permanent deformations due to the Sierra Madre event to also be less than 1 inch. These estimates are in good agreement with the observed maximum deformations of 1.61-inch vertical and 0.63-inch horizontal at the dam crest, and with previous experiences regarding the performance of rockfill dams during earthquake loading.

SUMMARY

Cogswell Dam, a 280-foot high concrete-faced, loosely dumped rockfill dam, experienced a peak transverse crest acceleration of 0.42 g during the 1991 Sierra Madre Earthquake. The dam performed very well with a maximum deformation of about 1.6-inch at the crest and with relatively minor cracking in limited portions of the upstream concrete facing. The good performance of the dam is consistent with previous experiences and with simplified seismically-induced permanent deformation analyses.

Preliminary results of FEM dynamic response analyses of Cogswell dam during the Whittier Narrows and Sierra Madre earthquakes were presented. An initial assessment of the results indicate that the two-dimensional dynamic response analyses were limited in their ability to accurately model the observed dam response and, in general, tended to overpredicted the recorded dam response. Three-dimensional response analyses are presently being performed to take full advantage of this valuable set of strong motion records. Together, the two- and three-dimensional dynamic response analyses are expected to enable a more reliable estimation of the dynamic properties of the loosely dumped rockfill comprising the body of Cogswell dam.

ACKNOWLEDGEMENTS

The authors would like to thank Mr. Robert Kroll of the Los Angeles County Department of Public Works for his assistance and discussions regarding the history of the dam and its recent performance. Financial support for this project was partially provided by Woodward-Clyde Consultants. This research project was supported by the California Department of Conservation, Division of Mines and Geology, Strong Motion Instrumentation Program, Contract 1091-352. All of this support is greatly appreciated.

REFERENCES

Boulanger, R. W., Bray, J. D., Chew, S. H., Seed, R. B., Mitchell, J. K., and Duncan, J. M. (1991). "SSCOMPPC: A Finite Element Analysis Program for Evaluation of Soil-Structure Interaction and Compaction Effects." Geotechnical Engineering Report No. UCB/GT/91-02, University of California, Berkeley, April.

Duncan, J. M., Byrne, P., Wong, K. S., and Mabry, P. (1980). "Strength, Stress-Strain and Bulk Modulus Parameters for Finite Element Analyses of Stresses and Movement in Soil Masses." Geotechnical Engineering Research Report No. UCB/GT/80-01, University of California, Berkeley.

Lefebvre, G. and Duncan, J. M. (1971). "Three Dimensional Finite Element Analyses of Dams." Geotechnical Engrg. Report No. TE 71-5 to U.S. Army Engineers Waterways Experiment Station, University of California, Berkeley, May.

Harder, L. F. Jr. (1992). "Performance of Earth Dams During the Loma Prieta Earthquake." Proc. 2nd International Conference on Recent Advances in Geotechnical Earthquake Engineering and Soil Dynamics, March 11-15, St. Louis, MO. pp. 1613-1629.

Kagawa, T., Mejia, L. H., Seed, H. B., and Lysmer, J. (1981). "TLUSH: A Computer Program for the Three-Dimensional Analysis of Earth Dams." Report No. UCB/EERC-81-14, Univ. of California, Berkeley, September.

Los Angeles County Flood Control District (1980). "Geotechnical Investigation of Cogswell Dam." An internal report prepared by the LACFCD, October.

Lysmer, J., Udaka, T., Tsai, C.F. and Seed, H. B. (1975). "FLUSH: A Computer Program for Approximate 3-D Analysis of Soil-Structure Interaction Problems." Report No. UCB/EERC-75-30, Univ. of California, Berkeley, November.

Makdisi, F. I., and Seed, H. B. (1978). "Simplified Procedure for Estimating Dam and Embankment Earthquake-Induced Deformations." Journal of the Soil Mechanics and Foundations Division, ASCE, Vol. 104, No. GT7, July, pp. 849-867.

Mejia, L. H. and Seed, H. B. (1983). "Comparison of 2-D and 3-D Dynamic Analyses of Earth Dams." Journal of the Soil Mechanics and Foundation Division, ASCE, Vol. 109, No. GT11, November, pp. 1383-1398.

Seed, H. B., and Idriss, I. M. (1970). "Soil Moduli and Damping Factors for Dynamic Response Analysis." Earthquake Engineering Research Center, Report No. EERC 70-10, University of California, Berkeley, December.

Seed, H. B., Wong, R. T., Idriss, I. M., and Tokimatsu, K. (1984). "Moduli and Damping Factors for Dynamic Analyses of Cohesionless Soils." Earthquake Engineering Research Center, Report No. EERC 84-14, University of California, Berkeley, September.

State of California (1986). Cogswell Dam, 32-5, Safety Review Report. Prepared by the Division of Safety of Dams, Department of Water Resources, State of California, June.

SEISMIC PERFORMANCE AND DESIGN CONSIDERATION OF A LONG-SPAN SUSPENSION BRIDGE

Wen David Liu, Roy A. Imbsen
Imbsen & Associates, Inc., Sacramento

Armen Der Kiureghian
University of California, Berkeley

ABSTRACT

A 3D analytical model of the Vincent Thomas Bridge is calibrated using the measured structure responses during the 1987 Whittier Narrows earthquake. Vibrational characteristics which are sensitive to multiple-support excitations were identified.

An analytical model for the ground motion incoherency was evaluated based on motions recorded at 10 stations at Caltech during the earthquake. The motions at four stations were selected as input to the bridge supports whose spatial variation is consistent with the coherency model. A multiple-support response spectrum method is described to illustrate the application to long structures.

INTRODUCTION

The seismic performance of major long-span bridges during a strong earthquake shaking would have significant effects on the regional economy and activities of the population. This was evidenced following the 1989 Loma Prieta earthquake. For important structures, not only collapse failure must be prevented, but also that the extent of damage due to an earthquake must be limited and the function of the bridge must be restored quickly. The new requirement for maintaining functionality following a major earthquake poses a greater demand on the seismic evaluation technology:

- A sufficiently detailed analytical model to capture the essential 3D vibrational characteristics of the structure;
- A clear understanding of the ground motion input to the structure supports; and
- A methodology to conduct seismic evaluation efficiently under the multiple-support excitation input.

The available instruments on the bridge site are not sufficient to define the multiple support ground motion input. To supplement the existing instrumentation, the ground motions recorded at the Caltech array during the 1987 earthquake (processed by CDMG) were used to establish the spatial variations as described by the coherency function. Ground motions recorded at four stations were selected for use in the direct-integration, multiple-support-excitation, time history analysis. Given the response spectrum and the coherency function consistent with the ground motion time histories, the applicability of the multiple-input response spectrum method can be evaluated.

THE VINCENT THOMAS BRIDGE

Description of the Bridge – The Vincent Thomas Bridge on State Sign Route 47 spans the main channel of Los Angeles Harbor between San Pedro on the west and Terminal Island on the east. Its 6060 foot length is made up of the 1500 foot suspended main span, two 507 foot long suspended side spans and 19 steel plate girder approach spans of from 150 to 230 feet in length. The suspended span consists of two stiffening trusses, transverse floor trusses, and a lower-chord wind bracing system of the K-truss type. The vertical sag of the cable at midspan is 150 feet. Roadway width is 52 feet between 2-foot wide curbs.

At the time of construction (1961-'63) it was thought to be the only suspension bridge in the world supported entirely on piles. The 14 BP 117 steel H-piles used at the anchorages, cable bents and main towers were driven to Elevation -75 at the Terminal Island Tower and -135 at the San Pedro Tower. Indicated bearing value was 145 tons for each pile.

The towers each consist of two steel box section legs fabricated in seven vertical segments with five lateral truss members separating the legs. Cross section of each leg is roughly that of a cross with the inside vertical and the outside tapering uniformly from the base elevation of 25.00 feet to the top elevation of 360.67 feet. Individual segments are made up of welded 3/4-inch plate, and segments are bolted to one another with one inch diameter high strength bolts. The base segment is held to the pier with 78 2-1/2-inch diameter steel rods, each stressed to 360,000 pounds.

The suspender ropes do not hang vertically as they do on some suspension bridges. Center-to-center spacing is 66'-6" at the top of main towers, 59'-2" at the cable bents and 55'-0" at the cable anchorages. The elevation and plan views of the cable are shown in Figure 1.

Description of the Instrumentation – Figure 2 shows the layout of the strong-motion instrumentation installed on the bridge (CSMIP Station No. 14406). A total of 26 sensors are used including: 13 sensors on the stiffening-truss deck; 3 sensors on top of the east tower; and 10 sensors at the base level (East anchorage, East Tower and West Tower).

Analytical Model – A 3D analytical model of the suspension bridge was developed as shown in Figure 3. The stiffening trusses and transverse floor trusses were represented by statically equivalent girders located at appropriate locations as shown in Figure 3b. The stiffness matrix derived from the idealization involving equivalent girders and bottom K bracings was evaluated against the "exact" generalized stiffness matrix for the actual 3D truss structure. Very close correlation was obtained for all diagonal as well as off-diagonal terms in the stiffness matrix indicating that all essential behavior of the original truss system is captured by the idealized model.

The model of the tower is shown in Figure 3c. All members in the transverse trusses were included in the model. At the intersection of the tower and the deck, both main-span and side-span trusses are free to slide longitudinally within a guided bearing assembly passing through the tower shaft, are supported vertically by hangers, and are restrained in the transverse direction. All rotational degrees of freedom at the tower-deck connection are unrestrained.

VIBRATION CHARACTERISTICS OF THE TOWER

The instrumentation layout was apparently devised to monitor the vertical,. lateral and torsional responses of the truss system. To this end, detailed correlation studies were carried out by Niazy (1991) to correlate analytical predictions with measured responses during the Whittier earthquake.

For the transverse vibration of the towers, there are three transducers installed at the top of the tower shaft (channel 8), the roadway level (channel 6), and the top of the pier (channel 9). The tower vibration in the transverse direction is strongly affected by the lateral vibration of the cable. Three types of modes are calculated as shown in Figure 4. There are a number of modes calculated which have essentially the same deformed configuration of the tower as shown in Figure 4a, but have periods ranging from 1.36 to 2.26 seconds depending on the participation of lateral cable vibration. From the measured data, similar modes were identified with periods 1.5 and 1.7 seconds. The second transverse mode with a period of 0.85 seconds involves the bending of the tower shaft starting at the roadway level as shown in Figure 4b. The corresponding measured mode was identified with a period of 0.79 seconds. The third transverse mode with a period of 0.47 seconds (Figure 4c) was not identified from the measurements.

Because of the high cable tension, the top of the tower where two transducers were located is essentially stationary. Therefore, longitudinal vibration modes of the towers can only be derived from the analytical model. Eight modes involving significant tower longitudinal vibration are shown in Figure 5:

- Modes 23 and 24 (T = 1.58 seconds) involve the longitudinal vibration of the two towers, respectively, and the in-phase motion of the adjacent side span (Figures 5a and 5b).
- Modes 31 and 32 (T = 1.27 seconds) involve similar vibration of the towers, but with out-of-phase motion of the side span trusses (Figures 5c and 5d).
- Modes 25 and 26 (T = 1.53 seconds) involve the simultaneous longitudinal motion of both towers. The two towers are in-phase for mode 25 and out-of-phase for mode 26 (Figures 5e and 5f).
- Mode 62 (T = 0.64 seconds) and Mode 67 (T = 0.58 seconds) involve the higher-order tower vibration with two towers vibrating in-phase and out-of-phase, respectively (Figures 5g and 5h).

These closely-spaced vibration modes are very important if the bridge structure is subjected to out-of-phase input motions at multiple supports.

MULTIPLE-SUPPORT-EXCITATION SEISMIC ANALYSIS

For long structures extended over many supports, the spatial variation of ground motion may induce structural responses in the following ways:

1. quasi-static responses, and
2. vibrational responses.

If the seismic ground motion input at the multiple supports is completely defined in terms of ground acceleration and displacement time histories, the most direct method is the direct-integration time history analysis method. However, this is rarely the case. Typically, there is high uncertainty in the ground motion specifications. A response spectrum analysis method that will account for the spatial variation of the seismic input would be very desirable.

Multiple-Support Ground Motion – The spatial variations of ground motion can be attributed to attenuation effect, wave passage effect, ray-path incoherency and extended source effect. (Abrahamson et al, 1991) The spatial incoherency is expressed as a complex-valued function of frequency and separation distances. Given recorded ground motions at closely spaced stations,

the coherency function can be quantitatively determined. In practice, the empirically derived coherency functions are used to define ground motion input. By varying the parameters involved, the sensitivity of the structural response to the spatial variation of ground motion can be assessed rather quickly using the multiple-support response spectrum method.

Multiple-Support Response Method – This method was recently developed by Der Kiureghian and Neuenhofer (1992) that would account for the multiple-support input. This is a direct extension of the CQC modal combination method under uniform input. (Der Kiureghian, 1980) Based on random vibration theory, the mean value of maximum responses (any displacement and member force component) can be expressed in terms of:

- peak ground displacements at each support,
- response spectrum at each support, and
- several cross-correlation coefficients.

In equation form, this is expressed as the sum of three terms as follows:

$$E\left[\max|z(t)|\right] = \left\{ \sum_k \sum_l a_k a_l \rho_{u_k u_l} u_{k,max} u_{l,max} \right.$$

$$+ \; 2 \sum_k \sum_l \sum_j a_k b_{lj} \rho_{u_k s_{lj}} u_{k,max} D_l(\omega_j, \xi_j)$$

$$\left. + \; \sum_k \sum_l \sum_i \sum_j b_{ki} b_{lj} \rho_{s_{ki} s_{lj}} D_k(\omega_i, \xi_i) D_l(\omega_j, \xi_j) \right\}^{1/2}$$

where

$z(t)$ = response quantities of interest.
a_k, a_l = effective quasi-static influence factors associated with supports k and l, respectively.
b_{ki}, b_{lj} = effective modal influence factors for mode i (j) and support degree of freedom k (l).
$u_{k,max}$ = peak ground displacement at support k.
$D_k(\omega,\xi)$ = displacement response spectrum associated with support k.
$\rho_{u_k u_l}$, $\rho_{u_k s_{lj}}$, and $\rho_{s_{ki} s_{lj}}$ = cross-correlation coefficients.

The three terms in the above equation account for:

1. the quasi-static effect,
2. the coupled quasi-static and dynamic effect, and
3. the dynamic effect.

The cross-correlation coefficients used account for the effects of spatial ground motion variation and the cross modal correlation. The method has been used in the study of the Golden Gate Bridge (Nakamura et al, 1993). The data flow diagram for the multiple-support response spectrum analysis is summarized in Figure 6.

In this study, an evaluation of the ground motion coherency model was carried out based on measured time histories. The time histories were selected to conduct the time history response

analysis using the calibrated structural model. The coherency model and the ground motion response spectra are used to derive all necessary correlation coefficients. The multiple-support response spectrum analysis will be carried out to compare with the time history analysis results.

ACKNOWLEDGMENTS

This study was supported through funding from the California Strong Motion Instrumentation Program, California Division of Mines and Geology. Partial funding was also provided by the In-House Research Program of Imbsen & Associates, Inc. These supports are gratefully acknowledged. Dr. Paul Somerville is a consultant for the evaluation of ground motion coherency function. Mr. Po Lam assisted in the calculation of foundation stiffness coefficients of all piers. Dr. Julie Cohen assisted in the calibration of the structural model.

REFERENCES

Der Kiureghian, A. and Neuenhofer A. (1991), A Response Spectrum Method for Multiple-Support Seismic Excitations, UCB/EERC 91/08, Earthquake Engineering Research Center, University of California, Berkeley, August 1991.

Nakamura, Y., A. Der Kiureghian and W.D. Liu (1993), Multiple-Support Response Spectrum Analysis of the Golden Gate Bridge, Earthquake Engineering Research Center, University of California, Berkeley, 1993.

Abrahamson, N.A., F. Schneider and J.C. Stepp (1991), Empirical Spatial Coherency Functions for Application to Soil-Structure Interaction Analysis, Earthquake Spectra, Vol. 7, No. 1.

Niazy, A.S.M. (1991), Seismic Performance Evaluation of Suspension Bridges, Ph.D. Dissertation, University of Southern California, December 1991.

Der Kiureghian, A. (1980), Structural Response to Stationary Excitation, Journal of Engineering Mechanics, ASCE Vol. 106 pp 1195-1213.

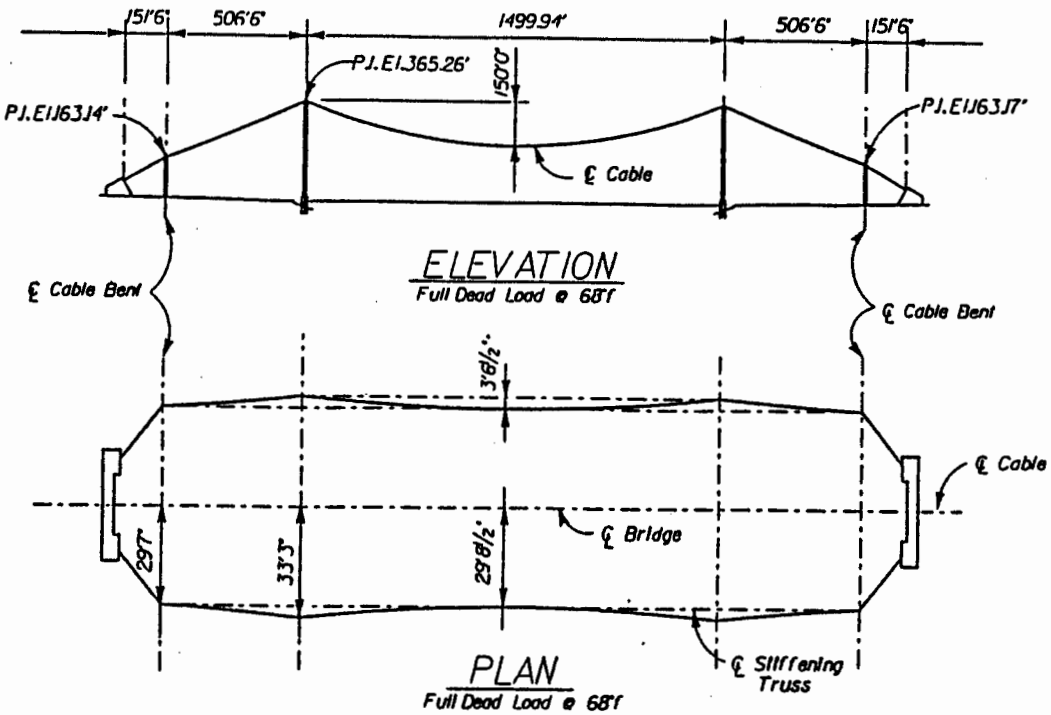

Figure 1 Cable Profiles-Vincent Thomas Bridge

Figure 2 Sensor Layout

Los Angeles – Vincent Thomas Bridge

(CSMIP Station No. 14406)

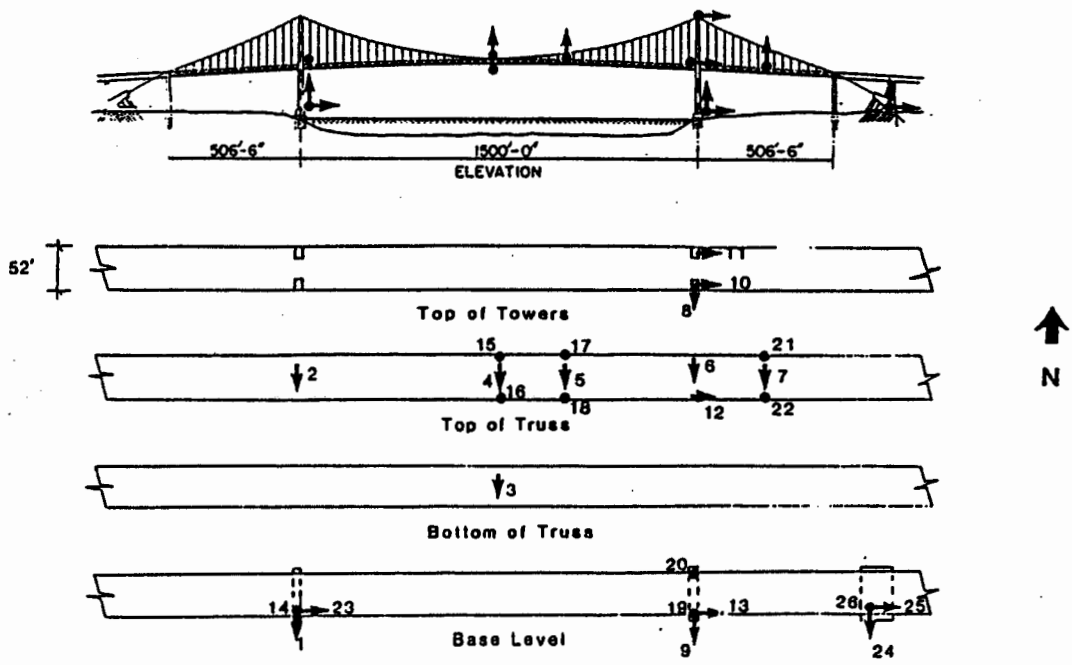

PLAN VIEWS

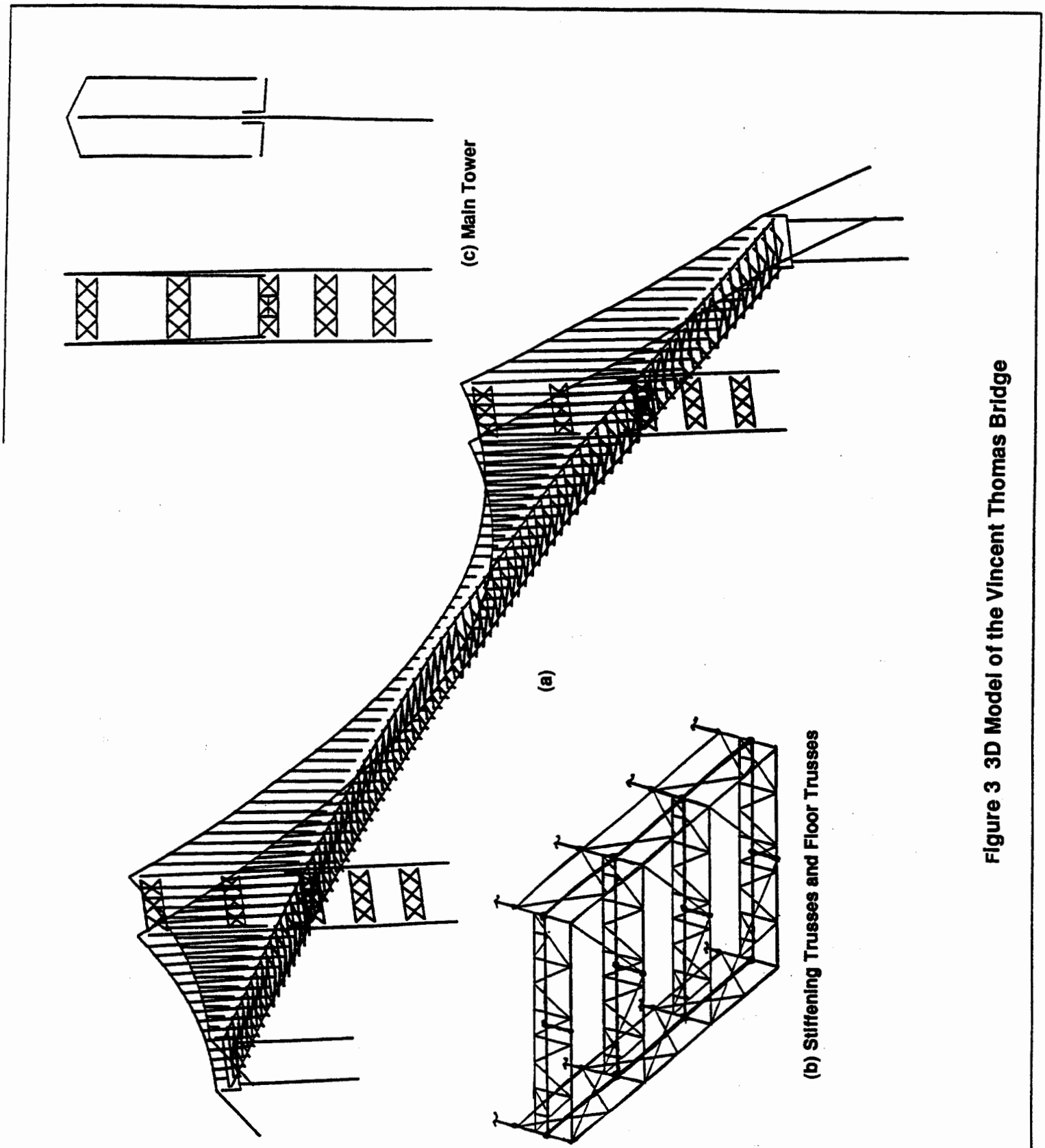

Figure 3 3D Model of the Vincent Thomas Bridge

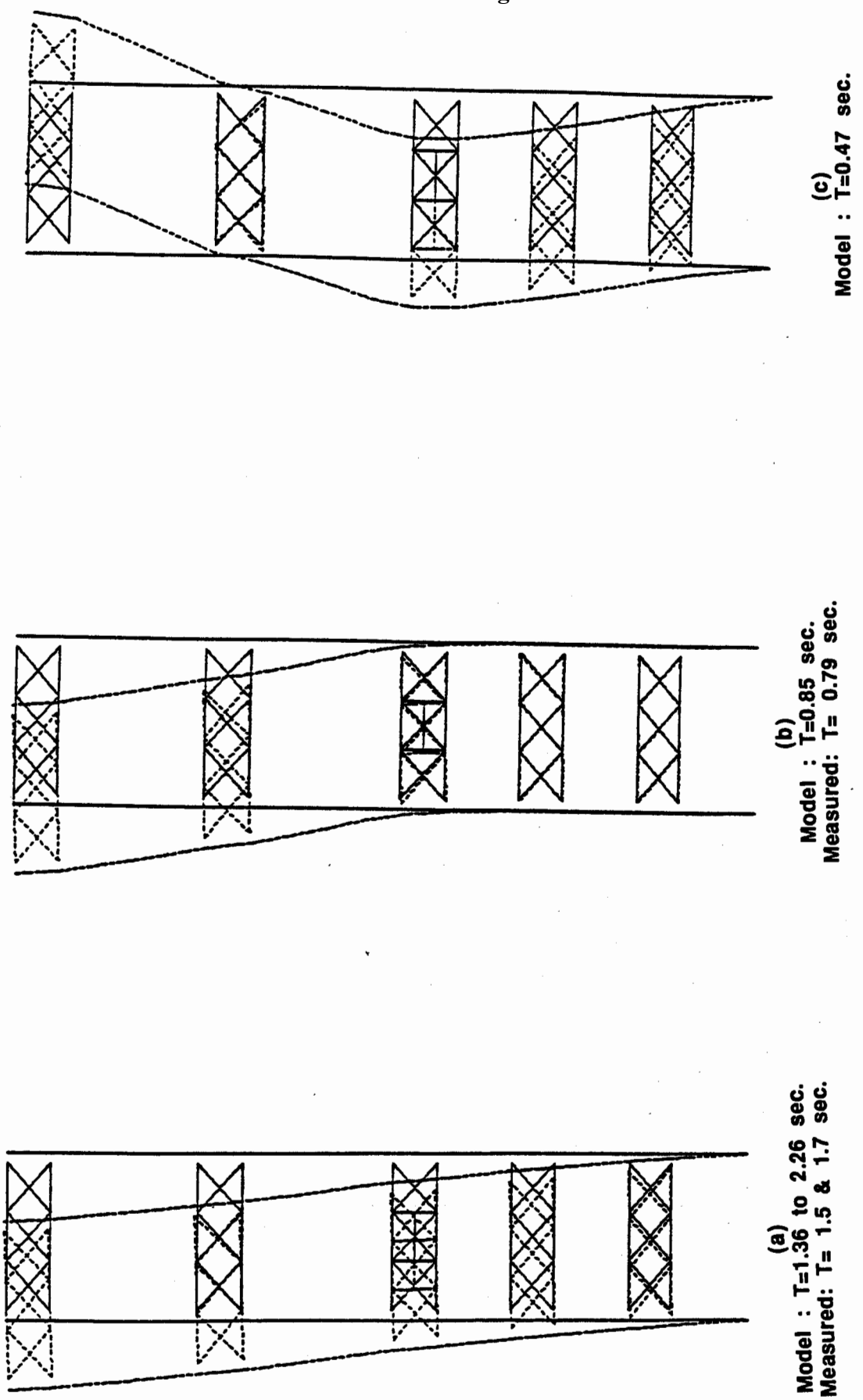

Figure 4 Transverse Vibration Modes - Vincent Thomas Bridge

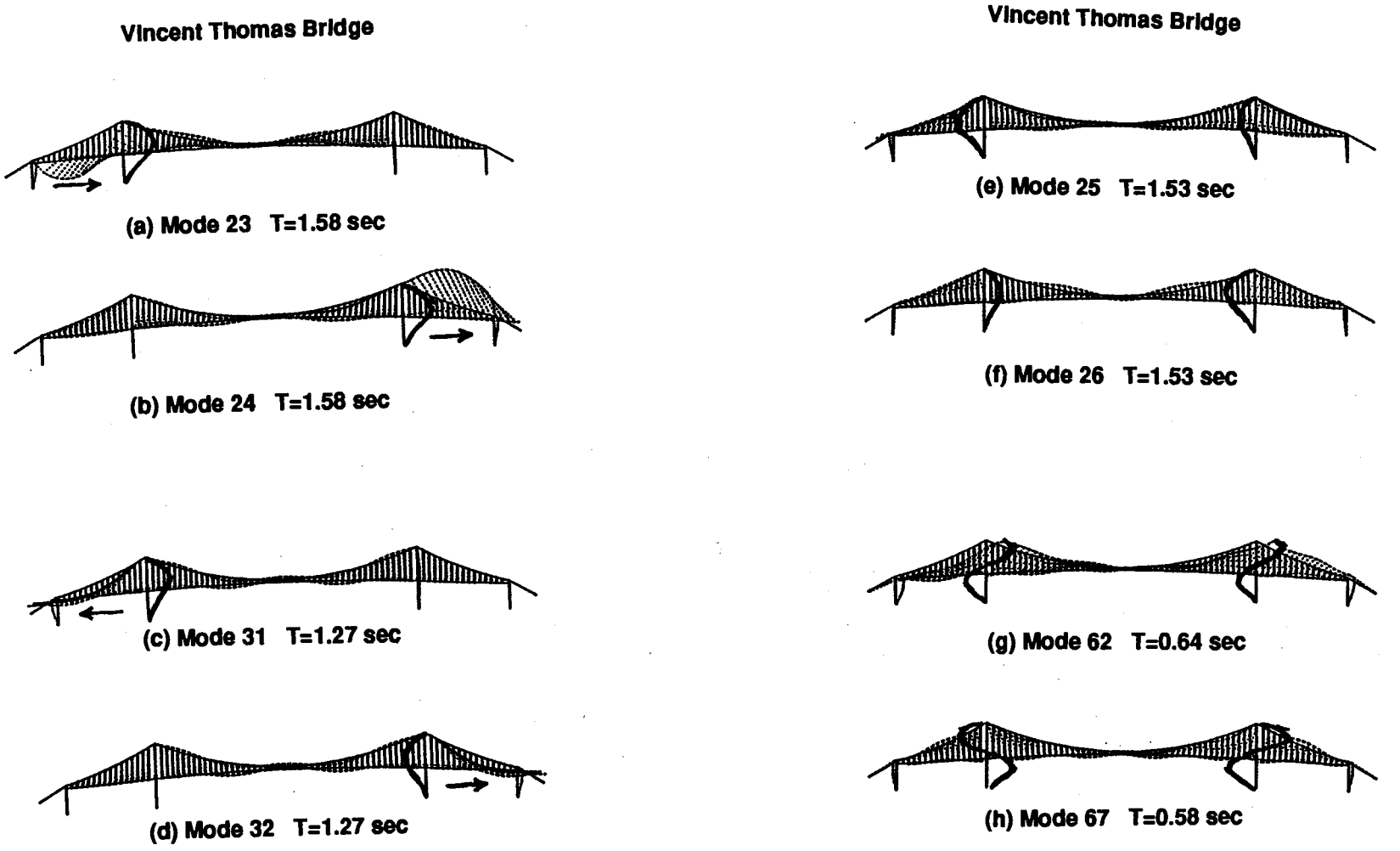

Figure 5 Longitudinal Vibration Modes

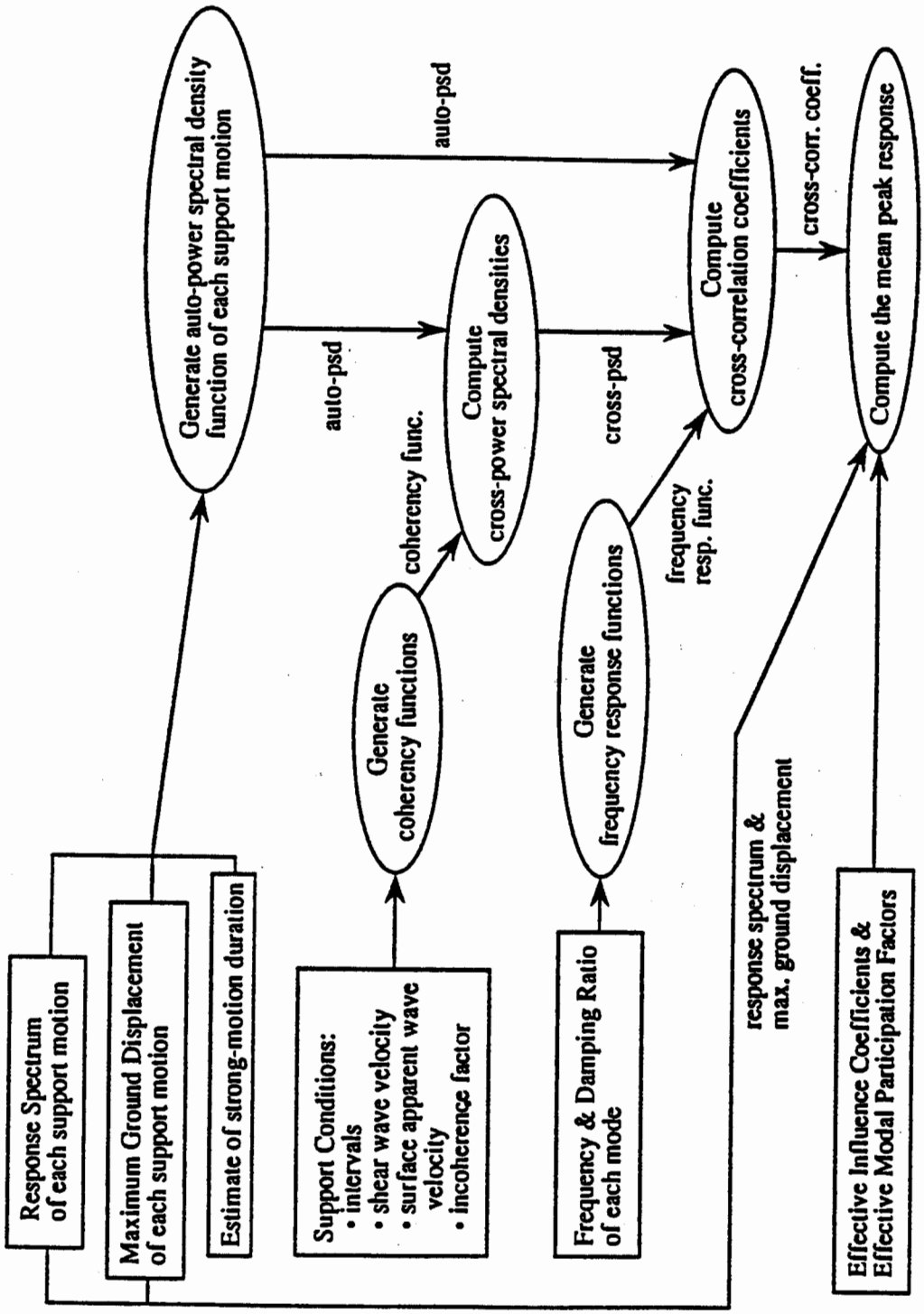

Figure 6 Data Flow Diagram for Multiple-Support Response Spectrum Analysis (Nakamura, et al 1993)